

European Journal of Biomedical and Life Sciences

2024, No 3

European Journal of Biomedical and Life Sciences

Scientific journal

2024, No 3

ISSN 2310-5674

Editor-in-chief

Todorov Mircho, Bulgaria, Doctor of Medicine

International editorial board

Inoyatova Flora Ilyasovna, Uzbekistan, Doctor of Medicine, Republican Specialized Scientific and Practical Medical Center of Pediatrics (RSNPMC Pediatrics)

Kurdzeka Aliksandr, Kazakhstan, Doctor of Veterinary Medicine, Kazakh National Agrarian University

Kushaliyev Kaissar Zhalitovich, Kazakhstan, Doctor of Veterinary Medicine, Zhangir Khan Agrarian Technical University

Mambetullaeva Svetlana Mirzamuratovna, Uzbekistan, Doctor of Biological Sciences, Karakalpak Research Institute of Natural Sciences

Nikitina Veronika Vladlenovna, Russia, Doctor of Medical Sciences, Associate Professor, PSPb State Medical University named after Academician I.P. Pavlov of the Ministry of Health of the Russian Federation

Petrova Natalia Guryevna, Russia, Professor, Doctor of Medical Sciences, First St. Petersburg State Medical University named after I.P. Pavlov

Skopin Pavel Igorevich, Russia, Doctor of Medicine, Mordovian State University

Spasennikov Boris Aristarkhovich, Russia, Doctor of Medicine, Doctor of Law, Institute of Industry Management (IOM) RANEPa

Suleyman Suleymanov, Uzbekistan, Senior Researcher, Associate Professor, PhD in Medical science, Bukhara State Medical University

Suleymanov Suleyman Fayzullaevich, Uzbekistan, Ph.D. of Medicine, Bukhara State Medical Institute (BukhGosMI)

Tegza Alexandra Alexeevna, Kazakhstan, Doctor of Veterinary Medicine, Kostanay State University

Vijaykumar Muley, India, Doctor of Biological Sciences, Institute of Neurobiology, National Autonomous University of Mexico (UNAM)

Proofreading

Kristin Theissen

Cover design

Andreas Vogel

Additional design

Stephan Friedman

Editorial office

Premier Publishing s.r.o.
Praha 8 – Karlín, Lyčkovo nám. 508/7, PSČ 18600

E-mail:

pub@ppublishing.org

Homepage:

ppublishing.org

European Journal of Biomedical and Life Sciences is an international, English language, peer-reviewed journal. The journal is published in electronic form.

The decisive criterion for accepting a manuscript for publication is scientific quality. All research articles published in this journal have undergone a rigorous peer review. Based on initial screening by the editors, each paper is anonymized and reviewed by at least two anonymous referees. Recommending the articles for publishing, the reviewers confirm that in their opinion the submitted article contains important or new scientific results.

Premier Publishing s.r.o. is not responsible for the stylistic content of the article. The responsibility for the stylistic content lies on an author of an article.

Instructions for authors

Full instructions for manuscript preparation and submission can be found through the Premier Publishing s.r.o. home page at: <http://ppublishing.org>.

Material disclaimer

The opinions expressed in the conference proceedings do not necessarily reflect those of the Premier Publishing s.r.o., the editor, the editorial board, or the organization to which the authors are affiliated.

Premier Publishing s.r.o. is not responsible for the stylistic content of the article. The responsibility for the stylistic content lies on an author of an article.

Included to the open access repositories:



Scientific Journal Impact Factor Value for 2024 – 6.671

© Premier Publishing s.r.o.

All rights reserved; no part of this publication may be reproduced, stored in a retrieval system, or transmitted in any form or by any means, electronic, mechanical, photocopying, recording, or otherwise, without prior written permission of the Publisher.

Typeset in Berling by Ziegler Buchdruckerei, Linz, Austria.

Printed by Premier Publishing s.r.o., Vienna, Austria on acid-free paper.



Section 1. Clinical medicine

DOI: 10.29013/EJBL-24-3-3-20



FIRST-IN-CLASS SMALL MOLECULE BTLA INHIBITORS AS POTENTIAL CANCER THERAPIES

Brian Kuo¹

¹ Cupertino High School

Cite: Kuo B. (2024). *First-In-Class Small Molecule Btla Inhibitors as Potential Cancer Therapies*. *The European Journal of Biomedical and Life Sciences 2024, No 3* <https://doi.org/10.29013/EJBL-24-3-3-20>

Abstract

Modern cancer treatments have developed to a great extent – however, various factors such as cancer types and resistance continue to make effective treatments difficult to create for many cancers. Among different cancer treatments, immunotherapy shows promise because of its utilization of one's own body's immune system in fighting off cancerous cells. Immune checkpoints instruct the body to stop producing anti-cancer cells, and blocking these checkpoints can be effective in reactivating an immune system. B and T Lymphocyte Attenuator (BTLA) is an immune checkpoint that shows promise as an immunotherapy target, but current clinical trials focus solely on large monoclonal antibodies that can have severe side effects and other limitations due to larger molecular size. By identifying small molecule BTLA inhibitors, the development of anti-cancer immunotherapy treatments could be vastly improved. In this paper I utilize a variety of experiments to virtually screen small molecules and identify potential BTLA inhibitors. First, I located suitable binding sites in BTLA using 3 different methods (geometric, energetic, and machine learning methods). I identified compounds using virtual screening in two different experiments, by identifying HVEM B-chain pharmacophore maps, then scanning the ZINC compound library for matches. Then, I verified the compounds' site binding on BTLA with molecular docking in SwissDock. Finally, the druggability of the remaining compounds were evaluated twice, for drug properties and for toxicity, in SwissADME and ProTox 3.0 respectively. In the end, two promising compounds with favorable energetic interactions with BTLA, strong drug properties according to Lipinski's rule, and low toxicity were identified as drug candidates for different applications, which hold potential for being pivotal milestones in the field of cancer therapy.

Keywords: *B and T Lymphocyte Attenuator (BTLA), immunotherapy, cancer, cancer therapy, immune checkpoints, drug discovery, small molecule inhibitor*

Introduction

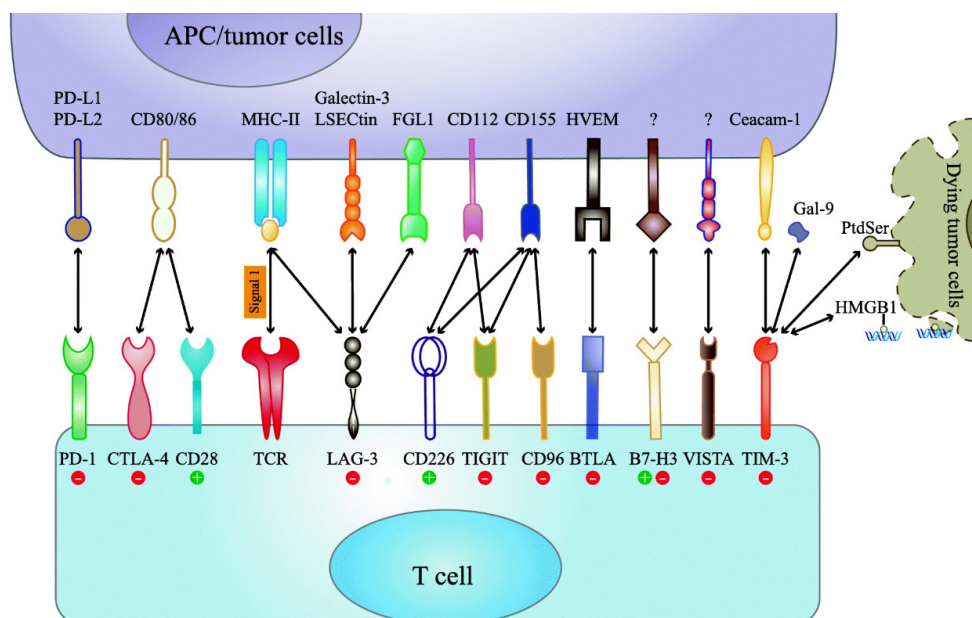
Cancer, a disease caused by uncontrolled, abnormal cell growth, is becoming more prominent of a global issue than ever, and with it comes human ingenuity in discovering cancer treatments. Modern treatments range from chemotherapy, which utilizes chemicals to kill dividing cancer cells, to radiation therapy, which induces damage to the DNA of cancer cells using radiation (Hossain *et al.*, 2023; Jaffray *et al.*, 2015). In addition, scientists have found that combining multiple treatments can be effective at an affordable cost (Bayat Mokhtari *et al.*, 2017). However, the large variability in different cancer types, cancer resistance to drugs, and the side effects of toxic drugs continue to make universal treatments nigh impossible (Barot *et al.*, 2023).

Among different types of cancer treatments, immunotherapy utilizes one's own body's immune system to fight off cancer. Currently, a better understanding of the immune system and immune surveillance has slowly made immunotherapy more viable – however, it is still a juvenile cancer treatment

due to the difficulty of predicting its effectiveness and toxicity (Esfahani *et al.*, 2020). But compared to conventional treatment methods such as chemotherapy, which can see harmful damage to parts of the human body that aren't cancerous, immunotherapy could potentially have fewer side effects (Shahid *et al.*, 2019).

Immune checkpoints allow the immune system to keep itself in check – they can inhibit or stimulate molecules, allowing the immune system to either attenuate or activate T-cell proliferation and activity. Immune checkpoints are necessary in maintaining homeostasis in the immune system, and to prevent any collateral damage done by one's own immune system. Because of its regulatory nature, some cancers have been found to slip under an immune system and halt T-cell proliferation through immune checkpoint pathways. On the other hand, immune checkpoints can be blocked in order to activate T-cells, which can target cancers (Lee *et al.*, 2016). The function of immune checkpoint pathways and our ability to inhibit them mark a promising avenue in immuno-oncology.

Figure 1. Various immune checkpoints found on T-cells, and their binding counterparts found on antigen-presenting or tumor cells (Qin *et al.*, 2019)



Inhibitors for immune checkpoints PD-1 and CTLA-4 are currently the forefront of immunotherapy, having received FDA approval (Zhang *et al.*, 2021). However, the inhibitors for these pathways are limited – immune checkpoint monotherapies for PD-1 and

CTLA-4 have been found to show responses in only 20%-30% of patients (Padmanee *et al.*, 2021). In addition, various cancers currently exhibit complete resistance to the current treatment methods (Pilard *et al.*, 2021). Because of this, research of newer inhibitors

for immune checkpoints could mean great strides in the field of cancer treatment.

B and T Lymphocyte Attenuator (BTLA), is an immune checkpoint most commonly found on B and T lymphocytes and dendritic cells, and negatively regulates immune responses to maintain immune homeostasis when bound with Herpesvirus Entry Mediator (HVEM), which is found on similar cells (Sedy *et al.*, 2005; Ning *et al.*, 2021). Similarly to PD-1 and CTLA-4, BTLA's negatively regulatory nature in the immune system means it is involved in many immune disorders and immune system functions (Watanabe *et al.*, 2003). For example, mice have been found to have a greater risk of autoimmune diseases when deficient of BTLA (Oya *et al.*, 2008).

BTLA on T-cells inhibits activity when activated by HVEM, which can prevent T-cells from being able to fight against cancer cells. Since cells deficient in BTLA are found to have increased T-cell activity and proliferation, inhibiting BTLA could potentially be pursued as an immunotherapy target (Andrzejczak *et al.*, 2024). However, the current main molecule for inhibiting BTLA is the monoclonal antibody (mAb) icatolimab, which was approved for clinical trials in 2019. Its larger size may provide challenges for immunotherapy in the future, such as longer lasting side effects and lower maneuverability, highlighting a need for discovering new, viable BTLA inhibitors that are of smaller molecular sizes.

Method

Locating Suitable Binding Sites on BTLA

Before beginning to find small molecules that could bind to BTLA, possible binding locations must first be identified. This was done using 3 different methods, all utilizing BTLA's Protein Database (PDB) Code: 1XAU. This code represents the 3D structure of BTLA when it is not interacting with external molecules, which gives a strong base to identify binding sites for the use of small molecule binding.

Geometric Method

The aim of the geometric method was to find binding sites on BTLA that are the right size for small molecules to target. First, the PDB code 1XAU was typed into the web structure-based modeling server, proteins.plus, to identify the

correct BTLA model (Schöning-Stierand *et al.*, 2022). Then, the geometric based binding sites were calculated using the default parameters of DoGSiteScorer, which detected binding sites based solely on the 3D structure of BTLA (Volkamer *et al.*, 2010).

Energetic-based Method

The second method was the energetic-based method using FTSite at ftsitesite.bu.edu, which identified binding sites using multiple molecular probes that account for charge and energy at the binding sites (Kozakov *et al.*, 2015). BTLA's PDB code was entered into FTSite, where the job was queued, completed, and later viewable on the website.

Machine Learning Method

The last method used to identify suitable binding sites on BTLA was the machine learning method, using prankweb.cz (Jakubec *et al.*, 2022). This method uses a variety of factors, from geometric to energetic, to identify binding sites. To use the model, the PDB code for BTLA was entered and submitted.

Virtual Screening with Pharmacophore

In order to narrow down suitable compounds to bind with BTLA and prevent its binding with HVEM, a virtual screening process must be undergone. First pharmacophore maps were identified with PocketQuery, then the ZINC library was screened with ZINCPharmer. Pharmacophore maps utilized the PDB code 2AW2, and were of the B-chain of HVEM, representing the interaction between BTLA and HVEM.

Pharmacophore Mapping

To identify the best pharmacophore maps on the BTLA/HVEM interaction, I used pocketquery.csb.pitt.edu. The PDB code 2AW2 was entered and searched, and the clusters with the highest scores on the B-chain were used. The B-chain is the HVEM side of the interaction, and using these maps will enable the discovery of small compounds that mimic its interaction with BTLA. The maps were then exported to ZINCPharmer through the website's in-built export function.

Small Molecule Virtual Screening

In zincpharmer.csb.pitt.edu, the pharmacophore maps were isolated by hiding the ligand and receptor residues in the viewer tab. Then, the submit query button scanned and identified matching compounds from

the ZINC library, which were then organized from lowest to highest Root Mean Square Deviation (RMSD) score to pick the best compound matches based on the pharmacophore map.

Molecular Docking

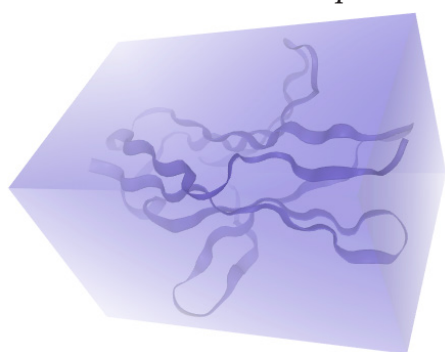
In order to quantify the energy between 20 chosen compounds and different bind-

ing sites on BTLA, I used molecular docking using the newest version of swissdock.ch. For each ligand, the SMILES format is found with the ZINC library website, and the PDB code for BTLA, 1XAU, was used. To define the search space, the sizes shown in Table 1 were used. Parameters were set to the default of 1.

Table 1. Search space used for molecular docking of BTLA in SwissDock experiment

Search box center (Å)	30	28	14
Search box size (Å)	28	25	41

Figure 2. Search space used for BTLA in the SwissDock experiment



Drug Properties Evaluation using SwissADME

With the top 5 compounds from the molecular docking experiment, I utilized swissadme.ch to evaluate the drug properties of the molecules. The respective SMILES were entered into the website and the evaluations were run. I looked at the 4 elements of Lipinski's rule as well as water solubility, GI absorption, and BBB permeability to evaluate the drug effectiveness of these compounds.

Toxicity Prediction using ProTox 3.0

The purpose of the toxicity prediction experiment is to see if the toxicity of the two remaining compounds are within an acceptable

toxicity range. This was done using Tox Prediction from ProTox 3.0, where the SMILES format and all models were selected. I then compared the predicted values (LD50, toxicity class, etc) as well as the predicted active elements and models between the two compounds to determine drugging suitability.

Results

Geometric Method

Results

Figure 3. Six suitable binding sites on BTLA, color labeled, based on geometric methods and identified using the DoGSiteScorer

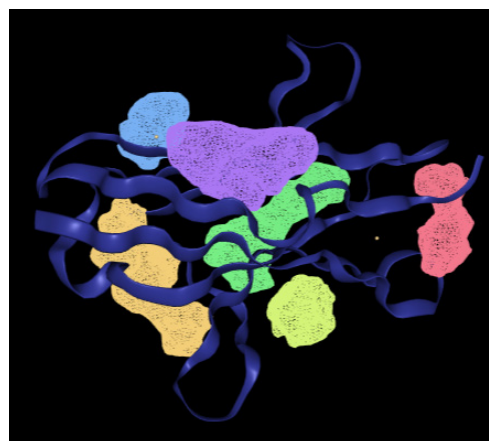


Table 2. Volume, Surface Area, and Drug Score assigned to each binding site with the Geometric method, using DoGSiteScorer at proteins. plus

Name	Volume (Å ³)	Surface Area (Å ²)	Drug Score
P_0 (Orange)	323.84	479.33	0.62
P_1 (Violet)	243.01	322.2	0.42
P_2 (Lime Green)	184.51	439.5	0.58
P_3 (Red)	121.98	306.51	0.36
P_4 (Blue)	113.98	326.8	0.21
P_5 (Green)	103.68	242.98	0.17

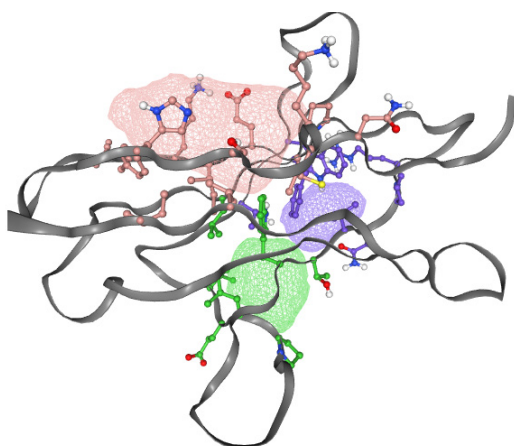
Discussion

Using the geometric method, 6 binding sites were identified with Protein.plus (DoGSiteScorer), each with varying volumes (103.68 to 323.84 Å³) and surface areas (242.98 to 479.33 Å²). The top binding site (P_0) in BTLA (PDB: 1XAU) based on Protein.plus had a volume of 323.84 Å³ and surface area of 479.33 Å². This binding site is highlighted in orange in Figure 3. Because Protein.plus is only based on the 3D shape of BTLA and not any other factors, such as the energetic ability of small molecules to bind at the site, there are more binding sites than testing with other methods.

Energetic-Based Method

Results

Figure 4. Three suitable binding sites, color labeled, identified based on the energetic-based method, using FTSite



Discussion

From the energetic-method tested using FTSite, 3 suitable binding sites were identified,

labeled in pink, green, and purple. These represent binding sites on BTLA (PDB: 1XAU) that are more energetically-favorable for small compounds to potentially bind to.

Machine Learning Method

Results

Figure 5. First suitable binding site of BTLA (labeled in red) based on the machine learning method, identified using PrankWeb

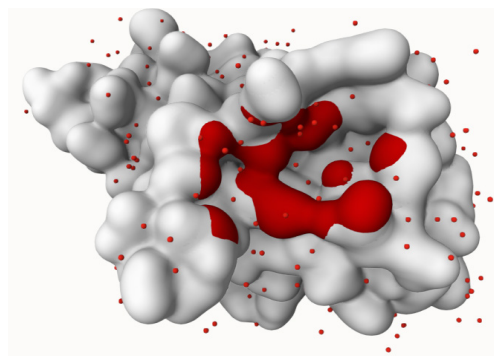


Figure 6. Second suitable binding site of BTLA (labeled in yellow) based on the machine learning method, identified using PrankWeb

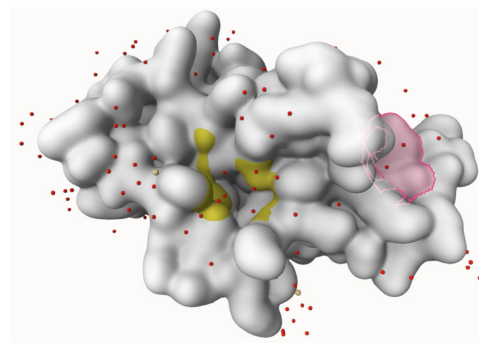


Table 3. Suitable binding site rankings, drug scores, and residue information for the two binding site results from the machine learning method, using PrankWeb

Binding Site Ranking	Drug Score	# of Residues	Residues
1 (red)	2.58	10	LYS50 ASN52 VAL 57 PRO 58 LEU59 GLU60 LEU65 HIS86 SER88 ASP 89

Binding Site Ranking	Drug Score	# of Residues	Residues
2 (yellow)	1.08	9	ILE17 LYS18 SER21 HIS23 LYS32 ILE33 GLU34 PRO 36 VAL 109

Discussion

The machine learning method shows two suitable binding sites, fewer than the other two methods used, because it combines a variety of factors instead of using just one. The binding sites must fit structural, physico-chemical, and evolutionary factors – the stricter criteria means that fewer sites are

selected (Kufareva I., Abagyan R. 2012). The top binding site identified with PrankWeb (labeled as red in Figure 4) has a drug score of 2.58 and consists of 10 amino acid residues.

Pharmacophore Mapping

Results

Table 4. PocketQuery pharmacophore mapping results for top five scoring clusters on the B chain of HVEM (Koes et al, 2012)

Ranking	Score	Distance (Å)	Size (residues)	Residues
1	0.771762	9.1795	3	GLU31 LEU32 GLY34
2	0.754979	7.298	2	LEU32 GLY34
3	0.731909	0	1	LEU32
4	0.730782	9.1795	4	GLU31 LEU32 THR33 GLY34
5	0.726755	11.9219	4	PRO 17 GLU31 LEU32 GLY34

Figure 7. Top PocketQuery match for HVEM B-chain

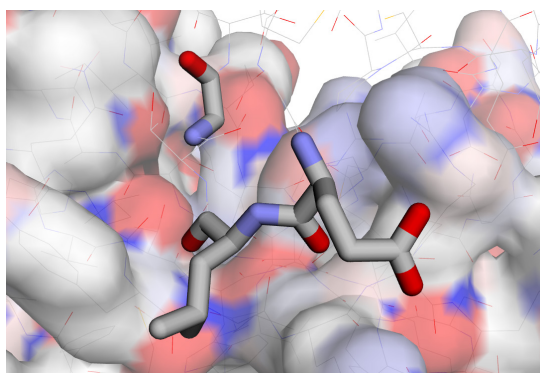


Figure 8. Second top PocketQuery match for HVEM B-chain

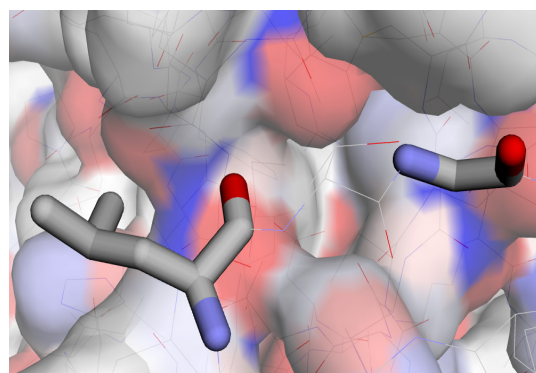
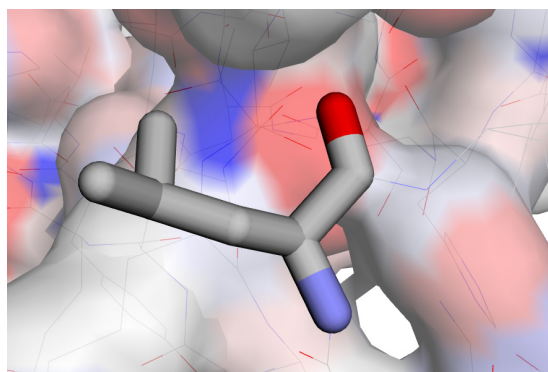


Figure 9. Third top PocketQuery match for HVEM B-chain



Discussion

PocketQuery search results for the BTLA/HVEM complex (PDB code: 2AW2) on the B chain showed the highest scoring results (with higher score being suitability for the design of small molecule inhibitors) generally having the residues GLU31, LEU32, and GLY34. The top five best scoring clusters for the B chain had varying distances (7.298 to 11.9219 Å) and sizes (1 to 4 residues), with

the best scoring cluster having a distance of 9.1795 Å and size of 3.

Small Molecule Virtual Screening Results

Figure 10. Pharmacophore map for top PocketQuery match

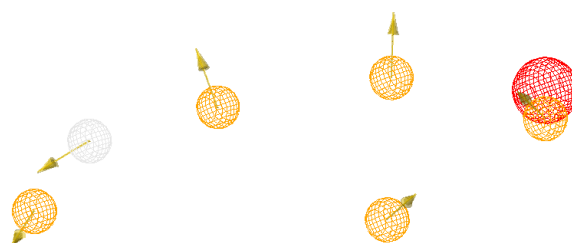


Figure 11. Pharmacophore map for top PocketQuery match after isolating 3 closest interactions



Table 5. Top compound match results from ZINCPharmer for highest scoring pharmacophore map of HVEM B-chain (Koes et al., 2012)

Name	RMSD Score	Mass (daltons)	Residue Binds
ZINC37452229	0.013	288	6
ZINC38148338	0.016	560	8
ZINC34781361	0.017	494	15
ZINC38867909	0.018	224	5

Table 6. Highest scoring pharmacophore map overlaid with compounds that showed lowest RMSD scores in ZINCPharmer

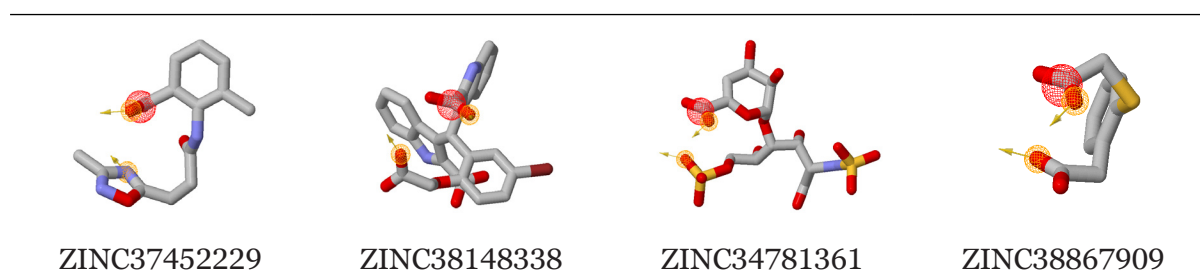


Figure 12. Pharmacophore map for second top PocketQuery match



Table 7. Top compound match results from ZINCPharmer for second highest scoring pharmacophore map of HVEM B-chain

Name	RMSD Score	Mass (daltons)	Residue Binds
ZINC49601555	0.008	445	15
ZINC93485320	0.009	289	6
ZINC83429713	0.011	463	13
ZINC83429714	0.011	463	13
ZINC06624253	0.011	414	10
ZINC12664461	0.011	414	10
ZINC39223733	0.012	360	14
ZINC81245051	0.012	316	9

Table 8. Second highest scoring pharmacophore map overlaid with compounds that showed lowest RMSD scores in ZINCPharmer

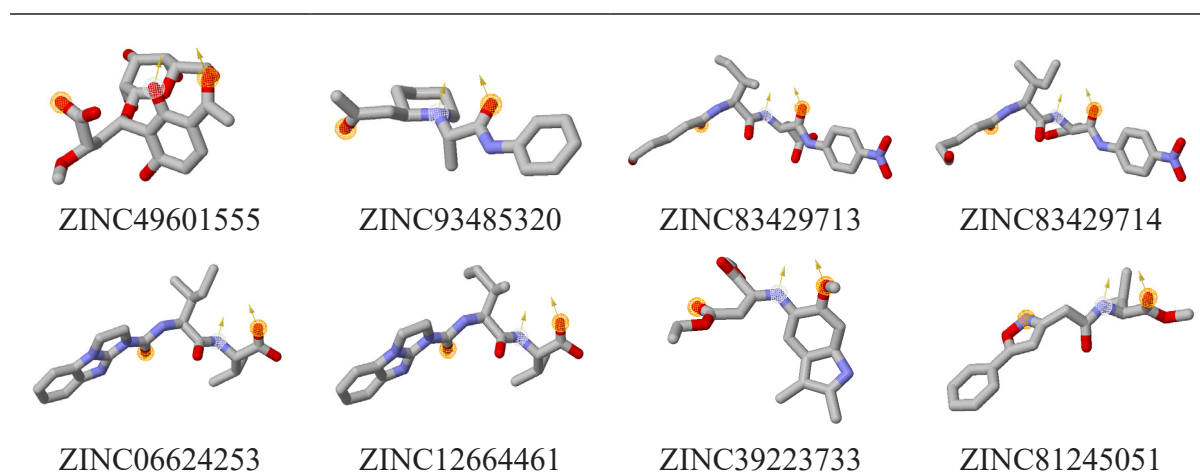


Figure 13. Pharmacophore map for third top PocketQuery match

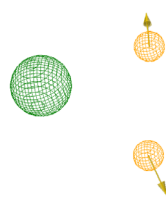
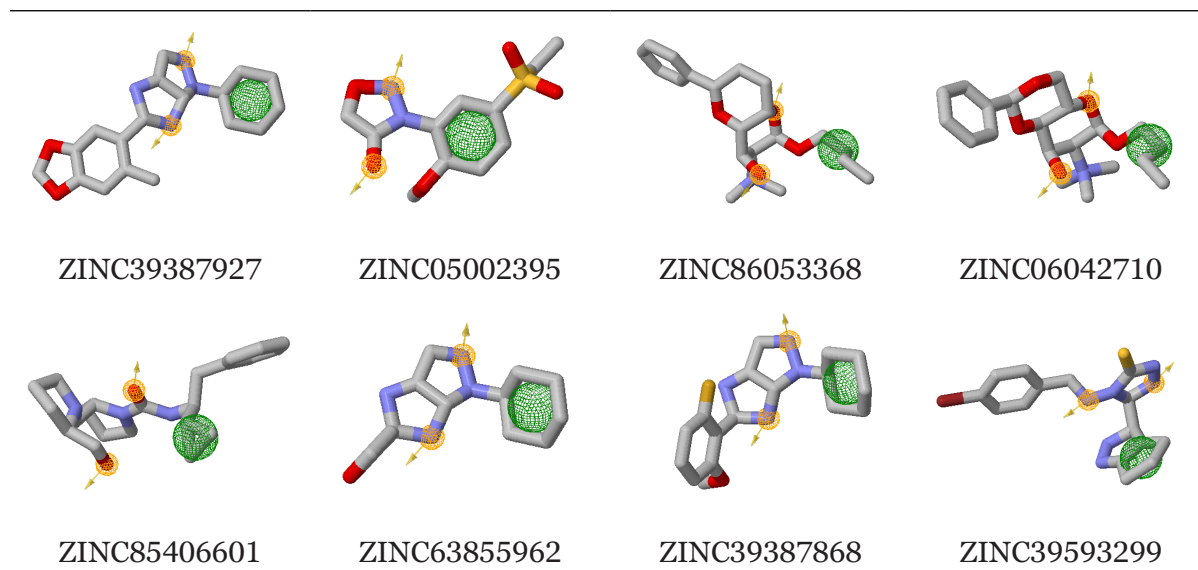


Table 9. Top compound match results from ZINCPharmer for third highest scoring pharmacophore map of HVEM B-chain

Name	RMSD Score	Mass (daltons)	Residue Binds
ZINC39387927	0.008	326	3
ZINC05002395	0.009	286	7
ZINC86053368	0.009	364	11
ZINC06042710	0.010	366	11
ZINC85406601	0.011	373	8
ZINC63855962	0.012	258	2
ZINC39387868	0.012	316	4
ZINC39593299	0.012	390	3

Table 10. Third highest scoring pharmacophore map overlaid with compounds that showed lowest RMSD scores in ZINCPharmer



Discussion

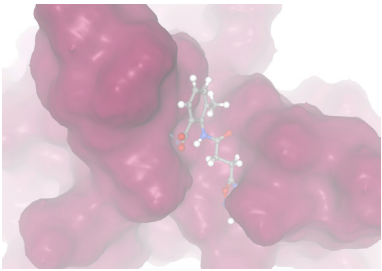
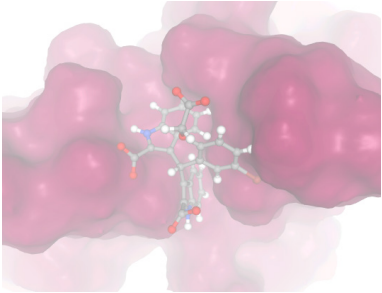
The RMSD values signal level of deviation the molecule has from the pharmacophore map (Kufareva *et al.*, 2012). Out of the 20 selected compounds with low RMSD values, from 3 different pharmacophore maps of the B chain on the BTLA-HVEM complex, there were varying masses (224 to 560) and residue binds (2 to 15). The compounds with the

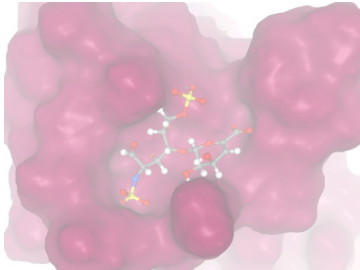
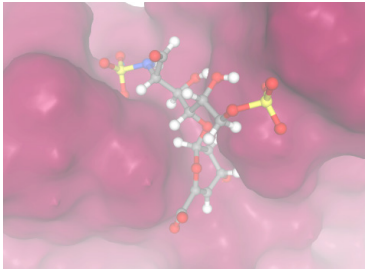
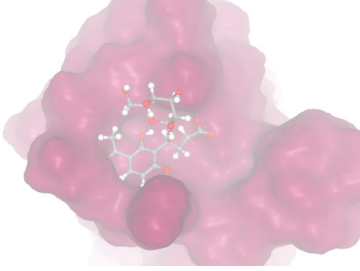
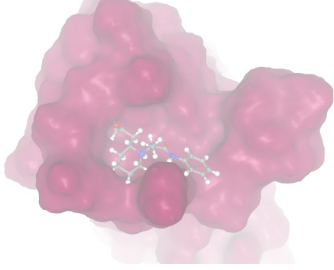
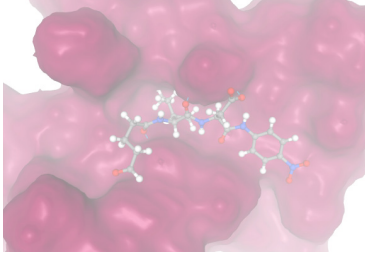
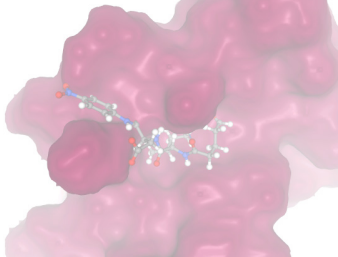
lowest RMSD values were ZINC49601555 and ZINC39387927 with RMSD values of 0.008. Masses for the compounds were 445 and 326 daltons respectively, and the compounds had residue binds of 15 and 3.

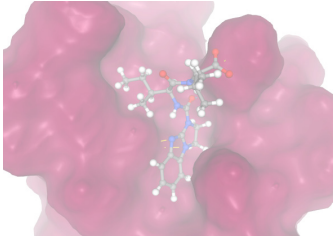
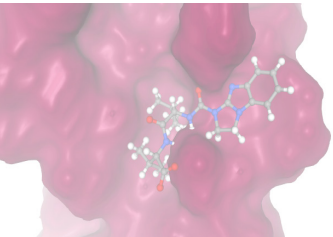
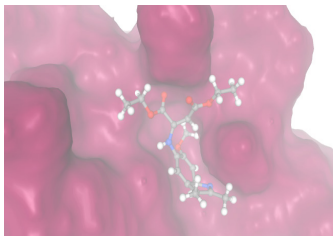
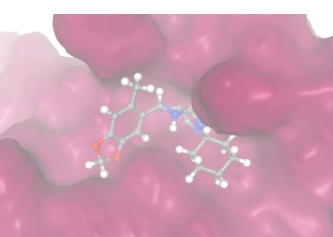
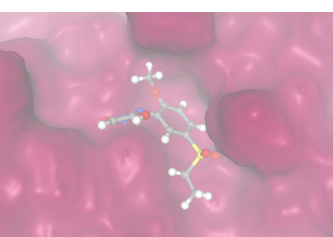
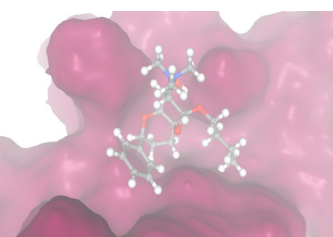
Molecular Docking

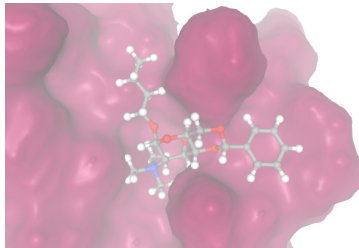
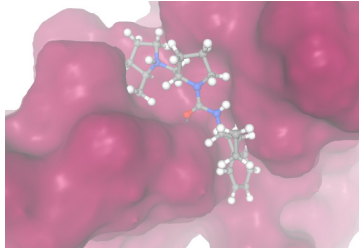
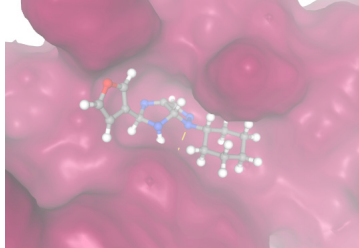
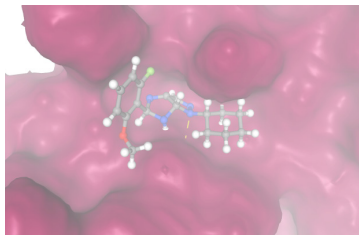
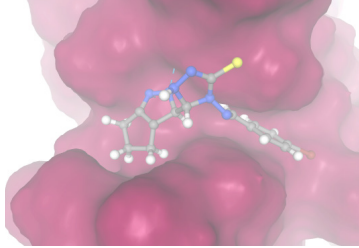
Results

Table 11. Molecular docking results for the 20 compounds with lowest RMSD scores, using the updated version of Swiss Dock.ch.

Compound	Highest SwissParam Score (kcal/mol)	Highest SwissParam Cluster	Highest Interaction
ZINC37452229	-6.6440	1	
ZINC38148338	-6.5126	13	

Compound	Highest SwissParam Score (kcal/mol)	Highest SwissParam Cluster	Highest Interaction
ZINC34781361	-6.5749	27	
ZINC38867909	-7.0349	3	
ZINC49601555	-6.8794	0	
ZINC93485320	-6.7812	1	
ZINC83429713	-7.1073	3	
ZINC83429714	-7.4917	2	

Compound	Highest SwissParam Score (kcal/mol)	Highest SwissParam Cluster	Highest Interaction
ZINC06624253	-7.0473	0	
ZINC12664461	-7.1827	0	
ZINC39223733	-7.2914	9	
ZINC81245051	-7.1301	4	
ZINC39387927	-7.3083	0	
ZINC05002395	-6.7593	4	
ZINC86053368	-6.5743	9	

Compound	Highest SwissParam Score (kcal/mol)	Highest SwissParam Cluster	Highest Interaction
ZINC06042710	-6.7704	0	
ZINC85406601	-7.1930	0	
ZINC63855962	-7.2660	0	
ZINC39387868	-7.4206	1	
ZINC39593299	-7.2100	0	

Discussion

Out of the 20 selected compounds, 12 compounds were able to achieve a SwissParam score of below -7 kcal/mol. The highest SwissParam scores for each compound ranged from -6.5126 to -7.4917 kcal/mol, with the top 5 compounds according to score being ZINC83429714, ZINC39387868, ZINC39387927, ZINC39223733, and ZINC63855962, from highest to lowest score. The SwissParam score

represents free energy, so these 5 compounds with the largest numerical scores have the most optimal energy interactions. The locations of these interactions were on clusters 2, 1, 0, 9, and 0 respectively.

Drug Properties Evaluation Results

Table 12. Drug properties of top 5 compounds, identified with SwissADME

Compound	Hydrogen Bond Donors (<5)	Hydrogen Bond Acceptors (<10)	Calculated LogP (1–5)	Mass (<500 daltons)	Lipinski's rule violations	Water Solubility ESOL (moderate or more)	GI Absorption (high)	BBB Permeability (no)
ZINC83429714	3	8	2.11	463.46	0	–2.10 (Soluble)	Low	No
ZINC39387868	1	5	3.19	316.37	0	–3.69 (Soluble)	High	Yes
ZINC39387927	1	5	2.99	326.39	0	–3.88 (Soluble)	High	Yes
ZINC39223733	1	6	4.06	360.40	0	–2.89 (Soluble)	High	No
ZINC63855962	1	4	2.51	258.32	0	–2.76 (Soluble)	High	No

Discussion

After evaluating all 5 compounds, the two molecules that successfully pass the set benchmarks for druggability were ZINC39223733 and ZINC63855962. Both of these molecules fit the elements of Lipinski's rule (<5 H bond donors, <10 H bond acceptors, 1–5 CLogP, <500 daltons) as well as being soluble, having High GI absorption and

not being BBB permeable. ZINC39387868 and ZINC39387927 also passed Lipinski's rule, and were soluble with high GI absorption. However, they are BBB permeable, potentially posing risks of side effects.

Toxicity Prediction*Results***Table 13.** Predicted Toxicity Data using Tox-Prediction from Pro Tox 3.0.

Compound	LD50 (mg/kg)	Toxicity Class	Toxic Elements
ZINC39223733	187	3	Nephrotoxicity Respiratory Toxicity Nutritional Toxicity
ZINC63855962	800	4	Neurotoxicity Respiratory Toxicity Carcinogenicity BBB-barrier Eco Toxicity Clinical Toxicity

Figure 14. Toxicity Radar Chart for Compound ZINC39223733, showing active toxic areas in nutritional, respiratory, and nephrotoxicity, lower than the average of its class of FDA-approved drugs

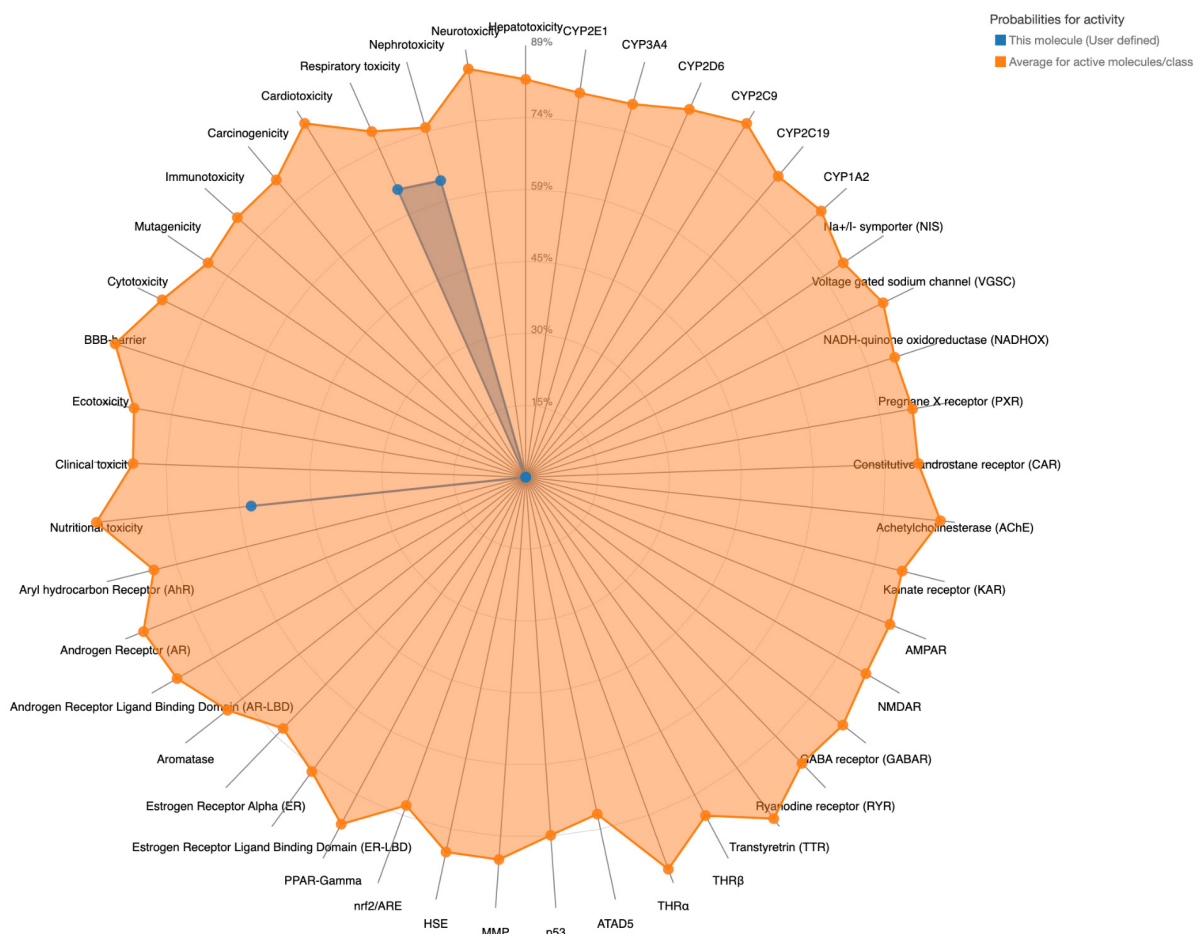


Figure 15. Network Charts for Compound ZINC39223733, showing the active and inactive clusters from the ProTox 3.0 experiment

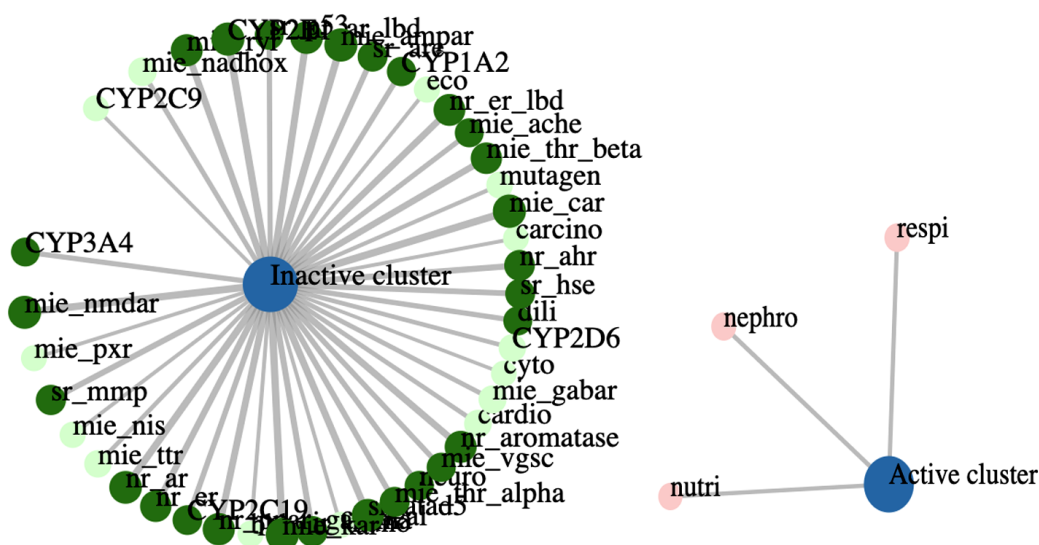


Figure 16. Toxicity Radar Chart for Compound ZINC63855962, showing active toxic areas in Clinical toxicity, eco toxicity, BBB-barrier toxicity, carcinogenicity, respiratory toxicity, and neurotoxicity, with BBB-barrier and respiratory toxicity being slightly higher compared to the average of its class of FDA-approved drugs

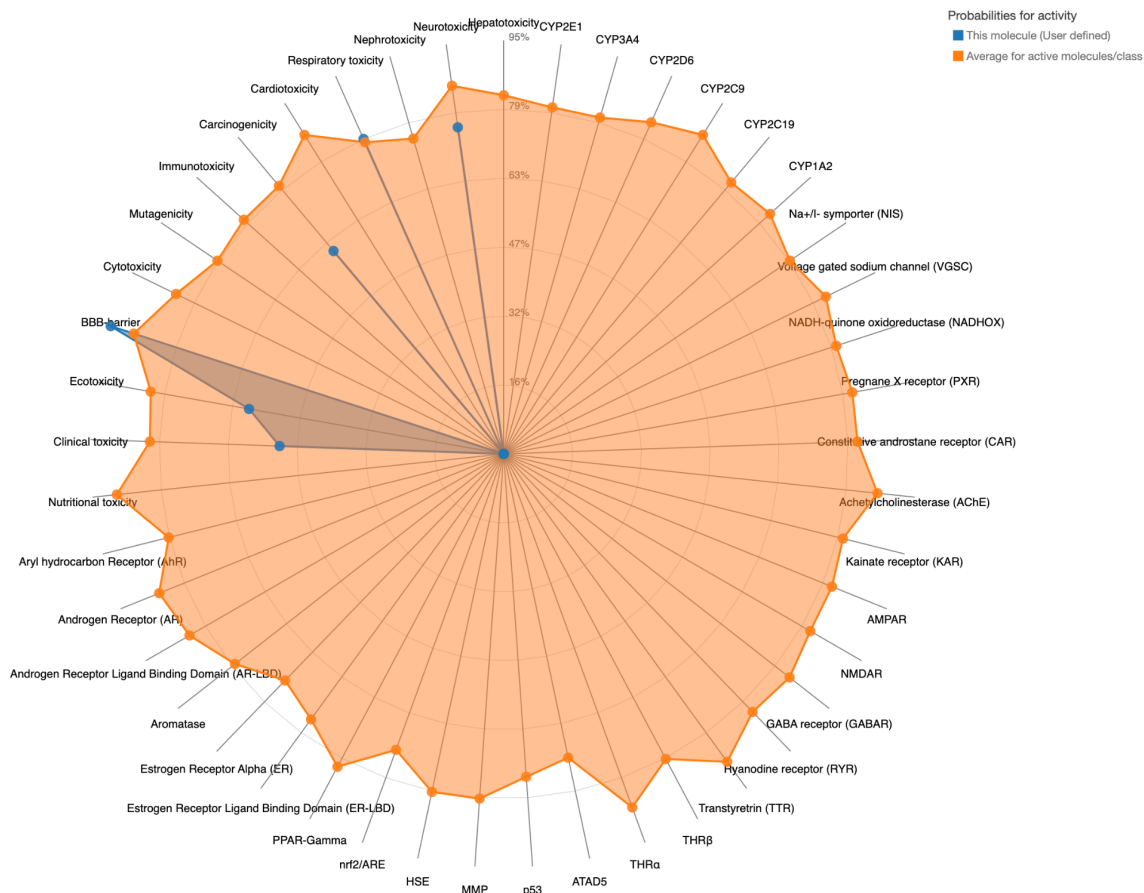
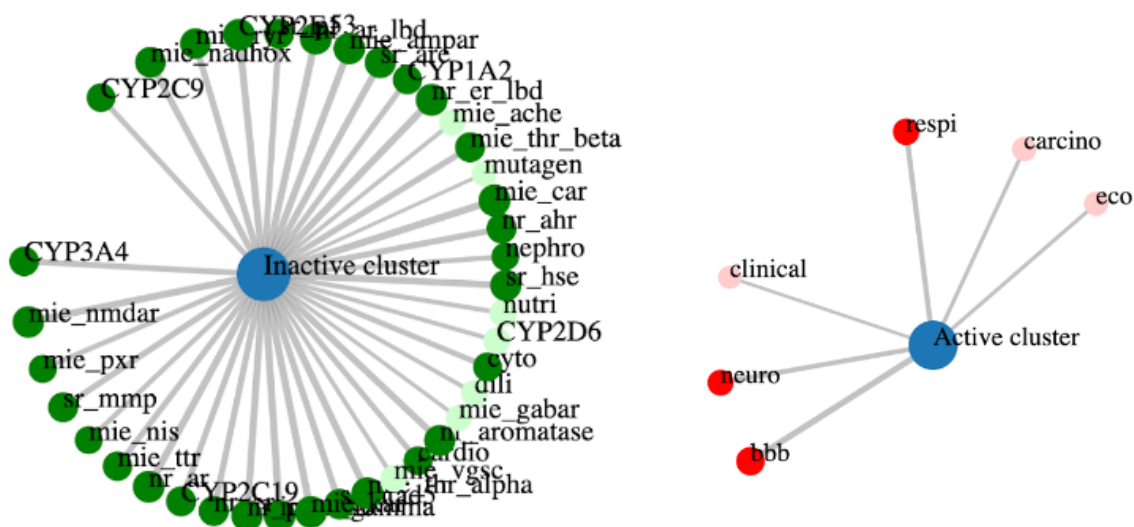


Figure 17. Network Chart for Compound ZINC63855962, showing the active and inactive clusters from the ProTox experiment



Discussion

Screening both compounds with the toxicity prediction method found that ZINC39223733 was the better drug candidate, with a lower LD50 of 187 mg/kg and toxicity class of 3, but fewer active toxic elements. As seen in Figure 14, the 3 active toxic elements of ZINC39223733 were all within an acceptable range.

ZINC63855962 had a higher LD50 of 800 mg/kg and toxicity class of 4 – however, it had a total of 6 toxic elements, with 2 elements, the blood-brain barrier and respiratory toxicity elements, being slightly above the average FDA-approved drug of its class.

Comparing the two drug candidates, ZINC39223733 stands out as a better candidate overall because of its fewer toxic elements. On the other hand, ZINC63855962's ability to penetrate the blood-brain barrier means it could be used to target tumors in the brain, which is only made possible because of the compound's BBB permeability.

Statement of Limitations

The main limitation of these experiments is that they are virtual, and may not reflect accurate real-life test results for binding and toxicity. Going forward, *in vitro* or *in vivo* experiments should be performed to evaluate the effectiveness of the compounds as BTLA inhibitors. Another limitation is that the PrankWeb evaluation of the first experiment only resulted in two binding sites on BTLA. PrankWeb was the most accurate binding site evaluator of the three methods used because it included the most factors, which brings up limitations for the ability of compounds to bind to BTLA. Finally, another limitation was in the Molecular Docking experiment, where many of the selected top 20 compounds had SwissParam scores above -7 kcal/mol, which were not ideal for moving into the drug property evaluation. This meant less compounds in the final drug and toxicity evaluation stages, which could have cut down on the number of promising compounds identified.

Conclusion

The first experiment identified two main binding sites on BTLA that accounted for all three binding site testing methods. In the next experiment, PocketQuery identified pharmacophore maps for molecules from the Zinc compound library to bind to, of which three maps were selected. From these three maps, I used ZincPharmer to select 20 of the best compounds with the lowest RMSD scores on these maps. In the third experiment, I used molecular docking in SwissDock to compare the binding efficacy of the 20 compounds, and the top five compounds for numerical SwissParam score were selected. These five compounds were evaluated for drug properties in the SwissADME experiment, where two passed Lipinski's rule as well as additional drug property factors. In the last experiment, ProTox 3.0 identified both of these final two compounds, ZINC39223733 and ZINC63855962 as suitable drug targets due to acceptable LD50s and low number of active clusters. Between the two, ZINC39223733 is a better candidate overall, with less toxic elements – this choice is also backed by its lower SwissParam score of -7.4206 kcal/mol, compared to ZINC63855962's score of -7.2660 kcal/mol. On the other hand, ZINC63855962's blood-brain barrier permeability shows potential for use in treatment of brain tumors. Ultimately, this research has concluded two promising compounds for small molecule BTLA inhibitors as potential cancer therapies.

Going forward, the next steps would involve biophysical interactions with BTLA, to overcome the uncertainty of virtual model interactions. In the long term, these inhibitors can be tested in animal studies and eventually clinical trials. By doing so, the effectiveness of these two top compounds, ZINC39223733 and ZINC63855962, as BTLA inhibitors can be evaluated, bringing the field to cancer immunotherapy a new ray of hope

References

- Hossain M. B., Haldar Neer A. H. Chemotherapy. *Cancer Treat Res.* 2023; 185: 49–58.
Jaffray D. A., Gospodarowicz M. K. Radiation Therapy for Cancer. In: Gelband H., Jha P., San-
karanarayanan R., Horton S., editors. *Cancer: Disease Control Priorities, Third Edition*

- (Volume 3). Washington (DC): The International Bank for Reconstruction and Development / The World Bank; 2015.– Nov 1. Chapter 14.
- Bayat Mokhtari R., Homayouni T.S., Baluch N., Morgatskaya E., Kumar S., Das B., Yeger H. Combination therapy in combating cancer. *Oncotarget*. 2017. Jun 6; 8(23): 38022–38043.
- Barot S., Patel H., Yadav A., Ban I. Recent advancement in targeted therapy and role of emerging technologies to treat cancer. *Med Oncol*. 2023. Oct 7; 40(11): 324.
- Esfahani K., Roudaia L., Buhlaiga N., Del Rincon S.V., Papneja N., Miller W.H. Jr. A review of cancer immunotherapy: from the past, to the present, to the future. *Curr Oncol*. 2020. Apr; 27 (Suppl 2): S87–S97.
- Shahid K., Khalife M., Dabney R., Phan A. T. Immunotherapy and targeted therapy – the new roadmap in cancer treatment. *Ann. Transl. Med*. 2019; 7. Doi: 10.21037/ATM.2019.05.58. 595–595.
- Lee L., Gupta M., Sahasranaman S. Immune Checkpoint inhibitors: An introduction to the next-generation cancer immunotherapy. *J Clin Pharmacol*. 2016. Feb; 56(2): 157–69.
- Zhang H., Dai Z., Wu W., Wang Z., Zhang N., Zhang L., Zeng W.J., Liu Z., Cheng Q. Regulatory mechanisms of immune checkpoints PD-L1 and CTLA-4 in cancer. *J Exp Clin Cancer Res*. 2021. Jun 4; 40(1): 184.
- Padmanee Sharma, Bilal A. Siddiqui, Swetha Anandhan, Shalini S. Yadav, Sumit K. Subudhi, Jianjun Gao, Sangeeta Goswami, James P. Allison; The Next Decade of Immune Checkpoint Therapy. *Cancer Discov* 1 April 2021; 11 (4): 838–857.
- Pilard C., Ancion M., Delvenne P., Jerusalem G., Hubert P., Herfs M. Cancer immunotherapy: it's time to better predict patients' response. *Br J Cancer*. 2021. Sep; 125(7): 927–938.
- Sedy J.R., Gavrieli M., Potter K. G., Hurchla M.A., Lindsley R. C., Hildner K., et al. B and T lymphocyte attenuator regulates T cell activation through interaction with herpesvirus entry mediator. *Nat Immunol*. 2005; 6(1): 90–8.
- Ning Z., Liu K., Xiong H. Roles of BTLA in Immunity and Immune Disorders. *Front Immunol*. 2021. Mar 29; 12: 654960.
- Watanabe N., Gavrieli M., Sedy J.R., Yang J., Fallarino F., Loftin S. K., et al. BTLA is a lymphocyte inhibitory receptor with similarities to CTLA-4 and PD-1. *Nat Immunol*. 2003; 4(7): 670–9.
- Oya Y., Watanabe N., Owada T., Oki M., Hirose K., Suto A., et al. Development of autoimmune hepatitis-like disease and production of autoantibodies to nuclear antigens in mice lacking B and T lymphocyte attenuator. *Arthritis Rheum*. 2008; 58(8): 2498–510.
- Andrzejczak, A., Karabon, L. BTLA biology in cancer: from bench discoveries to clinical potentials. *Biomark Res* 12, 8 (2024).
- Qin, S., Xu, L., Yi, M. et al. Novel immune checkpoint targets: moving beyond PD-1 and CTLA-4. *Mol Cancer* 18, 155. (2019).
- Schöning-Stierand, K., Diedrich, K., Ehrt, C., Flachsenberg, F., Graef, J., Sieg, J., Penner, P., Poppinga, M., Ungethüm, A., Rarey, M. (2022). ProteinsPlus: a comprehensive collection of web-based molecular modeling tools. *Nucleic Acids Research*, 50: W611–W615.
- Volkamer, A., Griewel, A., Grombacher, T., Rarey, M. Analyzing the topology of active sites: on the prediction of pockets and subpockets. *J Chem Inf Model* 2010. 50 (11), 2041–52.
- Kozakov D., Grove L. E., Hall D. R., Bohnuud T., Mottarella S. E., Luo L., Xia B., Beglov D., Vajda S. The FT Map family of web servers for determining and characterizing ligand-binding hot spots of proteins *Nature Protocols* 2015. 10(5): 733–755.
- Dávid Jakubec, Petr Škoda, Radoslav Krivák, Marian Novotný and David Hoksza. PrankWeb 3: accelerated ligand-binding site predictions for experimental and modelled protein structures. *Nucleic Acids Research*. May, 2022.
- David Ryan Koes, Carlos J. Camacho, Small-molecule inhibitor starting points learned from protein–protein interaction inhibitor structure, *Bioinformatics*,– Volume 28.– Issue 6. March 2012.– P. 784–791.

David Ryan Koes, Carlos J. Camacho, ZINCPharmer: pharmacophore search of the ZINC database, *Nucleic Acids Research*,– Volume 40.– Issue W1. 1 July, 2012, P. W409–W414.
Kufareva I., Abagyan R. Methods of protein structure comparison. *Methods Mol Biol.* 2012; 857: 231–57.

submitted 14.08.2024;
accepted for publication 31.08.2024;
published 29.10.2024
© Kuo B.
Contact: mrkuo787@gmail.com



Section 2. Chemistry biology

DOI:10.29013/EJBLS-24-3-21-38



IDENTIFYING CEACAM 1-TARGETED DRUG CANDIDATES FOR CANCER IMMUNOTHERAPY

*Guanrong (Rain) Cheng*¹

¹ Garden International School, Malaysia

Cite: *Guanrong (Rain) Cheng. (2024). Identifying Ceacam1-Targeted Drug Candidates For Cancer Immunotherapy. The European Journal of Biomedical and Life Sciences 2024, No 3. <https://doi.org/10.29013/EJBLS-24-3-21-38>*

Abstract

Carcinoembryonic antigen-related cell adhesion molecule 1 (CEACAM1) is a key regulatory protein in immune modulation and tumor progression, making it a promising target for cancer immunotherapy. Immunotherapy is promising because it harnesses the body's own immune system to identify and eliminate cancer cells, often leading to more durable responses compared to traditional therapies like chemotherapy and radiation. By targeting immune checkpoints, such as those regulated by CEACAM1, immunotherapy can reinvigorate exhausted immune cells, enhancing their ability to fight tumors. CEACAM1 is particularly promising as a target because it plays a key role in immune checkpoint pathways that tumors exploit to evade immune detection. By interacting with immune cells, CEACAM1 can inhibit the immune response against tumors, allowing them to grow unchecked. This study uses computational docking methods to evaluate potential interactions between CEACAM1 and a variety of compounds from the ZINC database. The docking process involved multiple steps, including target and ligand selection, docking simulation, and binding affinity calculation. SwissADME and ProTox 3.0 tools were employed to assess the drug-like properties and toxicity profiles of the top candidates. From an initial pool of 20 compounds, five candidates had the most favorable binding energies (ΔG). Further analysis revealed that while ZINC71788521 and ZINC67902861 exhibited good target affinity, they violated Lipinski's rule of five. Conversely, ZINC08820313, ZINC38617077, and ZINC41591046 adhered to Lipinski's rule, demonstrating promising drug-like characteristics. In the end, ZINC08820313 was chosen as a potential drug candidate due to its high ΔG and low toxicity levels compared to the other compounds chosen. The study identifies potential CEACAM1 inhibitors with favorable energetic interactions and acceptable drug-like properties. Future work will involve in vitro and in vivo validation to substantiate these computational predictions.

Keywords: *Cancer, CEACAM1, Immunotherapy, Immune checkpoints, Drug candidates*

Introduction:

Cancer is a broad group of diseases characterized by uncontrolled cell growth and the ability of those cells to invade other tissues. There are over 200 different types of cancer affecting various parts of the body (Cancer Research UK, 2023). Common cancer treatment approaches include surgery, radiation, chemotherapy, targeted therapy, immunotherapy and combinations of these which are normally referred to as combination therapy. These therapies each have distinct mechanisms and limitations, such as surgery and radiation, which are often localized treatments, while chemotherapy uses drugs to target rapidly dividing cells, affecting both cancerous and healthy cells. Modern treatments allow many people to survive cancer, seen through the increase of 5-year survival rate for lung and bronchus cancer from 20.5% in 2010–2016 (Chaitanya Thandra et al., 2021) to 26.7% in 2024 (National Cancer Institute, 2018). However, cancer still remains one of the leading causes of death worldwide. The development of new and more effective therapies is an active area of research, with combination treatments of targeted therapy and immunotherapy showing particular promise due to them being specific to the cell or protein.

Immunotherapy is a form of treatment that uses the body's own immune system to fight disease. It presents new opportunities for more effective and less toxic cancer therapies by enhancing existing anti-tumor immune responses or counteracting strategies employed by tumors to evade immunity (Zhang & Zhang, 2020). Different types of cancer immunotherapies include monoclonal antibodies, immune checkpoint inhibitors, cancer vaccines, and adoptive cell therapies. Immune checkpoint inhibitors in particular are one of the more powerful approaches in immunotherapy, producing durable responses in around 20–25% of patients with advanced melanoma, non-small cell lung cancer, and other cancers (Hodi et al., 2010). However, response rates can vary significantly across different cancer types, with checkpoint inhibitors showing the most benefit in cancers with a high mutational burden like melanoma and lung cancer, and less efficacy in cancers like prostate cancer (Zappasodi et al., 2018).

Immune checkpoints are regulatory proteins expressed on immune cells that act as stimulatory or inhibitory switches to modulate the immune response (Alsaab et al., 2017). Well-known examples of inhibitory immune checkpoints include CTLA-4, PD-1, TIM-3, LAG-3, and VISTA. CTLA-4 is expressed on activated T cells and inhibits early stages of T cell activation. PD-1 is induced on activated T cells, B cells, and myeloid cells and inhibits effector functions in peripheral tissues (Pauken and Wherry, 2015). In normal physiology, immune checkpoints play an important role in preventing autoimmunity by raising the threshold for T cell activation and proliferation, thereby limiting chronic inflammation and autoimmune damage to healthy cells (Darvin et al., 2018). They provide inhibitory signals that counterbalance costimulatory signals, maintaining self-tolerance and modulating the intensity and duration of immune responses against foreign antigens (Buchbinder and Desai, 2016).

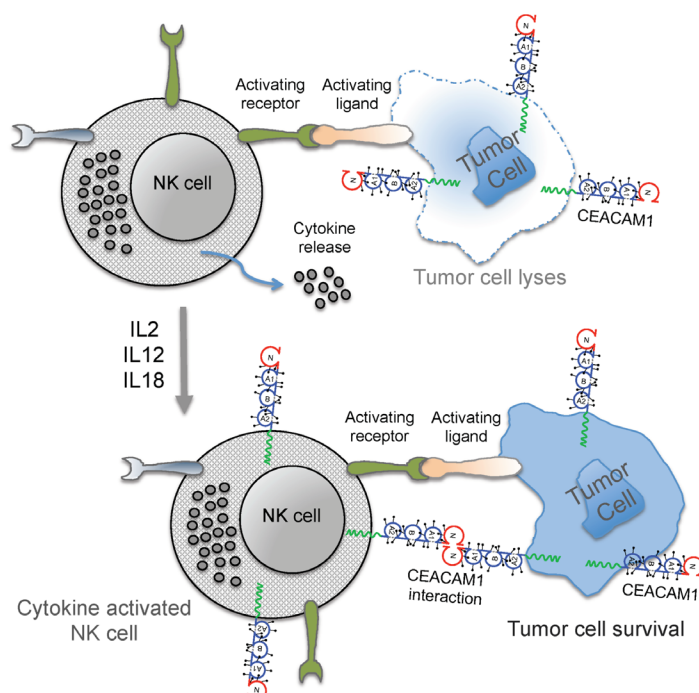
Carcinoembryonic antigen-related cell adhesion molecule 1 (CEACAM1) is a transmembrane glycoprotein of the immunoglobulin superfamily that plays roles lots of functions in the human body such as cell adhesion, angiogenesis, insulin metabolism, and immune regulation (Kim et al., 2019). It is widely expressed on epithelial cells, endothelial cells, and immune cells including T cells, B cells, and natural killer (NK) cells (Tucru et al., 2016). CEACAM1 functions by mediating homotypic and heterotypic cell-cell adhesion interactions through binding to other CEACAM family members or integrin receptors (Klaile et al., 2009). Its expression is highly regulated, with different isoforms generated by alternative splicing and its presence modulated by cytokines and other factors (Nagaiishi et al., 2008). Other than homophilic binding, CEACAM1 also binds heterophilically to CEACAM5, CEACAM6, and CEACAM8 (Kim et al., 2019), as well as integrin receptors like $\alpha\beta3$ (Brümmer et al., 2001).

CEACAM1 has a strong relationship with both cancer progression and suppression. Upregulation of CEACAM1 is observed in many cancers like colon, breast, prostate, and non-small cell lung cancer, and increased CEACAM1 expression correlates with higher tumor stage, metastasis, and poor prognosis

(Danker et al., 2017). CEACAM1 promotes tumor angiogenesis by disrupting endothelial cell-cell junctions and enhancing vascular permeability (Horst et al., 2009). It also facilitates immune evasion by inhibiting tumor-killing by NK cells and cytotoxic T cells (Markel et al., 2009). However, CEACAM1 can also have tumor suppressive effects by inducing anoikis and impairing anchor-

age-independent growth (Benchimol et al., 1989). This dual role makes CEACAM1 an attractive cancer target, as inhibition could simultaneously block tumor angiogenesis and immune evasion while enhancing anoikis. Indeed, anti-CEACAM1 monoclonal antibodies enhance anti-tumor immunity and inhibit metastasis in preclinical models (Danker et al., 2017).

Figure 1. NK cells activated by CEACAM1 (top). CEACAM1 expressed by NK cells reduces the NK cells' ability to kill tumor cells (bottom). Figure obtained from (Helfrich et al., 2019)



Literature review:

Park and coauthors observed in hepatocellular carcinoma (HCC), CEACAM1 is a promising target due to its role in regulating immune cell functions. CEACAM1 expression is significantly upregulated in EpCAM+ cancer stem cells, which are typically resistant to NK cell-mediated cytotoxicity. Targeting CEACAM1 in these cells has shown potential to enhance NK cell effectiveness, showing that blocking CEACAM1 in EpCAM-high HCC cells increases NK cell degranulation and cytotoxicity. Moreover, the knock-down of CEACAM1 using shRNA has been found to reduce its expression, therefore improving the susceptibility of tumor cells to immune-mediated killing (Park et al., 2020).

Tsang and coauthors have developed a monoclonal antibody named NEO-201, which

specifically binds to CEACAM-5, a glycoprotein often overexpressed in various carcinomas including colorectal, gastric, pancreatic, non-small cell lung, and breast cancers. The binding of NEO-201 to CEACAM-5 inhibits its interaction with CEACAM-1, another cell adhesion molecule found on NK cells. This inhibition is significant because the CEACAM-5/CEACAM-1 interaction typically suppresses the cytotoxic activity of NK cells against tumor cells. By blocking this interaction, NEO-201 can potentially restore and enhance the ability of NK cells to kill tumor cells. Moreover, NEO-201 exhibits direct anti-tumor activity through mechanisms such as antibody-dependent cell-mediated cytotoxicity (ADCC) and complement-dependent cytotoxicity (CDC). These processes involve the recruitment of immune cells and the activation of the complement

system to target and destroy tumor cells expressing CEACAM-5 (Tsang et al., 2022).

These findings suggest that CEACAM1-targeted therapies could potentially boost the body's anti-tumor immune response by modulating the interactions between CEACAM1 and immune cells, such as CD8+ T-cells and NK cells. By enhancing the cytotoxic activity of these immune cells and overcoming cancer stem cell-mediated resistance, CEACAM1-targeted approaches improve the efficacy of existing cancer treatments. However, the studies discussed previously are focused on specific cancer types (melanoma and HCC), and further research is needed to understand the broader applicability of CEACAM1-targeted therapies across different cancer types and in combination with other therapies.

Methodologies:

Analysis of Binding Sites in CEACAM1:

Geometric method:

1. Open chrome browser
2. Enter the link <https://proteins.plus/> in the browser and enter
3. Type in the PDB-Code 5DZL
4. Click "Go!"
5. Click "DoGSiteScorer Binding site detection"
6. Click "DoGSiteScorer"
7. Click "Calculate"
8. Click on the eye icon in the second column to visualize the binding sites

Energetic-based method:

1. Open chrome browser
2. Enter the link <https://ftsites.bu.edu/> in the browser and enter
3. Enter job name
4. Type in the PDB-Code 5DZL
5. Type in the email address
6. Click "Find My Binding Site"
7. Wait for the job complete email
8. Download the attachment in the email
9. Click on the link in the email
10. Click "Finish"

Machine learning method:

1. Open chrome browser
2. Enter the link <https://prankweb.cz/> in the browser and enter
3. Type in the PDB-Code 5DZL
4. Click "Submit"

Obtaining compounds that binds to CEACAM1

Virtual Screening

1. Open chrome browser
2. Enter the link <http://pocketquery.csb.pitt.edu/> in the browser and enter
3. Click "Search"
4. Enter PDB ID7RQR4
5. Click "Search"
6. Choose cluster in B chain with a score closest to 1.0
7. Click "Export"
8. Click "Send to ZINCPharmer"
9. Go to the viewer tab
10. Unselect "Ligand" and "Receptor Residues"
11. If less than 3 pharmacophore visible, choose a different cluster
12. Click "Submit Query"
13. If no matches found, unselect one of the pharmacophore that is the furthest away from the rest in the pharmacophore tab and click "Submit Query" again
14. Choose the compounds with RMSD closest to 0.0
15. Repeat until 20 compounds chosen

Quantifying the energy between the interaction of compounds obtained and CEACAM1

Molecular Docking

1. Open chrome browser
2. Enter the link <https://zinc12.docking.org/> in the browser and enter
3. Paste in one of the ZINC id from experiment 3.2.1. in the "Quick Search" bar and click "Go"
4. Copy the SMILES formate
5. Open another tab
6. Enter the link <https://datascience.unm.edu/tomcat/biocomp/convert> in the browser and enter
7. Under "Input" in the "Format" section, select "smiles – SMILES"
8. Under "Output" in the "Format" section, select "mol2 – Tripos mol2"
9. Under "Output" in the "generic" section, select "+3D"
10. Paste the SMILES format from step 4 in the box under "Input"
11. Click "Go Convert"
12. Click "download convert_out.mol2"
13. Rename the file into the ZINC id
14. Open another tab

15. Enter the link <http://old.swissdock.ch/docking> in the browser and enter
16. Under “Target selection” click “upload file”
17. Click “Choose file”
18. Upload file with PDB code of 5DZL
19. Under “Ligand selection” click ‘upload file”
20. Click “Choose file”
21. Choose the file renamed in step 13
22. Make sure it says “Successful setup” under both “Target selection” and “ligand selection”
23. Enter job name
24. Enter email
25. Click “Start Docking”
26. Wait for Job Terminated email
27. Click on the link attached in the Job Terminated email
28. Find the highest estimated ΔG
29. Repeat for 20 compounds and select 5 with the highest estimated ΔG compared to others for the next experiment

Drug properties

SwissADME

1. Collect and copy the SMILES code of the compound selected in 3.3.1.
2. Open Firefox browser
3. Enter the link <http://www.swissadme.ch/> and enter
4. Paste in the SMILES formate in the box
5. Press “Run!” and wait for results

Toxicity prediction

ProTox 3.0

1. Select the compound from experiment 3.4.1. that had no violations in Lipinski’s rule of 5
2. Open Firefox browser
3. Enter the link <https://tox.charite.de/protox3/index.php?site=home#> and enter
4. Click on the box with orange borders titled “Tox Prediction”
5. Paste in the SMILES format of compound selected in the “Canonical Smiles” section
6. Click on “smiles”
7. Scroll down to select models to predict, click “all”
8. Click “Start Tox-Prediction”

Results and Discussion:

Analysis of Binding Sites in CEACAM1:

Geometric method:

Using the geometric method, ProteinPlus identified ten potential binding sites in CEACAM1. The most promising site, P_0, displayed the largest volume (1177.38 Å³) and surface area (1364.93 Å²), coupled with the highest drug score (0.78) and simple score (0.62), which may suggest its suitability for drug binding. Other promising sites include P_1 and P_2, which also had relatively high volumes and scores, suggesting they could be viable targets as well. However, sites like P_4 through P_9 had significantly lower scores and smaller volumes, making them less favorable for drug binding. The results indicate there are many binding sites in CEACAM1, therefore making it a very promising drug target.

Figure 2. 10 possible binding sites in CEACAM 1(PDB code: 5DZL) detected by ProteinPlus based on size

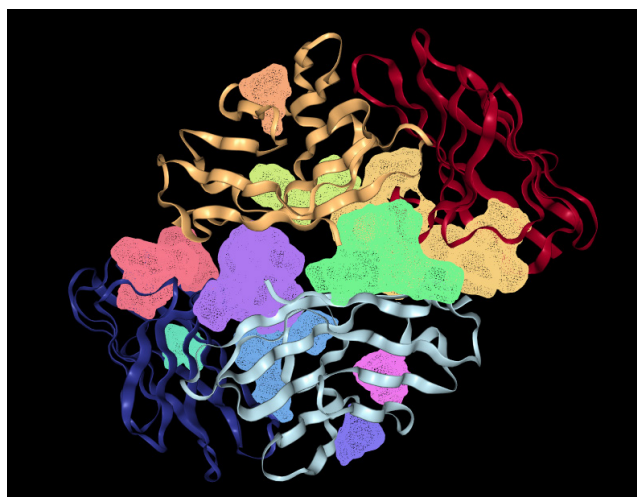
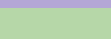
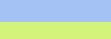
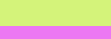


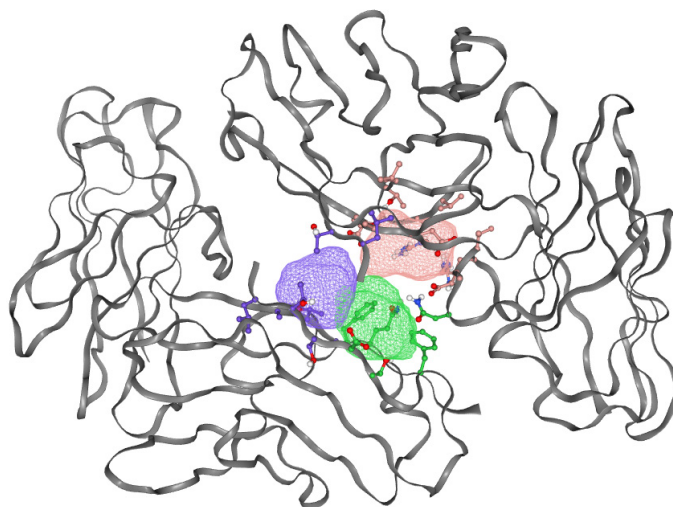
Table 1. Binding sites predicted by ProteinPlus in CEACAM1(PDB code: 5DZL).

Color	Name	Volume(Å ³)	Surface Area(Å ²)	Drug Score	Simple Score
	P_0	1177.38	1364.93	0.78	0.62
	P_1	953.32	1102.57	0.76	0.59
	P_2	709.25	919.7	0.72	0.49
	P_3	477.3	609.26	0.64	0.27
	P_4	349.02	549.5	0.46	0.12
	P_5	202.01	496.25	0.42	0.01
	P_6	170.04	286.83	0.3	0.0
	P_7	117.07	152.53	0.38	0.0
	P_8	110.63	273.66	0.27	0.0
	P_9	100.55	212.03	0.2	0.0

Energetic-based method:

Using an energetic-based method, FT Site detected 3 possible binding sites on CEACAM1. This method assesses binding affinity or energy between a molecule and a target site. FT Site can calculate and predict

the interaction energy based on the physical and chemical properties of the molecules involved. The results suggest that 3 binding sites have enough energy to successfully allow molecules to bind to, which further confirmed CEACAM1 is a promising drug target.

Figure 3. 3 possible binding sites in CEACAM 1(PDB code: 5DZL) detected by FT Site based on energetic-based method*Machine learning method:*

Using a machine learning method, Prankweb detected 3 possible binding sites for CEACAM1. The most promising binding site, coloured red and ranked 1, has a score of 4.04 and 11 residues. This means through analyzed data and predictions made based on patterns and statistical models, the red binding site predicted binding affinity is the highest. Furthermore, 11 residues suggests that there is a large area for potential interactions. Yellow and orange binding sites are

ranked 2 and 3 respectively, with a score 2.27 and 1.09. These are both decent scores which conveys of them being a promising target. In this method, the promising targets found are more spread out around the sides of CEACAM1. However, in the energetic-based method, the promising targets are found close to the center of CEACAM1. This shows the large variety of binding sites in CEACAM1, which suggests that it will be a highly promising target.

Figure 4. 3 possible binding sites in CEACAM 1(PDB code: 5DZL) detected by Prankweb based on machine learning method

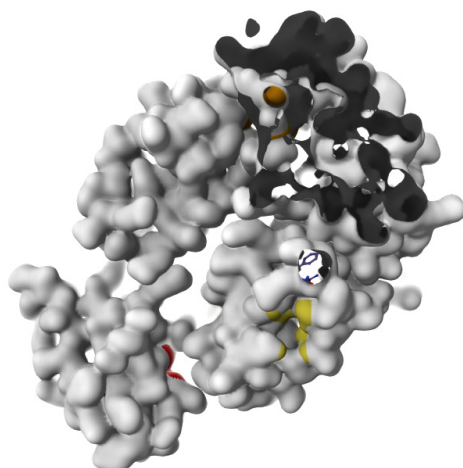


Table 2. Binding sites detected by Prankweb in CEACAM 1 (PDB code: 5DZL)

Color	Rank	Score	# of residues
	1	4.04	11
	2	2.27	8
	3	1.09	7

Virtual Screening:

By analyzing the interaction between CEACAM1 and HopQ (PDB ID: 7RQR4), PocketQuery identified key amino acid residues involved in their binding. It finds four distinct clusters of interactions, each with a high score (ranging from 0.819305 to 0.848688), indicating strong binding affinities. There are many different amino acids

present in these clusters, with some residues appearing in multiple clusters. Notably, LEU150 and VAL156 are present in three out of four clusters, suggesting they may play a role in the CEACAM1/HopQ interaction. THR appears in both clusters 1 and 2, while MET240 is found in clusters 2 and 4. This overlap indicates that certain amino acids contribute to multiple binding sites.

Figure 5. Visual representation of the 4 clusters of the CEACAM1 interaction with HopQ (PDB ID: 7RQR4) using Pocket Query

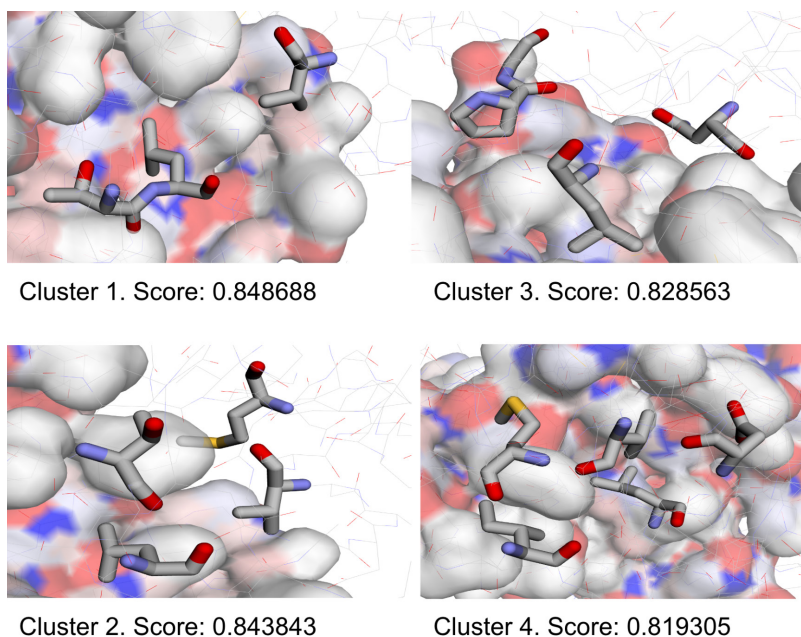
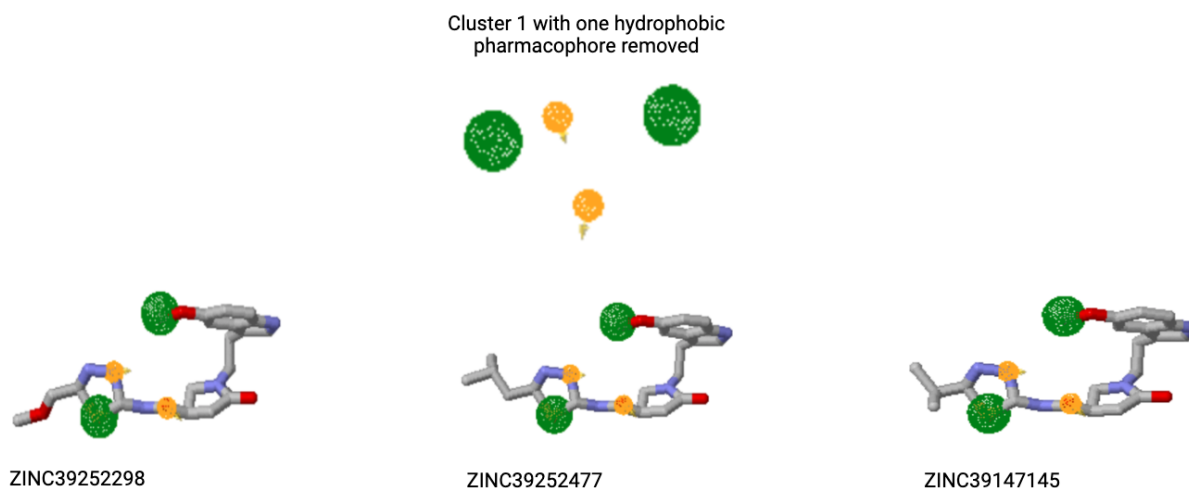


Table 3. The amino acids involved in the pharmacophore maps for CEACAM1/HopQ interaction(PDB ID: 7RQR4) found by Pocket Query

Cluster Number	Residues	#
1	THR	149
1	LEU	150
1	VAL	156
2	THR	147
2	LEU	150
2	VAL	156
2	MET	240
3	PRO	110
3	GLY	111
3	ASN	145
3	LEU	150
4	ILE	102
4	LEU	150
4	ASP	153
4	VAL	156
4	MET	240

This part of the experiment identified potential CEACAM1 hits across four distinct clusters using ZincPharmer. Cluster 1 compounds (ZINC39252298, ZINC39252477, ZINC39147145, ZINC39147149, ZINC39252325) all showed consistent RMSD values of 0.151 and masses ranging from 432–448 Da. Cluster 2 compounds (ZINC95379969, ZINC41591046, ZINC81530427, ZINC89851740, ZINC38617077) exhibited the lowest RMSD values (0.002–0.003) and lower masses (343–389 Da), indicating they most closely match the target pharmacophore and may have favorable drug-like proper-

ties. Cluster 3 compounds (ZINC67902861, ZINC71788521, ZINC80694653, ZINC80695211, ZINC08376405) showed intermediate RMSD values (0.047–0.067) and a wide mass range (332–653 Da). Cluster 4 compounds (ZINC08449618, ZINC36047021, ZINC36047023, ZINC08820313, ZINC08449640) had the highest RMSD values (0.152–0.199) and relatively high masses (478–592 Da). The outcome suggests that Cluster 2 compounds, particularly ZINC95379969 and ZINC41591046, are the most promising leads for CEACAM1 inhibition due to their fit to the pharmacophore model.

Figure 6. Top compounds as potential CEACAM1 hits with the lowest RMSD from each cluster selected using ZINCPharmer

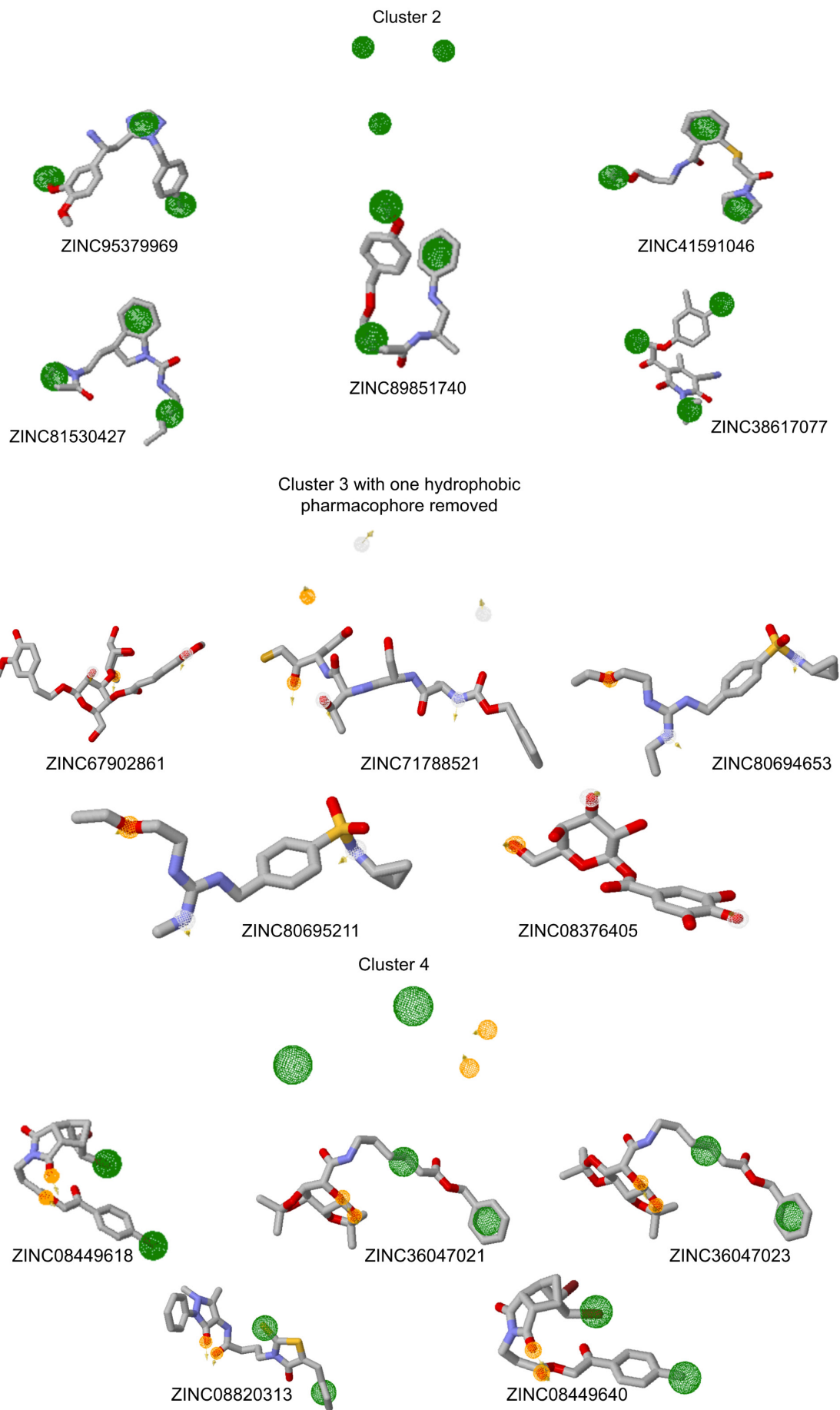


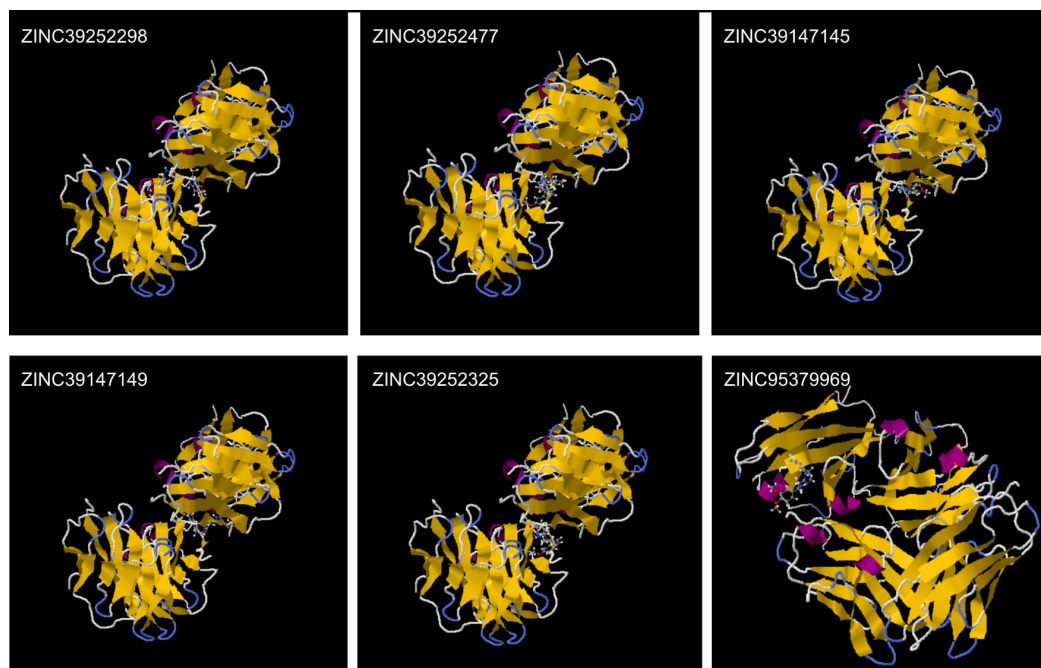
Table 4. Top 20 potential CEACAM1 hits with the lowest RMSD from each cluster using ZINCPharmer

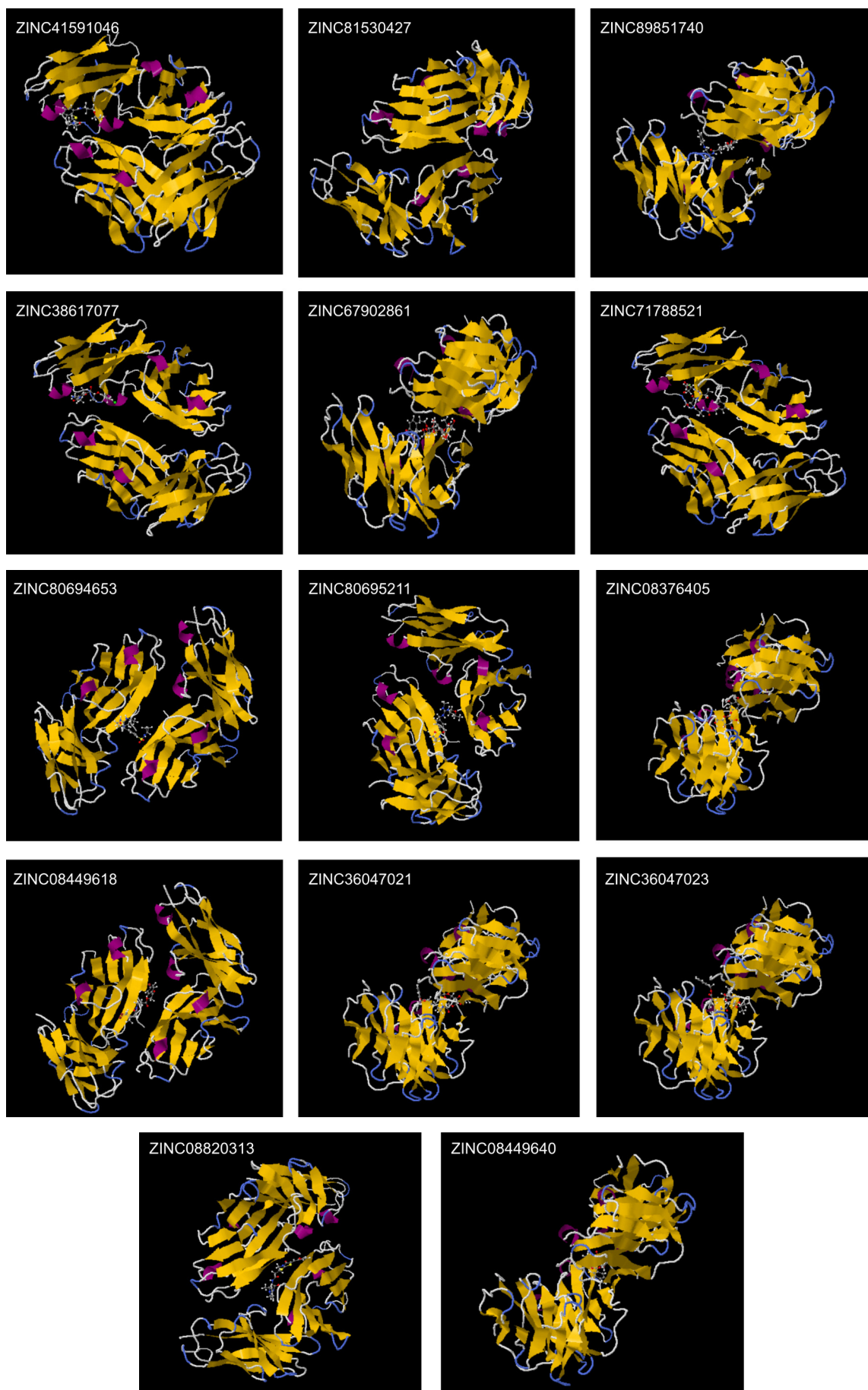
Cluster Number	Name	RMSD	Mass
1	ZINC39252298	0.151	434
1	ZINC39252477	0.151	446
1	ZINC39147145	0.151	432
1	ZINC39147149	0.151	446
1	ZINC39252325	0.151	448
2	ZINC95379969	0.002	353
2	ZINC41591046	0.002	350
2	ZINC81530427	0.003	343
2	ZINC89851740	0.003	356
2	ZINC38617077	0.003	389
3	ZINC67902861	0.047	653
3	ZINC71788521	0.047	542
3	ZINC80694653	0.062	370
3	ZINC80695211	0.062	355
3	ZINC08376405	0.067	332
4	ZINC08449618	0.152	592
4	ZINC36047021	0.179	478
4	ZINC36047023	0.181	478
4	ZINC08820313	0.191	483
4	ZINC08449640	0.199	527

Molecular Docking:

This experiment found the estimated binding energies (ΔG) between CEACAM1 and other compounds, aiming to identify

suitable drug candidates. The top 5 compounds with the most favorable (most negative) estimated ΔG values are highlighted in yellow:

Figure 7. Quantifying the energy between CEACAM1 and compounds, therefore choosing suitable drug candidates



ZINC71788521 (Cluster number 3): -10.90 kcal/mol
 ZINC67902861 (Cluster number 3): -10.00 kcal/mol
 ZINC08820313 (Cluster number 4): -9.97 kcal/mol
 ZINC38617077 (Cluster number 2): -9.89 kcal/mol

ZINC41591046 (Cluster number 2): -9.39 kcal/mol

These compounds show the strongest predicted binding to CEACAM1, with ZINC71788521 exhibiting the most favorable interaction.

Table 5. Quantifying the energy between CEACAM1 and compounds, therefore choosing suitable drug candidates (top 5 estimated ΔG highlighted in yellow)

ZINC id	Cluster	Estimated ΔG (kcal/mol)
ZINC39252298	15	-8.47
ZINC39252477	1	-8.55
ZINC39147145	6	-8.77
ZINC39147149	9	-8.26
ZINC39252325	7	-8.75
ZINC95379969	19	-9.0
ZINC41591046	1	-9.39
ZINC81530427	0	-8.03
ZINC89851740	4	-8.50
ZINC38617077	0	-9.89
ZINC67902861	1	-10.00
ZINC71788521	9	-10.90
ZINC80694653	26	-9.19
ZINC80695211	5	-9.24
ZINC08376405	8	-8.04
ZINC08449618	18	-8.50
ZINC36047021	16	-8.51
ZINC36047023	28	-8.49
ZINC08820313	2	-9.97
ZINC08449640	2	-7.94

Drug Properties:

This experiment shows the drug properties of the top 5 drug candidates selected for this experiment. The first two candidates (ZINC71788521 and ZINC67902861) violate Lipinski's rule of 5. The violations are due to their high number of H-bond acceptors (11 and 15 respectively) and molecular weights exceeding 500 g/mol. The remaining three candidates (ZINC08820313,

ZINC38617077, and ZINC41591046) comply with Lipinski's rule, having 0 violations, and are classified as drug-like. In conclusion, while the top two candidates show promising target affinity (as implied by their ranking), their drug-like properties are less ideal. The other three candidates offer better drug-like characteristics, making them possibly more suitable for further development.

Table 6. Inspecting the drug properties of the top 5 drug candidates chosen (violations of Lipinski's rule of 5 is highlighted in red)

ZINC id	Num. H-bond acceptors	Num. H-bond donors	Molecular weight g/mol	iLOGP	Num of violations	Druglike-ness
ZINC71788521	11	6	541.50	0.68	3	No
ZINC67902861	15	7	652.64	3.12	3	No
ZINC08820313	4	1	482.58	3.27	0	Yes
ZINC38617077	5	0	387.84	2.89	0	Yes
ZINC41591046	3	1	350.48	3.44	0	Yes

Toxicity Prediction:

In experiment 3.5.1., ZINC08820313 was selected for toxicity assessment using ProTox 3.0 due to its high ΔG . The results show a relatively low predicted LD50(3000 mg/kg) and a high toxicity class(5), which are favorable attributes for drug development. In figure 4.5.1, most probabilities for toxic activity are below the average active molecule thresh-

olds, indicating that ZINC08820313 shows little toxic behavior. Although the respiratory toxicity probability is slightly above average, it remains within acceptable limits. Furthermore, as shown in table 4.5.2 and figure 4.5.2, the compound demonstrates a low number of active/toxic sites. This shows the potential of ZINC08820313 as a viable drug candidate with manageable toxicity risks.

Table 7. Summary of toxicity of selected compound(ZINC08820313) using ProTox 3.0

Predicted LD50(mg/kg)	Predicted toxicity class
3000	5

Table 8. Detailing active and inactive parts of ZINC08820313 to measure toxicity (with active parts highlighted in red)

Classification	Target	Shorthand	Prediction
Organ toxicity	Hepatotoxicity	dili	Active
Organ toxicity	Neurotoxicity	neuro	Active
Organ toxicity	Nephrotoxicity	nephro	Inactive
Organ toxicity	Respiratory toxicity	respi	Active
Organ toxicity	Cardiotoxicity	cardio	Inactive
Toxicity end points	Carcinogenicity	carcino	Active
Toxicity end points	Immunotoxicity	immuno	Inactive
Toxicity end points	Mutagenicity	mutagen	Inactive
Toxicity end points	Cytotoxicity	cyto	Inactive
Toxicity end points	BBB-barrier	bbb	Active
Toxicity end points	Ecotoxicity	eco	Active
Toxicity end points	Clinical toxicity	clinical	Active
Toxicity end points	Nutritional toxicity	nutri	Inactive
Tox21-Nuclear receptor signalling pathways	Aryl hydrocarbon Receptor (AhR)	nr_ahr	Inactive
Tox21-Nuclear receptor signalling pathways	Androgen Receptor (AR)	nr_ar	Inactive

Classification	Target	Shorthand	Prediction
Tox21-Nuclear receptor signalling pathways	Androgen Receptor Ligand Binding Domain (AR-LBD)	nr_ar_lbd	Inactive
Tox21-Nuclear receptor signalling pathways	Aromatase	nr_aromatase	Inactive
Tox21-Nuclear receptor signalling pathways	Estrogen Receptor Alpha (ER)	nr_er	Inactive
Tox21-Nuclear receptor signalling pathways	Estrogen Receptor Ligand Binding Domain (ER-LBD)	nr_er_lbd	Inactive
Tox21-Nuclear receptor signalling pathways	Peroxisome Proliferator Activated Receptor Gamma (PPAR-Gamma)	nr_ppar_gamma	Inactive
Tox21-Stress response pathways	Nuclear factor (erythroid-derived 2)-like 2/antioxidant responsive element (nrf2/ARE)	sr_are	Inactive
Tox21-Stress response pathways	Heat shock factor response element (HSE)	sr_hse	Inactive
Tox21-Stress response pathways	Mitochondrial Membrane Potential (MMP)	sr_mmp	Inactive
Tox21-Stress response pathways	Phosphoprotein (Tumor Suppressor) p53	sr_p53	Inactive
Tox21-Stress response pathways	ATPase family AAA domain-containing protein 5 (ATAD5)	sr_atad5	Inactive
Molecular Initiating Events	Thyroid hormone receptor alpha (THR α)	mie_thr_alpha	Inactive
Molecular Initiating Events	Thyroid hormone receptor beta (THR β)	mie_thr_beta	Inactive
Molecular Initiating Events	Transthyretin (TTR)	mie_ttr	Inactive
Molecular Initiating Events	Ryanodine receptor (RYR)	mie_ryr	Inactive
Molecular Initiating Events	GABA receptor (GABAR)	mie_gabar	Inactive
Molecular Initiating Events	Glutamate N-methyl-D-aspartate receptor (NMDAR)	mie_nmdar	Inactive
Molecular Initiating Events	alpha-amino-3-hydroxy-5-methyl-4-isoxazole-propionate receptor (AMPA)	mie_ampar	Inactive
Molecular Initiating Events	Kainate receptor (KAR)	mie_kar	Inactive
Molecular Initiating Events	Achetylcholinesterase (AChE)	mie_ache	Inactive
Molecular Initiating Events	Constitutive androstane receptor (CAR)	mie_car	Inactive
Molecular Initiating Events	Pregnane X receptor (PXR)	mie_pxr	Inactive

Classification	Target	Shorthand	Prediction
Molecular Initiating Events	NADH-quinone oxidoreductase (NADHOX)	mie_nadhox	Inactive
Molecular Initiating Events	Voltage gated sodium channel (VGSC)	mie_vgsc	Inactive
Molecular Initiating Events	Na ⁺ /I ⁻ symporter (NIS)	mie_nis	Inactive
Metabolism	Cytochrome CYP1A2	CYP1A2	Inactive
Metabolism	Cytochrome CYP2C19	CYP2C19	Inactive
Metabolism	Cytochrome CYP2C9	CYP2C9	Inactive
Metabolism	Cytochrome CYP2D6	CYP2D6	Inactive
Metabolism	Cytochrome CYP3A4	CYP3A4	Inactive
Metabolism	Cytochrome CYP2E1	CYP2E1	Inactive

Figure 8. Toxicity radar chart comparing the probabilities for activity in ZINC08820313 and average active molecules

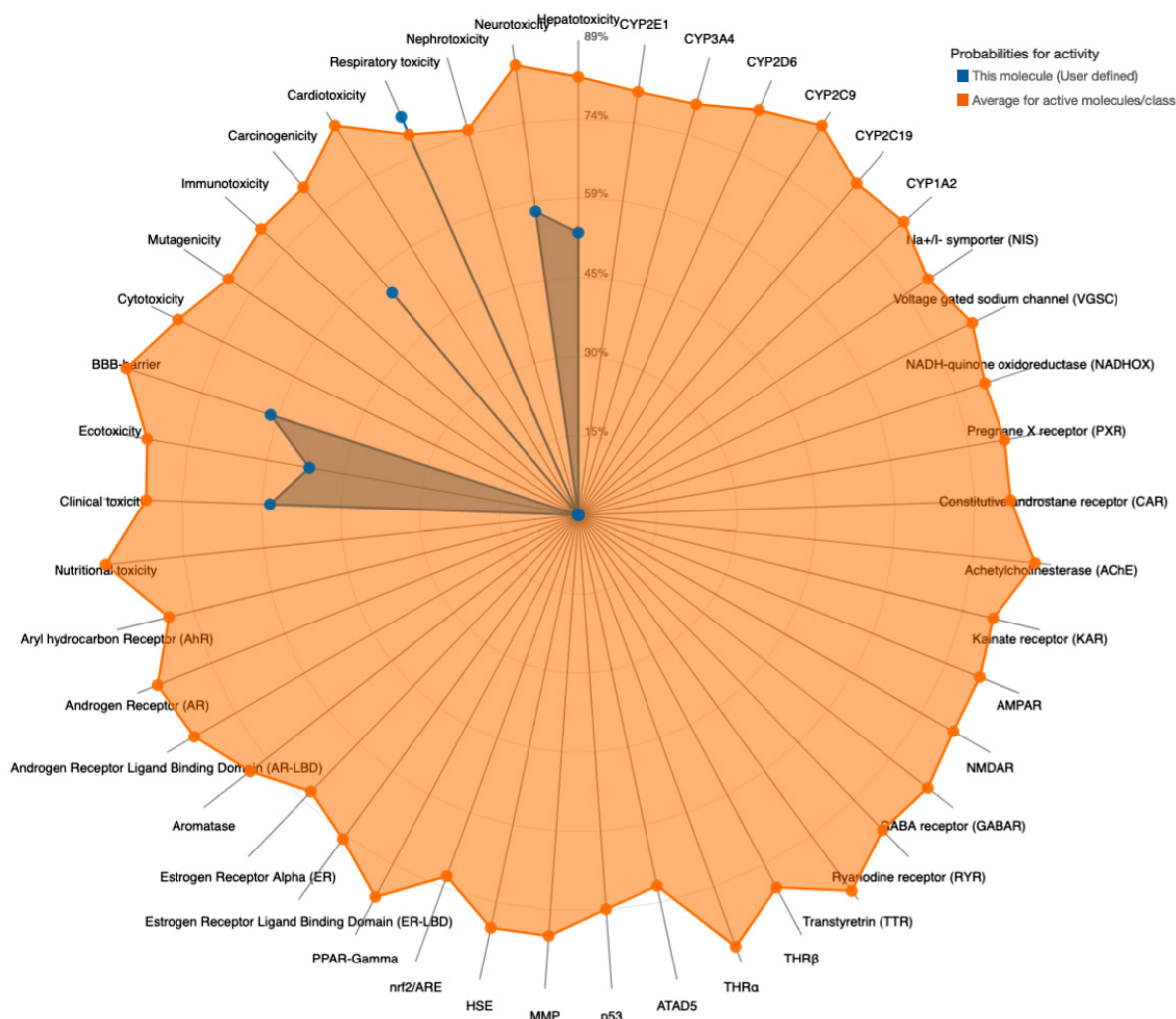
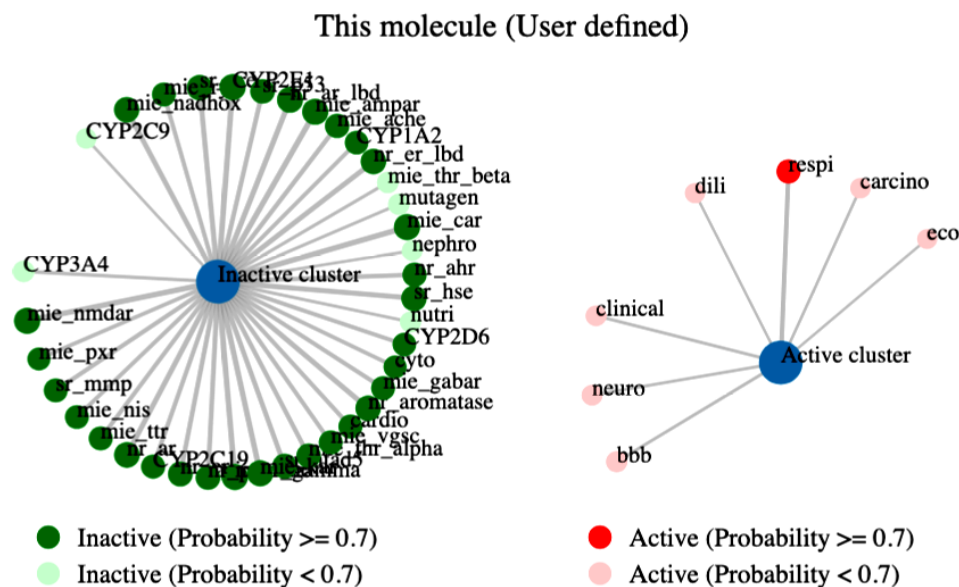


Figure 9. Network chart visually illustrating the active and inactive parts of ZINC08820313



5. Conclusion:

This study successfully identified several promising drug candidates targeting CEACAM1 through an extensive computational screening process. The primary objectives of this research were to identify compounds with high binding affinity for CEACAM1 and to evaluate their drug-like properties and toxicity profiles. The compounds ZINC71788521 and ZINC67902861, while initially promising due to their strong target affinities, were found to violate Lipinski's rules, thus making them not suitable as drug candidates. In contrast, ZINC08820313, ZINC38617077, and ZINC41591046 demonstrated strong binding potential and adhered to the pharmacokinetic properties outlined by Lipinski. After comparing toxicity and estimated ΔG values, ZINC08820313 was selected as the final drug candidate. By targeting an immune checkpoint molecule, the drug candidate offers an approach to overcoming immune evasion by cancer cells, potentially improving patient outcomes in cancer therapy. The drug-like properties of the identified compound suggest its potential for clinical application. With further development and testing, it could be integrated into existing cancer treatment regimens, allowing different combination therapies with immunotherapy targeting CEACAM1.

In the future, focus will be on conducting in vitro experiments to verify the binding affini-

ties of ZINC08820313 with CEACAM1. These experiments will help establish the efficacy of these compounds in a controlled biological environment. If successful in vitro validation, in vivo studies are necessary to evaluate the pharmacokinetics, bioavailability, and therapeutic efficacy of the identified compounds in animal models. Later, if in vivo experiment successes, clinical trials should be conducted, which could lead to the development of more comprehensive and effective cancer treatment protocols. While the study presents promising candidates for cancer immunotherapy, it is important to acknowledge certain limitations. First, this study relies heavily on computational methods for initial screening and evaluation. Although these methods provide valuable insights, experimental validation is essential to confirm the accuracy and applicability of the predictions. Secondly, cancer is a multifaceted disease, and targeting a single molecule may not be sufficient for effective treatment in all cases. A multi-target approach or combination therapies may be necessary to address the diverse mechanisms of cancer progression and immune evasion.

In conclusion, this research has laid a solid foundation for the development of CEACAM1-targeted therapies in cancer immunotherapy. The identification of ZINC08820313 as a promising drug candidate highlights the potential of targeting immune checkpoints to enhance the body's natural defense against

cancer. By continuing to explore innovative therapeutic strategies, the aim is to contribute to the ongoing efforts in developing more

effective and less toxic cancer treatments, ultimately improving the quality of life for cancer patients worldwide.

References

- Alsaab, H. O., Sau, S., Alzhrani, R., Tatiparti, K., Bhise, K., Kashaw, S. K., & Iyer, A. K. (2017). PD-1 and PD-L1 Checkpoint Signaling Inhibition for Cancer Immunotherapy: Mechanism, Combinations, and Clinical Outcome. *Frontiers in Pharmacology*, – 8(561).
- Benchimol, S., Fuks, A., Jothy, S., Beauchemin, N., Shiota, K., & Stanners, C. P. (1989). Carcinoembryonic antigen, a human tumor marker, functions as an intercellular adhesion molecule. *Cell*, – 57(2), 327–334.
- Brümmer, J., Ebrahimnejad, A., Flayeh, R., Schumacher, U., Löning, T., Bamberger, A. M., & Wagener, C. (2001). cis Interaction of the cell adhesion molecule CEACAM1 with integrin beta(3). *The American journal of pathology*, – 159(2), 537–546.
- Buchbinder, E. I., & Desai, A. (2016). CTLA-4 and PD-1 Pathways: Similarities, Differences, and Implications of Their Inhibition. *American journal of clinical oncology*, – 39(1), 98–106.
- Cancer Research UK. (2023, October 28). Types of Cancer. Cancer Research UK. Assessed on June 24th 2024. Retrieved from URL: <https://www.cancerresearchuk.org/about-cancer/what-is-cancer/how-cancer-starts/types-of-cancer>
- Chaitanya Thandra, K., Barsouk, A., Saginala, K., Sukumar Aluru, J., & Barsouk, A. (2021). Epidemiology of lung cancer. *Współczesna Onkologia*, – 25(1), 45–52.
- Dankner, M., Gray-Owen, S. D., Huang, Y. H., Blumberg, R. S., & Beauchemin, N. (2017). CEACAM1 as a multi-purpose target for cancer immunotherapy. *Oncoimmunology*, – 6(7), e1328336.
- Darvin, P., Toor, S. M., Sasidharan Nair, V., & Elkord, E. (2018). Immune checkpoint inhibitors: recent progress and potential biomarkers. *Experimental & molecular medicine*, – 50(12), 1–11.
- Helfrich, I., & Singer, B. B. (2019). Size Matters: The Functional Role of the CEACAM1 Isoform Signature and Its Impact for NK Cell-Mediated Killing in Melanoma. *Cancers*, – 11(3), 356.
- Hodi, F. S., O'Day, S. J., McDermott, D. F., Weber, R. W., Sosman, J. A., Haanen, J. B., Gonzalez, R., Robert, C., Schadendorf, D., Hassel, J. C., Akerley, W., van den Eertwegh, A. J., Lutzky, J., Lorigan, P., Vaubel, J. M., Linette, G. P., Hogg, D., Ottensmeier, C. H., Lebbé, C., Peschel, C., ... Urba, W. J. (2010). Improved survival with ipilimumab in patients with metastatic melanoma. *The New England journal of medicine*, – 363(8), 711–723.
- Horst, A. K., Bickert, T., Brewig, N., Ludewig, P., van Rooijen, N., Schumacher, U., Beauchemin, N., Ito, W. D., Fleischer, B., Wagener, C., & Ritter, U. (2009). CEACAM1+ myeloid cells control angiogenesis in inflammation. *Blood*, – 113(26), 6726–6736.
- Kim, W. M., Huang, Y.-H., Gandhi, A., & Blumberg, R. S. (2019). CEACAM1 structure and function in immunity and its therapeutic implications. *Seminars in Immunology*, – 42, 101296.
- Klaile, E., Vorontsova, O., Sigmundsson, K., Müller, M. M., Singer, B. B., Ofverstedt, L. G., Svensson, S., Skoglund, U., & Obrink, B. (2009). The CEACAM1 N-terminal Ig domain mediates cis- and trans-binding and is essential for allosteric rearrangements of CEACAM1 microclusters. *The Journal of cell biology*, – 187(4), 553–567.
- Markel, G., Seidman, R., Cohen, Y., Besser, M. J., Sinai, T. C., Treves, A. J., Orenstein, A., Berger, R., & Schachter, J. (2009). Dynamic expression of protective CEACAM1 on melanoma cells during specific immune attack. *Immunology*, – 126(2), 186–200.
- Nagaishi, T., Chen, Z., Chen, L., Iijima, H., Nakajima, A., & Blumberg, R. S. (2008). CEACAM1 and the regulation of mucosal inflammation. *Mucosal Immunology*, – 1(1), S39–S42.
- National Cancer Institute. (2018). Cancer of the Lung and Bronchus – Cancer Stat Facts. National Cancer Institute. Accessed on June 18th 2024. Retrieved from URL: – <https://seer.cancer.gov/statfacts/html/lungb.html>
- Park, D. J., Sung, P. S., Kim, J. H., Lee, G. W., Jang, J. W., Jung, E. S., Bae, S. H., Choi, J. Y., & Yoon, S. K. (2020). EpCAM-high liver cancer stem cells resist natural killer cell-mediated

- ed cytotoxicity by upregulating CEACAM1. *Journal for immunotherapy of cancer*, – 8(1), e000301.
- Pauken, K. E., & Wherry, E. J. (2015). Overcoming T cell exhaustion in infection and cancer. *Trends in immunology*, – 36(4), 265–276.
- Tsang, K. Y., Fantini, M., Mavroukakis, S. A., Zaki, A., Annunziata, C. M., & Arlen, P. M. (2022). Development and Characterization of an Anti-Cancer Monoclonal Antibody for Treatment of Human Carcinomas. *Cancers*, – 14(13), 3037.
- Turcu, G., Nedelcu, R. I., Ion, D. A., Brînzea, A., Cioplea, M. D., Jilaveanu, L. B., & Zurac, S. A. (2016). CEACAM1: Expression and Role in Melanocyte Transformation. *Disease markers*, 2016, – 9406319.
- Zappasodi, R., Merghoub, T., & Wolchok, J. D. (2018). Emerging Concepts for Immune Checkpoint Blockade-Based Combination Therapies. *Cancer Cell*, 34(4), 690.
- Zhang, Y., & Zhang, Z. (2020). The history and advances in cancer immunotherapy: understanding the characteristics of tumor-infiltrating immune cells and their therapeutic implications. *Cellular & Molecular Immunology*, – 17(8), 1–15.

submitted 12.09.2024;
accepted for publication 29.09.2024;
published 29.10.2024
© Guanrong (Rain) Cheng
Contact: raincheng08@gmail.com



Section 3. Life sciences

DOI:10.29013/EJBLS-24-3-39-45



A REVIEW OF HARP THERAPY AND GENDER DEMOGRAPHICS ANALYSIS IN PUBLISHED STUDIES

*Yimiao Zou*¹

¹ Henry Gunn High School, United States

Cite: Yimiao Zou. (2024). A Review of Harp Therapy and Gender Demographics Analysis in Published Studies. *The European Journal of Biomedical and Life Sciences* 2024, No 3 <https://doi.org/10.29013/EJBLS-24-3-39-45>

Abstract

Harp therapy has been proven to help patients with pain and stress relief, the improvement of the pregnancy rate of reproductive medicine, the weight gain in newborns, and the palliative care for the terminally ill or dying ones. This article reviewed the application field of harp therapy, the music utilized during treatment, and the available training programs for harp therapy. Furthermore, the gender demographics of published studies were analyzed. The psychophysiological responses from different genders need to be investigated in future studies.

Keywords: Harp Therapy, Music Therapy, Gender Difference, Sex Bias, Pain and Stress

Introduction

Vibroacoustic therapy (VAT) was developed in Norway by Dr. Olav Skille in the 1980s (SKILLE, 1989). The vibration at low-frequency tones (30 Hz to 120 Hz) that penetrates the body was combined with music for therapy, which could massage both the body and the soul (Williams, 2005a). Dr. Skille observed the positive effects of VAT on 24 patients' symptoms, including Rett syndrome, Autism, Spastic conditions, etc (SKILLE, 1989). Found as early as 3500 BCE in Sumer (Galpin, 1929), harp instruments have strings that vibrate and penetrate the body, the pitches at varying frequencies could be felt by different parts of the body (Williams, 2005b). In 1990, vibroacoustic harp therapy (VAHT) was

begun with the combined use of an acoustic harp and a Genesis™ vibrotactile unit located in a chronic pain center (Williams, 2005 b). Dr. Sarajane did a tremendous amount of fundamental work in VAHT.

There are a few reports about the clinical study of harp therapy. In this paper, we reviewed the application of harp therapy, the harp music for treatment, and the training programs of the harp therapist. Additionally, the gender demographics of the published studies were analyzed.

Review of harp therapy *Application of harp therapy*

Harp therapy has been helping patients before and post-surgery, emergent medical

care, traumatic illness center, intensive care unit (ICU), reproductive medicine center, neonatal intensive care unit, department of pediatrics, and the terminally ill or dying ones.

Daleen Aragon and the coauthors applied harp therapy to Orlando Regional Medical Center patients in 2001. They proved that slow, soft, melodies of live harp music produced statistically significant differences in physiological measures of systolic blood pressure and oxygen saturation with a positive effect on patient perception of anxiety, pain, and satisfaction (Aragon, 2002). Studies from K. Sand-Jecklin and H. Emerson in 2010 showed that patients reported significant reductions in pain, anxiety, muscle tension, respiration rate, and systolic blood pressure (Sand-Jecklin, 2010).

Other studies demonstrated that harp music could help reduce preoperative pressure and anxiety (Gelatti, 2020), and there was a significantly larger decrease in state anxiety from pre- to post-embryo transfer and increased pregnancy rate (Murphy, 2014). Dr. Kathi J. Kemper and coauthors' study with 45 minutes of harp music showed reduced activity and increased weight gain in stable premature infants (Kemper, 2008).

In addition, harp therapy plays an important role in hospice (Ganzini, 2015). Dr. Linda Ganzini and coauthors surveyed 55 family members, whose terminally ill loved one experienced a music vigil during hospitalization. Family members perceived that the vigils resulted in modest improvement in the patients' breathing, relaxation, comfort, and ability to sleep, with fewer positive effects on pain, and almost no negative effects. In a clinical trial in 2006 (Freeman, 2006), 65 dying patients were administered a 25- to 95-minute intervention of prescriptive harp music. Data collected included vital signs and observational indicators before and after the vigil. Patients were more likely to experience decreased levels of agitation and wakefulness while also breathing more slowly and deeply with less effort at the conclusion of the music vigil.

Music Played for Harp Therapy

The reported harp therapy studies were with live harp music or recorded harp music with lengths from 10 minutes to 45 minutes. Dr. Sarajane Williams indicated the music compositions in the book 'Good Vibrations',

which included but were not limited to *Wind, Rain, and The Flight* (Williams); *Vibrations on a Theme by Mozart* (Anon./ Le Dentu); etc (Williams, 2005 c). The harp playing techniques of glissandos, damping the strings, and harmonics have special sensational effects. For live harp music therapy, a full-sized concert pedal harp could produce low, resonant tones (Williams, 2005 d). In a hospital setting, the small harp is an ideal instrument as well for bedside support.

Dr. Schneider and coauthor's study published in 2015 (Schneider, 2015) described a typical live harp music therapy procedure. The procedure is composed of live interaction between the harpist and the patient. The harpist introduced herself to the patient and asked a few questions about the symptoms based on the quality-of-life (QOL) variables to be studied such as "Are you in pain right now?" or "What would you like help with right now?" and "Is there any kind of music you do, or do not, want to hear?" Finally, "Would you like to receive the harp music now?" Because a standardized, recognized protocol for therapeutic harp technique does not exist, a therapeutic harp vibration protocol tailored to each study patient was created and administered. The music chosen in Dr. Schneider's study included 1) set of pieces chosen by the patient or by the therapeutic harpist including Celtic, classical, folk, country, inspirational, religious, or other styles; and 2) improvisations composed at the moment to address the patient's individual condition. The harpist examined the patient's verbal and nonverbal cues indicating their responses throughout the 30–40-minute intervention. These cues included respiration quality, patterns, and rates; movement of extremities; facial expression; emotional reaction such as tears or anger; body tension and position; and verbal comments. Based on these cues, the harpist adjusted different aspects of the music being administered, including tempo, key, rhythm, volume, chordal structure, and plucking techniques. The harpist employed classical Salzedo techniques and used a gut-strung Lyon & Healy Troubadour harp of 33 strings.

Gelatti F and coauthors' pilot study applied live harp music or recorded harp music to interventional or control groups (Gelatti, 2020). The intervention was carried out ac-

ording to the protocol and respecting some specific guidelines such as a gradual creation of the therapeutic sound space (regular beat, soft musical inputs-mainly 1st/5th intervals and almost no melody at first), a careful observation of the patient's reactions to the musical stimuli, the use of tunes in modal scales and subsequent modal improvisations on the basis of the perceived or declare mood of the patient, constant attention towards the respiratory patterns, and verbal feedback of the patient. The recorded music sessions used a stereo speaker and the same music that the harp-therapy student and professional harper had previously recorded. In both cases, the music was played at a volume of a minimum of 60 dB and a maximum of 85 dB. The live harp music was more effective in reducing HR ($P = 0.001$) and diastolic BP ($P = 0.007$), than was recorded harp music.

Available Training programs for harp therapy

Bedside Harp's Harp Therapy Certification Programs (Bedside Harp. (n.d.))

Bedside Harp program offers Certified Harp Therapist (CHT) and Certified Master of Harp Therapy (CMHT) programs accredited by the National Standards Board of Therapeutic Musicians (NSBTM). They are designed to train adult harpists and harpers to work as healthcare professionals in a variety of medical and wellness settings including acute care and behavioral health hospitals, hospices, long-term care facilities, assisted living, memory care, cancer centers, dialysis centers as well as doctors' and dentists' offices.

International Harp Therapy Program (International Harp Therapy Program. (n.d.))

The International Harp Therapy Program (IHTP) was founded by Christina Tourin, a pioneer and leader in the world of harp and healing, in the early 1990s. The program is accredited by NSBTM. The IHTP offers a comprehensive training program through a combination of two separate attendance modules, independent (at-home) study, and an internship.

Harp for Healing, LLC (Harp for Healing. (n.d.)) offers three levels of training:

1) Public Music for Medical Environments (PMME)–training in appropriate music for public areas of healthcare environ-

ments, such as lobbies, nurse's stations, hallways, and the like.

2) Clinical Musician Certification Program (CMCP)–training in the theory and practice of bedside therapeutic music. Accredited by NSBTM. Suitable for any therapeutic instrument – harp, keyboard, guitar, voice, dulcimer, etc.

3) Vibroacoustic Therapeutic Music (VATM) and Vibroacoustic Harp Therapy (VAHT)–Training in utilizing a harp or other instruments in combination with vibrotactile equipment to deliver the sounds and vibrations of music in what has been described as a “cellular massage”.

Vibroacoustic harp therapy training course (VAHT) (Vibroacoustic harp therapy. (n.d.))

Dr. Sarajane Williams introduced the vibroacoustic harp therapy training course to train harpists to provide VAHT and administrators/medical supervisors for VAHT practitioners.

Music-Thanatologists certification from Music-Thanatology Association International (Music Therapy Association of India. (n.d.))

Music-thanatology is a professional field within the broader sub-specialty of palliative care. It is a musical/clinical modality that unites music and medicine in end-of-life care. The music-thanatology utilizes harp and voice at the bedside to lovingly serve the physical, emotional, and spiritual needs of the dying and their loved ones with prescriptive music.

Members certified as music-thanatologists give evidence of the personal, musical, medical, clinical, thanatological, and professional competencies required to effectively offer the prescriptive qualities of music to meet the physical, emotional, and spiritual needs of people who are dying and their families, with harp and voice.

Gender demographics analysis with the published harp therapy studies

There are a few findings published focusing on the treatment study with harp music, among which there are 7 articles with gender information of the adult patients that signed the content for studies and 1 study with gender not reported. There is one study with 181

patients that underwent in vitro fertilization-embryo transfer procedure and that had to include only female subjects. In the remain-

ing six studies, female subjects accounted for 55% and male subjects accounted for 45% (Table 1).

Table 1. Gender information from published harp music therapy studies

Studies on harp therapy with adult patients	Authors and published year	Variables studied	Patients' gender		
			Female	Male	Not presented
1	Diane M. Schneider, et al. 2015	Quality of life variables: fatigue, anxiety, sadness, relaxation, and pain	65(72)	27(29)	
2	Fabrizia Gelatti, et al. 2020	Preoperative stress and fear related to minor surgery	25(54)	21(46)	
3	Daleen Aragon, et al. 2002	Postoperative. anxiety, pain, and satisfaction	7(41)	10(59)	
4	Freeman L, et al. 2006	Music thanatology--palliative care for dying patients	42(65)	23(35)	
5	Erin M. Murphy, et al. 2013	Anxiety from pre- to post-embryo transfer, clinical pregnancy rate	181 (100)	NA	
6	Lincoln, Valerie, et al. 2014	Inpatient acute care pain and anxiety			Not presented
7	AnnMarie Chiasson, et al. 2013	Pain, heart rate, respiratory rate, oxygen saturation, blood pressure	35(35)	65(65)	
8	Kari Sand-Jecklin, et al. 2010	Pain, anxiety, and muscle tension	17(55)	14(45)	
Overall cases except #5 and #6			191 (54)	160 (46)	

Discussion

Sex Bias in Clinical Research and Gender Differences in Music Therapy

Sex bias has existed in clinical research historically, medical studies have excluded female participants and research data have been collected from males and subsequently generalized to females (Dresser, 1992). A study was performed with an observational analysis of data from registered clinical trials published in three high-impact biomedical journals, Journal of the American Medical Association (JAMA), The Lancet, and The New England Journal of Medicine, from January 1, 2015 to December 31, 2019. One

thousand four hundred and forty-two manuscripts with 4,765,783 human subjects were included for analysis. Significantly more males (56%) than females (44%) were included in all three journals ($P < 0.0001$). Sex matching $\geq 80\%$ was found in 24.6% of publications. Industry funded 43.7% of all studies enrolling significantly more males than females (60.8% versus 39.2%, $P < 0.0001$). NIH funded 10.2% of studies enrolling significantly more females than males (52.7% versus 47.3%, $P < 0.0001$). North America and Europe contributed 82.6% of the studies with each enrolling significantly more males than females ($P < 0.0001$). The United

States was the country contributing the most studies (36.1%), enrolling significantly more males than females (55.5% versus 45.5%, $P < 0.0001$). Cardiovascular disease was the subject area of the most manuscripts among medical specialties (19%), enrolling significantly more males than females (64.9% versus 35.1%, $P < 0.0001$). According to the American Heart Association (AHA) Heart Disease and Stroke Statistics published in 2016 (WG members, 2016), among the 5.1 million cases of heart failure, 52.9% were men and 47.1% were women.

Nonetheless, music therapy showed a different trend in gender demographics with more female participants. A retrospective electronic health record (EHR) review (Rodgers-Melnick, 2024) was conducted across ten medical centers with hospitalized patients between January 2017 and July 2020. The music therapy team provided 14,261 sessions to 7378 patients across 9091 hospitalizations. In this study, patients were predominantly female (63.7%).

A systematic review and meta-analysis with a total of 154 results and 14 studies evaluated the effect of music therapy on anxiety and stress prior to dental treatments. More than 50% of female participants were enrolled in 8 out of the 14 studies (Lopez-Valverde, 2024).

Reasons for the Different Demographic Trends in Music Studies

There are possible explanations for the different sex demographics in music therapy studies.

Females have positive attitudes about music therapy. A survey with 184 participants on the attitudes toward and willingness to use music therapy was obtained between 2014 and 2015 (McDaniel, 2015), the study showed a significant difference in the scores of knowledge of music therapy for females ($M=4.27$, $SD=0.53$) and males ($M=4.09$, $SD=0.35$); $t(65)=1.99$, $p=0.01$. Females and adults ages 45–54 reported the most positive attitudes about music therapy. A randomized study of cardiovascular prevention trials with 783 participants across 13 clinical centers showed that women had lower distrust of medical researchers (Ding, 2007).

There are gender differences in psychophysiological responses to music listening

and music therapy. A study in 2016 presented a comparative account of psychophysiological responses to music listening in healthy males and females. The stimulus material was a slow-paced taped rāga Desi-Todi on a flute. The participants listened to music for 30 minutes a day for 20 days. The pre-and post-treatment procedure was adopted for assessments of psychophysiological measures. This study showed that the effects of music listening, that is, reduction in negative affect, enhancement of positive affect, and decrease in blood pressure and heart rate, were more intense in females than males (Uma Gupta, 2016). Gender differences in the outcome of guided imagery and music (GIM) therapy were explored in a study with a potentially gender-sensitive instrument, the Inventory of Interpersonal Problems (IIP), as well as the Symptom Checklist –90 (SCL-90) and Sense of Coherence (SOC) scale (Dag Körlin, 2001). The study revealed that women benefited more than men in relational aspects measured by the IIP. In the SOC, there were gender differences in subscale effects consistent with current assumptions of gender roles. There was also support for the observation that men have a higher threshold for seeking psychotherapeutic treatment.

In addition to the psychophysiological responses, there is a gender difference in pain tolerance and pain rating from music treatment. Sina Ghaffaripour and coauthors assessed the effect of two types of music (Iranian folkloric and preferred music) on pain tolerance and pain rating in a cold pressor test with 50 healthy Iranian medical students enrolled (Ghaffaripour, 2013). Mean tolerance time was significantly higher in preferred music compared to Iranian folkloric music ($F(1,48) = 25.44$, $p=0.0001$) and no music ($F(1,48) = 3.51$, $p=0.0001$) conditions. There was a significant interaction when tolerance time in no music condition was compared to preferred music condition, regarding sex; Tolerance time increased more in females ($F(1,48) = 5.53$, $p=0.023$). Music distracts the attention from pain and Women can be impressed and distracted more easily by music.

Conclusion

Harp has been more and more widely applied in therapy, such as pain, anxiety and

pressure and muscle tension relief; from the field of reproductive medicine, neonatal care, quality of life in the hospital, to Hospice. Certified training programs that are essential for effective and professional treatment are

available from different organizations. There is no gender difference study reported in the harp therapy field, psychophysiological responses from different genders need to be investigated in future studies.

References

- Aragon, D., et al., (2002). The effects of harp music in vascular and thoracic surgical patients. *Alternative Therapies in Health and Medicine*, 8(5), 52–54, 56–60.
- Bedside Harp. (n.d.). Harp therapy certification. Bedside Harp. URL: <https://www.bedside-harp.com/harp-therapy-certification>
- Chiasson, A.M., et al., (2013). The effect of live spontaneous harp music on patients in the intensive care unit. *Evidence-Based Complementary and Alternative Medicine*, 2013, – 428731.
- Dresser, R. (1992). Wanted: Single, white male for medical research. *Hastings Center Report*, – 22(1), 24–29.
- Ding, E.L., et al., (2007). Sex differences in perceived risks, distrust, and willingness to participate in clinical trials: A randomized study of cardiovascular prevention trials. *Archives of Internal Medicine*, – 167(9), 905–912.
- Freeman, L., et al., (2006). Music thanatology: Prescriptive harp music as palliative care for the dying patient. *American Journal of Hospice and Palliative Medicine*, – 23(2), 100–104.
- Galpin, F. W. (1929). The Sumerian harp of Ur, c. 3500 B.C.E. *Oxford Journal of Music and Letters*, – 10(2), 108–123.
- Ganzini, L., et al., (2015). Family members' views on the benefits of harp music vigils for terminally ill or dying loved ones. *Palliative & Supportive Care*, – 13(1), 41–44.
- Gelatti, F., et al., (2020). Efficacy of live versus recorded harp music in reducing preoperative stress and fear related to minor surgery: A pilot study. *Alternative Therapies in Health and Medicine*, – 26(3), 10–15.
- Ghaffaripour, S., Mohammadzadeh, M., Sahmeddini, M. A., & Alipour, A. (2013). Music can effectively reduce pain perception in women rather than men. *Pakistan Journal of Medical Sciences*, – 29(1), 128–131.
- Gupta, U., & Gupta, B. S. (2016). Gender differences in psychophysiological responses to music listening. *Music and Medicine*, – 8(1), 53–64.
- Harp for Healing. (n.d.). Harp for Healing. URL: <https://www.playharp.com/international-harp-therapy-program>
- International Harp Therapy Program. (n.d.). Play Harp. URL: <https://www.playharp.com/international-harp-therapy-program>
- Kemper, K. J., & Hamilton, C. (2008). Live harp music reduces activity and increases weight gain in stable premature infants. *Journal of Alternative and Complementary Medicine*, – 14(10), 1185–1186.
- Körlin, D., & Winberg, B. (2001). Gender differences in outcome of guided imagery and music (GIM) therapy. *Nordic Journal of Music Therapy*, – 10(2), 132–143.
- Lincoln, V., & Holmes, A. (2014). Impact of healing touch with healing harp on inpatient acute care pain: A retrospective analysis. *Holistic Nursing Practice*, – 28(3), 164–170.
- Lopez-Valverde, N., et al., (2024). Efficacy of music therapy on stress and anxiety prior to dental treatment: A systematic review and meta-analysis of randomized clinical trials. *Frontiers in Psychiatry*, – 15, – 1352817.
- McDaniel, M. E. (2015). Attitudes toward and willingness to use music therapy in Southern Mississippi (Doctoral dissertation, University of Southern Mississippi). The Aquila Digital Community.
- Murphy, E.M., et al., (2014). Randomized trial of harp therapy during in vitro fertilization-embryo transfer. *Journal of Evidence-Based Complementary & Alternative Medicine*, – 19(2), 93–98.

- Musiatory. (n.d.). Vibroacoustic harp therapy. Musiatory. URL: <https://www.musiatory.com/vibroacoustic-harp-therapy.html>.
- Music Therapy Association of India. (n.d.). Certification. MTAI. URL: <https://www.mtai.org/certification>
- Rodgers-Melnick, S.N., et al., (2024). Effectiveness of medical music therapy practice: Integrative research using the electronic health record: Rationale, design, and population characteristics. *Journal of Integrative and Complementary Medicine*, – 30(1), 57–65.
- Sand-Jecklin, K., & Emerson, H. (2010). The impact of a live therapeutic music intervention on patients' experience of pain, anxiety, and muscle tension. *Holistic Nursing Practice*, – 24(1), 7–15.
- Schneider, D.M., et al., (2015). Application of therapeutic harp sounds for quality of life among hospitalized patients. *Journal of Pain and Symptom Management*, – 49(5), 836–845.
- Skille, O. (1989). Vibroacoustic therapy. *Music Therapy*, – 8(1), 61–77.
- Williams, S. (2005a). Interview with Olav Skille, vibroacoustic therapy. In *Good vibrations: Principles of vibroacoustic harp therapy*, – P. 64–65.
- Williams, S. (2005b). Vibroacoustic harp therapy. In *Good vibrations: Principles of vibroacoustic harp therapy*, – P. 69–71.
- Williams, S. (2005c). Subjective responses to vibroacoustic therapy. In *Good vibrations: Principles of vibroacoustic harp therapy*, – 73 p.
- Williams, S. (2005d). Equipment. In *Good vibrations: Principles of vibroacoustic harp therapy*, – 87 p.
- Writing Group Members, et al. (2016). Executive summary: Heart disease and stroke statistics-2016 update: A report from the American Heart Association. *Circulation*, – 133(4), 447–454

submitted 02.09.2024;
accepted for publication 16.09.2024;
published 29.10.2024
© Yimiao Zou
Contact: yimiazou@gmail.com



Section 4. Pharmaceutical Sciences

DOI:10.29013/EJBLS-24-3-46-74



VIRTUAL SCREENING OF ACETYLCHOLINESTERASE-CENTERED INHIBITORS AS POTENTIAL THERAPIES FOR ALZHEIMER'S DISEASE

*Benjamin Liu*¹

¹ United States of America

Cite: Benjamin Liu. (2024). *Virtual Screening of Acetylcholinesterase-Centered Inhibitors as Potential Therapies for Alzheimer's Disease. The European Journal of Biomedical and Life Sciences 2024, No 3.* <https://doi.org/10.29013/EJBLS-24-3-46-74>

Abstract

Acetylcholinesterase inhibitors (AChE-Is) are currently one of the most popular treatments for Alzheimer's disease (AD). Despite their proven effectiveness in easing symptoms of cognitive decline, their limited efficacy and strong adverse side effects demand the urgent need to develop better treatment for AD patients. This study explores a new series of ligands targeted towards inhibiting AChE as an anti-AD drug. Findings from various binding site detection methods, such as geometric, machine learning, and energetic-based methods, showed that AChE is a suitable binding target for ligands. The research utilized ZINCPharmer to identify compounds with good binding interactions with different pharmacophore maps of AChE. Molecular docking using SwissDock revealed multiple ligands with an impressive SwissParam score range of -7.2 to -8.9 kcal/mol, confirming their strong binding interaction with AChE binding sites. The top compounds were tested for their absorption, distribution, metabolism, and excretion (ADME) using SwissADME. Three promising compounds L_6 (ZINC12232928), L_7 (ZINC92176885), and L_9 (ZINC92189850) were able to cross the Blood Brain Barrier while adhering to Lipinski's rule. The toxicity of the compounds was also examined using a computational prediction tool ProTox 3.0. Most compounds have acceptable toxicity, with compound L_18 (ZINC03302264) having the best predicted LD50 of 5240 mg/kg and predicted toxicity class 6. Finally, ligands L_7 and L_9 are the most promising candidates as potential lead compounds for future AChE-I studies as they maintained excellent results in all experiments.

Keywords: *Alzheimer's Disease, Acetylcholinesterase, Virtual Screening, Drug Discovery, Therapeutics*

Introduction

Alzheimer's disease (AD) is a progressive neurodegenerative disease characterized by

memory loss, cognitive deficit, and difficulties conducting personal daily activities. It is the main cause of dementia, accounting for

60–70% of the 50 million cases worldwide. It is estimated that there are around 50 million AD patients worldwide, and the numbers are projected to increase to 152 million by 2050 (Breijyeh et al., 2020; Chen et al, 2022). A meta-analysis of treatment costs for Alzheimer’s disease estimates that the total costs per patient per year determined by the meta-analysis is \$20,461 (Marešová et al, 2019). These studies emphasize the severity of the physical and mental toll and the financial burden on the patients and their families, demonstrating the urgent need for improved treatment for the disease (Tahami et al, 2022).

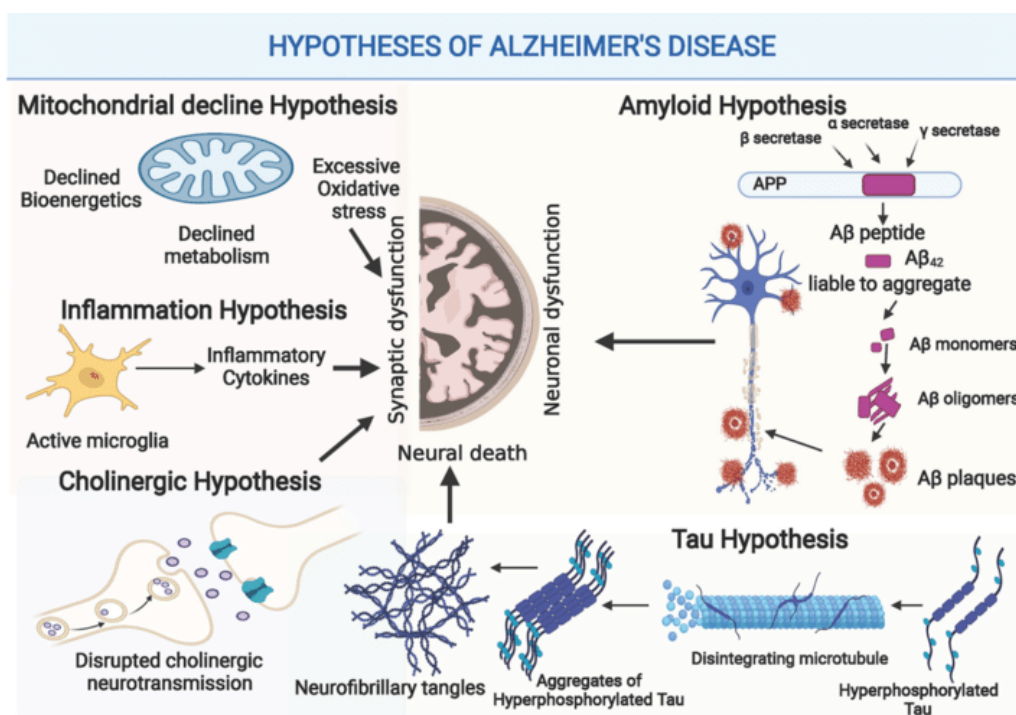
Although the trigger and driving force behind the progression of AD remain unclear, two main hypotheses have been proposed: the cholinergic hypothesis and the amyloid hypothesis. The cholinergic hypothesis attributes the cause of AD to the degeneration of cholinergic neurons, neurons that use and synthesize acetylcholine (ACh) (Stanciu et al, 2020).

ACh, first discovered in 1913 (Tansey, 2006), is an excitatory neurotransmitter involved in several physiological processes such as memory, learning, attention, arousal, and involuntary muscle movement (Sam et al, 2024). Due to its important role in cognition, the deficiency of ACh and the

cholinergic neurons is considered to play a significant role in the pathogenesis of AD (Ferreira-Vieira et al, 2016). ACh is synthesized by an enzyme called choline acetyltransferase (ChAT), which causes a reaction between choline and the acetyl group to create acetylcholine. To transmit chemical messages across nerve cells, ACh binds to two types of receptors: nicotinic receptors and muscarinic receptors. To repeat the process, ACh is broken down by the enzyme acetylcholinesterase (AChE) in the synapse into choline and acetate, which can then be reused. These compounds are reabsorbed and recycled to be reused in transmitting additional chemical messages (Cleveland Clinic Medical, n.d.).

The amyloid hypothesis attributes the cause of AD to the buildup of amyloid- β ($A\beta$) plaque in the brain parenchyma and the cerebral vasculature (Ricciarelli et al, 2017). Although amyloid plaques are found in healthy brains, the human body’s ability to properly break down $A\beta$ decreases with age or pathological conditions, thus leading to abnormal accumulation of $A\beta$ peptides. As a result, the buildup creates neurotoxicity and causes neuronal cell death and neurodegeneration (Murphy et al, 2010).

Figure 1. Illustration of the Cholinergic, Amyloid, Mitochondrial, Inflammation, and Tau Hypothesis of AD (Abuelezz et al, 2021)



Currently, there are only two types of drugs approved to treat Alzheimer's disease (AD). The most common type includes cholinesterase inhibitors, and the other type consists of N-methyl D-aspartate (NMDA) receptor antagonists such as memantine (Breijyeh, 2020). Recent clinical data has shown that the brains of patients with AD show severe damage to cholinergic neurons, a decrease in ACh levels, and reduced ChAT activity (Chen, 2022). Acetylcholinesterase inhibitors (AChE-Is) help restore cholinergic functions by blocking the breakdown of ACh by AChE and butyrylcholinesterase (BChE), which increase the ACh levels in the synaptic cleft. Currently, the three most used Food-and-Drug-Administration(FDA)-approved AChE-Is are donepezil, galantamine, and rivastigmine. All three types showed their ability to improve AD symptoms. However, rivastigmine has stood out as the most promising drug, with the most desirable safety, tolerability, and efficacy profile, likely due to its ability to inhibit both AChE and BChE (Grossberg, 2003). In July 2023, the FDA approved lecanemab, a new monoclonal antibody. A clinical trial demonstrated that lecanemab effectively removed A β plaques in early Alzheimer's disease and showed moderate success in reducing cognitive decline (Van Dyck et al, 2023). Despite showing favorable results, these drugs are associated with adverse side effects such as loss of appetite, diarrhea or vomiting, headaches, feeling tired or dizzy, and difficulty sleeping well ("Dementia Medication", n.d.). Therefore, further research is needed to develop new compounds that minimize these side effects.

Literature review

To tackle the complex multifactorial pathogenesis of AD, recent AChE-Is development focused on the multi-target-directed ligands (MTDLs) strategy which emerges as an advantageous approach compared to combination therapy, which involves using multiple medications to treat a single disease. The MTDL strategy demonstrated its potential by effectively addressing multiple pathological pathways using a single medication, offering additional benefits. These include avoiding potential risks from drug-drug interactions, reducing the likelihood

of worsening side effects, and providing a more convenient dosing regimen (Zou et al, 2023). Although the resulting compounds in this study are not experimented to be multi-targeted, they are strong starting points for the future development of this advantageous anti-AD therapy.

Dual AChE and MAO-B inhibitors

Despite AChE being the primary target in AD drug development, the discovery of overexpression of monoamine oxidase B (MAO-B) in the brains of AD patients has identified it as another promising enzyme target for AD therapy. To discover, design, and screen for AChE and MAO-B dual inhibitors, the research utilized nanotechnology and computer-aided drug design (CADD) and incorporated the pharmacophores of anti-AD molecules or drugs. Inhibitors such as chalcone, coumarin, chromone, benzo five-membered ring, imine, and hydrazone scaffolds were systematically classified based on their structure and analyzed by their design strategies, docking studies, and structure-activity relationships (SARs). While dual AChE and MAO-B inhibitors have strong potential to provide significant treatment to AD, there are limiting factors to overcome while developing such inhibitors. One limitation is the structural difference between the catalytic anionic site (CAS) of AChE and the active sites of MAO-B. This structural difference makes it extremely difficult to discover effective dual inhibitors for AChE and MAO-B, as both enzymes often cannot share the same pharmacophores (Zou et al, 2023).

Dual AChE and BACE-1 inhibitors

A new series of multi-targeted donepezil analogues as dual AChE and β -secretase 1 (BACE-1) inhibitors have been designed, synthesized, and evaluated. This new design targets both cholinergic dysfunction and amyloid- β plaque formation and is achieved by introducing backbone amide linkers to enhance BACE-1 inhibition and reduce extracellular cleavage of the amyloid precursor protein (APP). Molecular docking studies confirm the analogues' capability to inhibit both AChE and BACE-1. Additionally, in vitro cytotoxicity testing on SH-SY5Y neuroblastoma cells showed that the new analogues exhibited tolerable toxicity levels and did not negatively

impact cell viability compared to the controls. Furthermore, the analogues demonstrated passive permeability of the blood-brain barrier (BBB) comparable to donepezil, as measured by the parallel artificial membrane permeability assay for BBB (PAMPA-BBB). These encouraging results, particularly with compound 4, highlight the strong potential of these compounds as strong candidates for further therapeutic development (Moustafa et al, 2018).

Dual Targeting of AChE and Tau Aggregation

In search for inhibitors of AChE, BACE1, A β 1-42 fibrillation, tau aggregation, and α -syn aggregation, deoxyvasicinone analogues are designed, synthesized, and evaluated as potential multi-targeted therapy for AD. The research utilized a pharmacophore combination strategy to design new MTDLs. The compounds were then screened using biological assays to confirm their performance in inhibiting the five targets. Molecular docking studies were also conducted using the Autodock software to predict the binding interaction of the compounds. Finally, physicochemical properties and BBB permeability were analyzed to test their suitability as drug candidates. The result concluded that several MTDLs demonstrated their ability to effectively inhibit both AChE and cellular tau oligomerization. Interestingly, compound 11f has demonstrated greater neuroprotective efficacy, showing the effectiveness of multi-targeted drugs as therapeutic agents for AD and urging further investigation (Shoab et al, 2021).

Lecanemab clinical trial

Targeted for soluble aggregated A β plaques, Lecanemab, a humanized IgG1 monoclonal antibody, was approved by the FDA on July 6, 2023, and is currently undergoing clinical trials ("FDA Converts", 2023). The phase 2 clinical trial for lecanemab, specifically study 201 blinded period(core), was a multinational, multicenter, double-blind, placebo-controlled study of 856 patients randomized to one of five dose regimens or placebo. Subsequently, during the open-label extension (OLE) of the study, the patients were allowed to receive open-label lecanemab 10 mg/kg biweekly for up to 24 months, with an off-treatment period (gap period) ranging

from 9 to 59 months (mean 24 months). The study found a significant difference between the drug and placebo group over time and observed key changes to the pathophysiology of the AD patients and a continued drug effect during the gap period. These results indicated lecanemab's strong potential for reducing amyloid plaques and improving symptoms in AD patients. The study also proved the effectiveness of plasma biomarkers as indicators for lecanemab treatment responses. The ongoing phase three clinical trials will further explore these results and the therapeutic potential for lecanemab (McDade et al, 2022).

Research method

Binding Sites Identification

The availability of compatible binding sites for small molecules is crucial in developing drug candidates for enzymes. Multiple factors such as the size, composition, and energy interaction could indicate if an enzyme has suitable binding sites for ligands (Agu et al, 2023). Geometric, machine learning, and energetic-based methods were used to confirm the potential for AChE to provide binding sites for future drug developments. For the purpose of studying binding interactions with small molecules, we used Protein Data Bank(PDB) ID 3LII for AChE for all binding site prediction experiments (Berman et al, 2000).

Geometric Method

DoGSiteScorer is an automatic algorithm from Protein Plus that identifies potential binding pockets in a protein only using the 3D structure of the protein. It also assigns each pocket with a druggability score ranging from 0 to 1 using a support vector machine(SVM) algorithm trained and tested by a druggability dataset consisting of 1069 targets (Volkamer et al, 2010; Volkamer et al, 2012).

Machine Learning Method

Prankweb is an online tool that uses a combination of the 3D structure of a protein accessed through the PDB, evolutionary conservation analysis, and a previously developed machine learning algorithm P2Rank to predict potential ligand-binding sites in proteins (Dávid et al, 2022; Lukáš et al, 2019; Radoslav et al, 2018).

Energetic Based Method

FTSite is an energy-based binding sites detection method with a 94% success rate in

the LIGSITE test set (Kozakov et al, 2015; Ngan et al, 2012; Brenke et al, 2009).

Virtual Screening

Pharmacophore Identification with PocketQuery

To identify lead compounds that can modulate the function of AChE, we first used pocketquery with PDB code 4QWW to search for pharmacophore models that have a higher likelihood of supporting ligand binding. 4 pharmacophore maps were selected based on their high scores and their location in chains C and E which are the antibody chains.

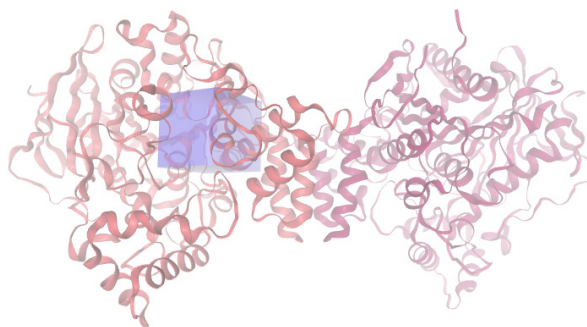
Large-scale Screening with ZINC-Pharmer

The 4 selected pharmacophore maps are then exported to the online tool ZINCPharmer. A large library of around 18 million compounds was virtually screened to identify ones that have desired fitting with the features of the imported pharmacophores. A few pharmacophore features are deselected before the query to prevent having 0 hits. Afterward, 5 compounds with the lowest Root-mean-square deviation(RMSD) from each of the 4 maps were selected and recorded. Compounds with lower RMSD values have better matching with the pharmacophore models and are thus selected for further experimentation. The 20 compounds are displayed in Tables 4, 6, 8, and 10.

Molecular Docking with Swiss-Dock

The binding affinity of the compounds to AChE was further examined using the Attracting Cavities (AC) 2.0 docking engine from the web service SwissDock (Bugnon et al, 2024; Röhrig et al, 2023). To start the docking session, follow these steps: (i) For the ligand preparations, submit the SMILES for each ligand. These can be accessed through the ZINC database. (ii) For the protein target preparation, submit the PDB ID 4QWW for AChE with only chains A and B being selected. In addition, select “None” for the heteroatoms parameter. (iii) The dimensions of the search box are 15Å by 15Å by 15Å with the center coordinates at (18, -75, -4)Å (Fig. 2.). This search region is considered as it is in proximity to the binding sites with high druggability score found from the results in the binding site identification experiments (4.1). (iv) The number of Random Initial Conditions (RIC) was kept at 1 and other parameters were kept as default. (v) Lastly, click on the “Starting Docking” button to initialize the session. The results from this experiment are displayed in Table 11 with the compound analyzed based on their SwissParam score.

Figure 2. Position and Size of the Purple Search Box Used for the SwissDock Experiment



Drug Effectiveness with SwissADME

In order to determine the drug effectiveness of our top compound from the SwissDock experiment, we assessed our compounds based on their absorption, distribution, metabolism, and excretion (ADME) properties. We utilized SwissADME, a free web tool, to determine the physicochemical properties, lipophilicity, water solubility,

druglikeness, and pharmacokinetics of our compounds. For lipophilicity specifically, we used the partition coefficient between n-octanol and water (logP) from SwissADME's in-house physics-based iLogP method (Daina et al, 2017). Using these pieces of information, we were able to first determine if each compound passed Lipinski's rule of 5 for good absorption and permeation. Specifically, we ex-

aminated if the ligand had a molecular mass of less than 500 daltons, no more than 5 hydrogen bond donors, no more than 10 hydrogen bond acceptors, and no more than 5 for log P. Lastly, we also considered the compound's ability to permeate the BBB and its GI absorption. To run SwissADME, we entered a list of SMILES files for our compounds and clicked "run" to start the calculations. Our results for the compounds with the top ADME result and compounds with the top SwissParam scores are recorded in Table 13.

Toxicity test with ProTox 3.0

Determining the toxicity of a ligand is crucial in developing lead drug compounds. Our study utilized ProTox 3.0, a virtual lab that runs the prediction of toxicities of small mol-

ecules (Banerjee et al, 2024). To run Tox-Prediction, we entered the SMILES files for our compounds and clicked "smiles" to upload the compound information. We then selected "all" for our prediction models and clicked "start Tox-Prediction" to run the prediction.

Results and discussion

Binding Sites Identification

AChE is well-suited as a target for drug development as we observed the availability of multiple binding sites for ligands and small molecules in all three of our used binding site detection methods.

Geometric Method Results

Figure 2. Molecular Model of AChE Binding Sites Predictions Using the DoGSiteScorer Method

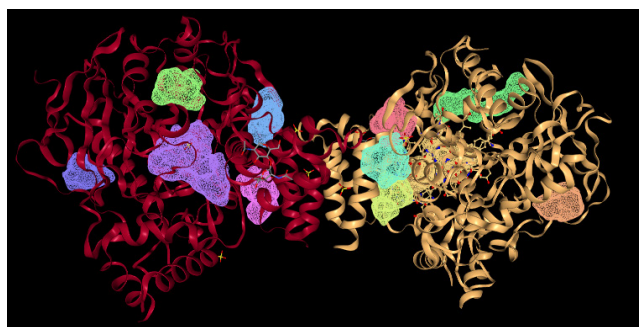


Table 1. Potential AChE Binding Subpockets And Their Drug Scores Predicted By DoGSiteScorer Ranked By Volume Using PDB ID: 3LII

Binding Pockets	Volume (cubic Å)	Surface (square Å)	Drug Score
P_0	796.24	650.39	0.82
P_1	771.85	643.47	0.83
P_10	235.02	378.65	0.35
P_11	228.41	169.54	0.36
P_12	223.39	318.79	0.49
P_13	221.57	341.31	0.34
P_14	193.3	134.38	0.55
P_15	188.06	315.58	0.38
P_16	186.01	147.47	0.57
P_17	176.89	286.69	0.45

The table above displays the top 10 binding sites predicted by DoGSiteScorer, ranked based on their volume. Binding sites P_0 and P_1 are the largest, with volumes of 796.24 and 771.85 cubic Å, surface areas of 650.39 and 643.47 square Å, and the best

drug scores of 0.82 and 0.83. Smaller binding sites like P_15 and P_17 showed significantly worse drug scores, indicating that larger binding sites potentially have better drug scores and stronger binding affinity for small molecules. One notable binding site is P_1

from Protein Plus. It showed up in similar locations as Rank 2 from Prankweb and the green highlighted site from FTSites. Results from DoGSiteScorer display that this binding site consists of 37 residues with the most abundant residues being tryptophan (TRP), tyrosine (TYR), and glycine (GLY), each ap-

pearing 7, 6, and 4 times respectively. Another promising binding site is P_0 from Protein Plus and Rank 1 from Prankweb. This binding site consists of 44 residues with the most abundant residues being glycine (GLY), tyrosine (TYR), and serine (SER), each appearing 8, 7, and 4 times respectively.

Machine Learning Method Results

Figure 3. Molecular Model of Predicted Binding Sites in AChE (PDB ID: 3LII) by PrankWeb

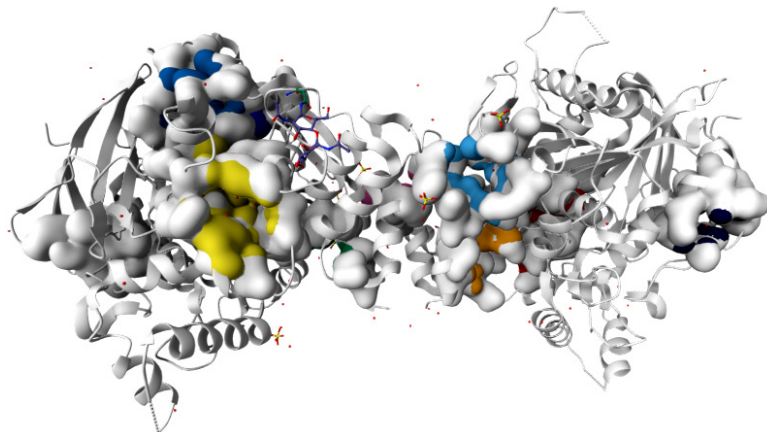


Figure 4. Close Up of Rank 1 AChE Binding Site

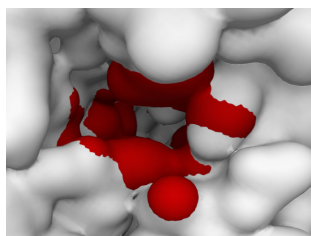


Figure 5. Close Up of Rank 2 AChE Binding Sites

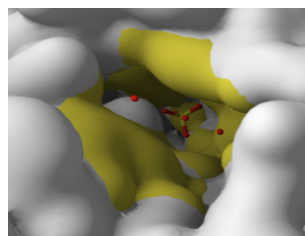


Table 2. Potential AChE Binding Pockets Predictions by PrankWeb3 Ordered by Score Using PDB Code 3LII

Rank	Score	Probability	# of residues	Avg conservation
1	29.65	0.915	24	0.765
2	24.12	0.877	25	0.808
3	1.8	0.033	10	0.082
4	1.78	0.032	14	0
5	1.77	0.032	7	0.146
6	1.5	0.021	12	0.09
7	1.4	0.018	6	0
8	1.21	0.012	12	1.606
9	1.18	0.011	12	1.916
10	1.12	0.009	8	0

The table above displays the top 10 binding sites predicted by PrankWeb3, ranked based on their score. Binding sites Rank 1 and Rank 2 are the largest, with 24 and 25

residues and significantly higher drug scores of 29.65 and 24.12.

Energetic-Based Method Results

Figure 6. Molecular Model of Predicted Binding Sites by FTSite Server in AChE Using PDB code 3LII. Binding Sites are Highlighted with the Colors Pink, Green, and Purple

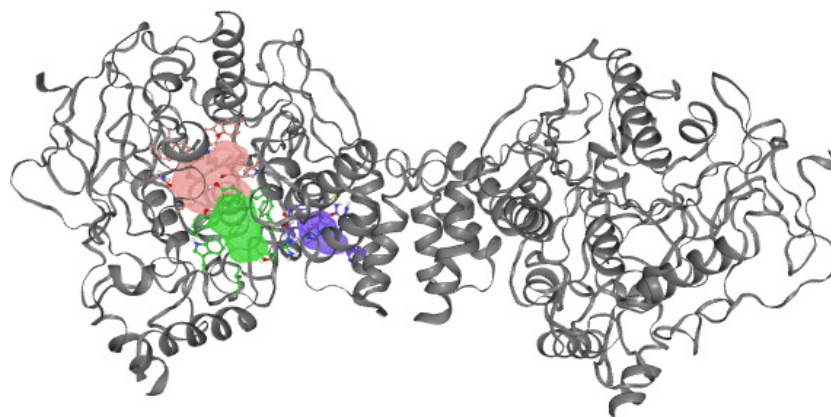
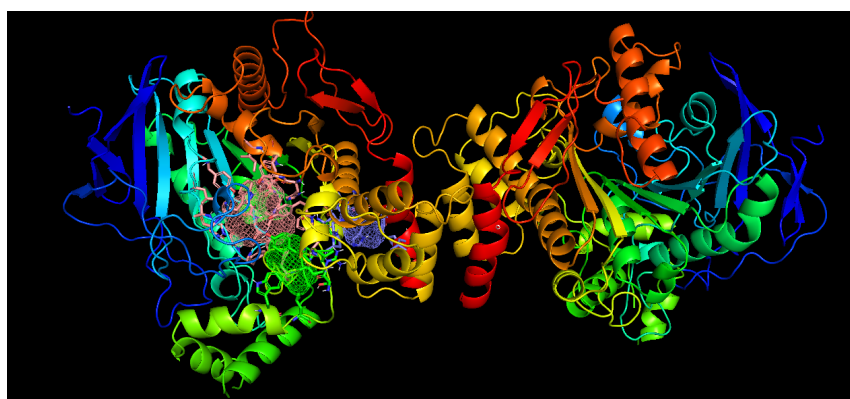


Figure 7. Molecular Model of Predicted Binding Sites In AChE By PyMol Session Using PDB Code 3LII. Binding Sites are the Blob Shapes Highlighted with the Colors Pink, Green, And Purple. FTsite Identified Three Binding Sites for AChE



ZINCPharmer Ligand Binding Result

Table 3. Pharmacophore Map 1 Information Containing Cluster Model, Chain Letter, Residues, Score and Features Considered

Figure 8. PharmMap 1 Model	Chain	Residue	#	Pocket Query Score	Features Considered
	C	TYR	90	0.986921	Hydrogen Donor Hydrogen Donor Hydrogen Acceptor Hydrophobic
		HIS	93		

Table 4. ZINCPharmer Results Based on Pharmacophore Map 1 for the Interaction of 5 Top Compounds with AChE (PDB ID: 4QWW)

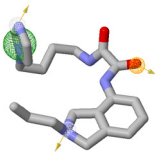
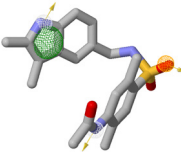
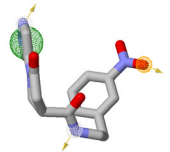
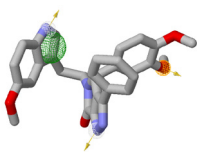
Name	ZINC64380746	ZINC67533629	ZINC19567459	ZINC89306446	ZINC95101290
Structure					
RMSD	0.137	0.137	0.177	0.180	0.184
Mass	390	371	400	343	509

Table 3 provides information about pharmacophore map 1. PocketQuery identifies that pharmacophore map 1 belongs in the C chain with two crucial residues Tyrosine at position 90 and Histidine at position 93. It has a high PocketQuery score of 0.986921. The key features we used for the ZINCPharmer query

are 2 hydrogen donors, 1 hydrogen acceptor, and 1 hydrophobic interaction. Table 4 presents the top 5 ligands for pharmacophore map 1. The RMSD values for these ligands range from 0.137 to 0.184, with the median value at 0.177. This indicates that these ligands are a good fit for the Pharm Map 1.

Table 5. Pharmacophore Map 2 Information Containing Cluster Model, Chain Letter, Residues, Score and Features Considered

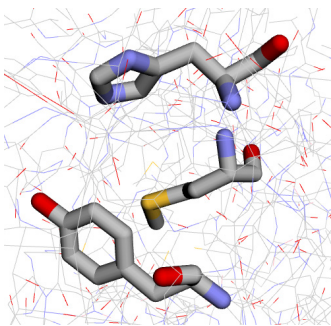
Figure 9. Pharm Map 2 Model	Chain	Residue #	PocketQuery Score	Features Considered
	C	TYR 90	0.984095	Hydrogen Donor Hydrogen Acceptor Hydrophobic
		HIS 93		
		MET 95		

Table 6. ZINCPharmer Results Based on Pharmacophore Map 2 for the Interaction of 5 Top Compounds with AChE (PDB ID: 4QWW)

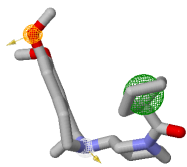
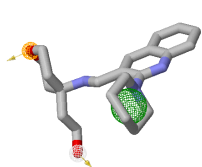
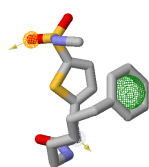
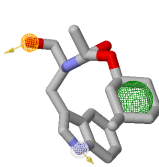
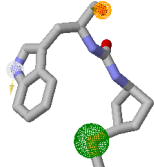
Name	ZINC12232928	ZINC92176885	ZINC69328766	ZINC92189850	ZINC74888813
Structure					
RMSD	0.005	0.007	0.007	0.008	0.010
Mass	388	371	396	358	362

Table 5 provides information about pharmacophore map 2. PocketQuery identifies that pharmacophore map 2 belongs in the C chain with three crucial residues Ty-

rosine at position 90, Histidine at position 93, and Methionine at position 95. It has a high PocketQuery score of 0.984095. The key features we used for the ZINCPharmer

query are 1 hydrogen donor, 1 hydrogen acceptor, and 1 hydrophobic interaction. Table 6 presents the top 5 ligands for pharmacophore map 2. The RMSD values for these

ligands range from 0.005 to 0.010, with the median value at 0.007. This indicates that these ligands are an exceptional fit for the PharmMap 2.

Table 7. Pharmacophore Map 3 Information Containing Cluster Model, Chain Letter, Residues, Score and Features Considered

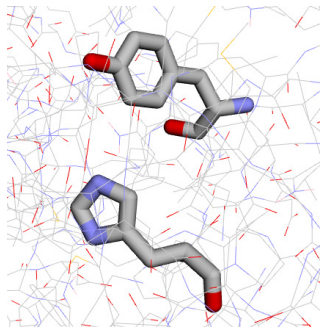
Figure 10. Pharm Map 3 Model	Chain	Residue	#	PocketQuery Score	Features Considered
	E	TYR	90	0.981743	Hydrogen Donor Hydrogen Acceptor Hydrogen Acceptor Hydrophobic
		HIS	93		

Table 8. ZINCPharmer Results Based on Pharmacophore Map 3 for the Interaction of 5 Top Compounds with AChE (PDB ID: 4QWW)

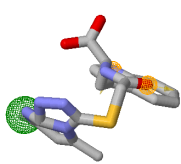
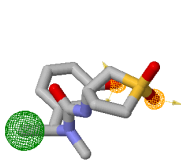
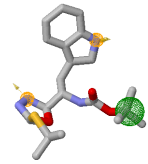
Name	ZINC64684329	ZINC31156228	ZINC67580654	ZINC12249875	ZINC63426782
Structure					
RMSD	0.018	0.021	0.022	0.024	0.025
Mass	426	486	312	424	406

Table 7 provides information about pharmacophore map 3. PocketQuery identifies that pharmacophore map 3 belongs in the E chain with 2 crucial residues Tyrosine at position 90 and Histidine at position 93. It has a high PocketQuery score of 0.981743. The key features we used for the ZINCPharmer query

are 1 hydrogen donor, 2 hydrogen acceptors, and 1 hydrophobic interaction. Table 8 presents the top 5 ligands for pharmacophore map 3. The RMSD values for these ligands range from 0.018 to 0.025, with the median value at 0.022. This indicates that these ligands are a great fit for the PharmMap 3.

Table 9. Pharmacophore Map 4 Information Containing Cluster Model, Chain Letter, Residues, Score and Features Considered

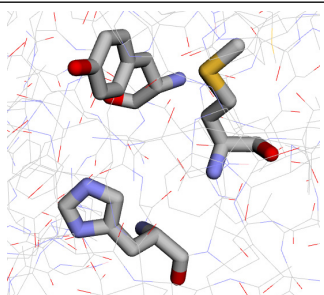
Figure 11. PharmMap 4 Model	Chain	Residue	#	PocketQuery Score	Features Considered
	E	TYR	90	0.981391	Hydrogen Donor Hydrogen Acceptor Hydrophobic
		HIS	93		
		MET	95		

Table 10. ZINCPharmer Results Based on Pharmacophore Map 4 for the Interaction of 5 Top Compounds with AChE (PDB ID: 4QWW)

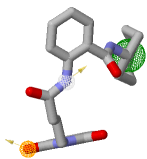
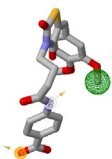
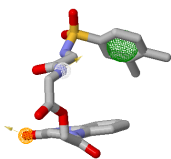
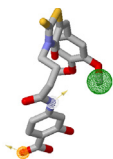
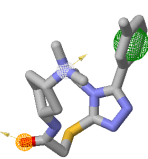
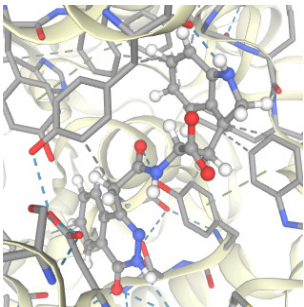
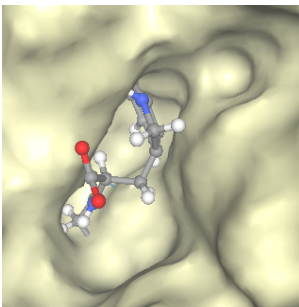
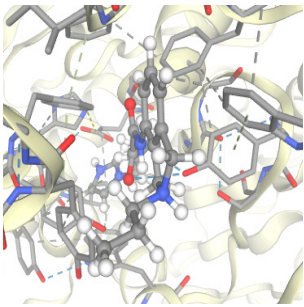
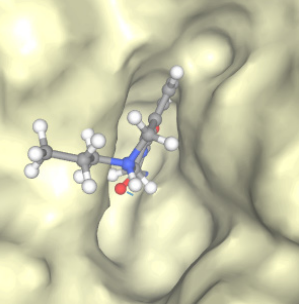
Name	ZINC01211703	ZINC33417589	ZINC03302264	ZINC35638852	ZINC93796225
Structure					
RMSD	0.016	0.018	0.020	0.021	0.021
Mass (dalton)	448	469	489	502	389

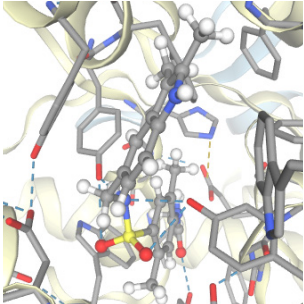
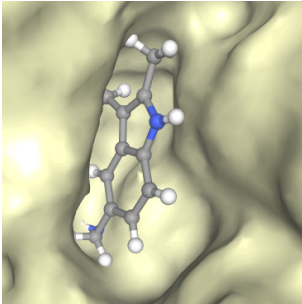
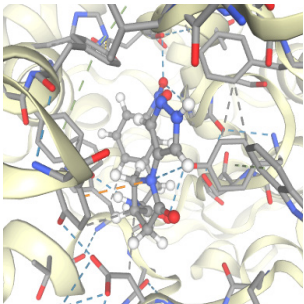
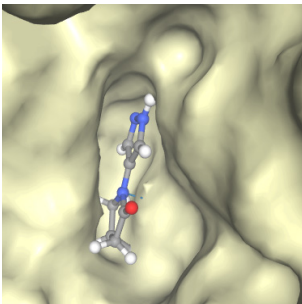
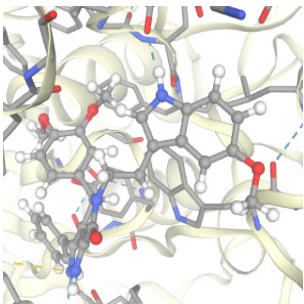
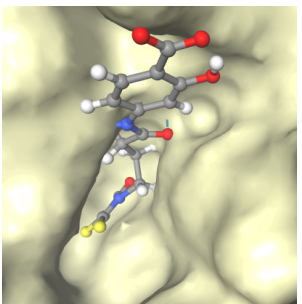
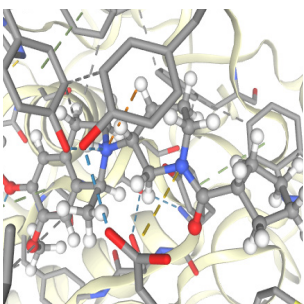
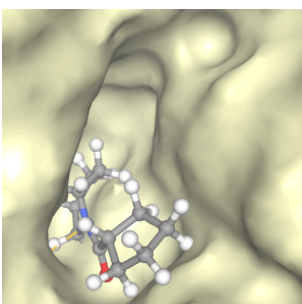
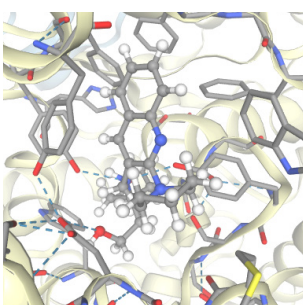
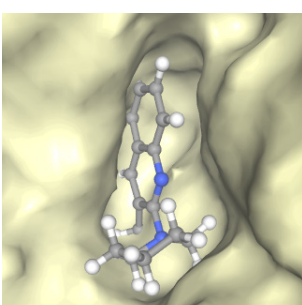
Table 9 provides information about pharmacophore map 4. PocketQuery identifies that pharmacophore map 2 belongs in the C chain with three crucial residues Tyrosine at position 90, Histidine at position 93, and Methionine at position 95. It has a high PocketQuery score of 0.981391. The key features we used for the ZINCPharmer query are 1

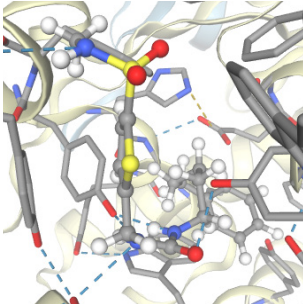
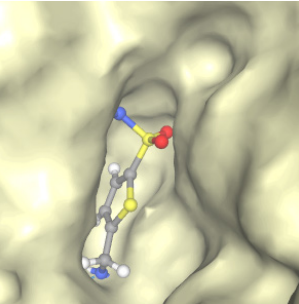
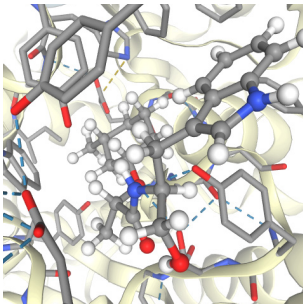
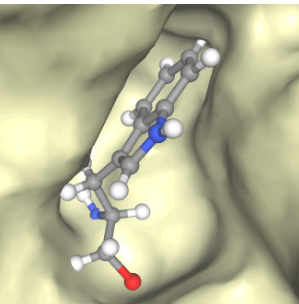
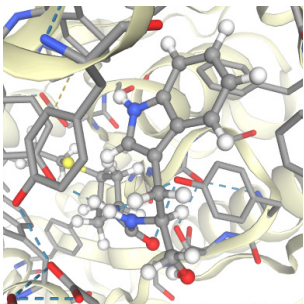
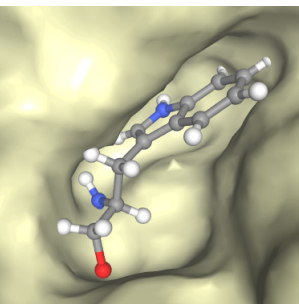
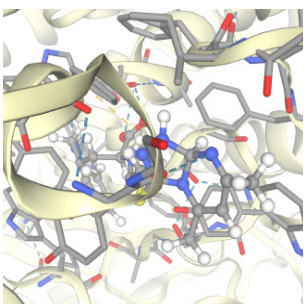
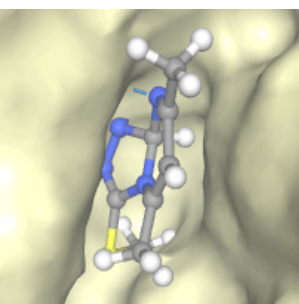
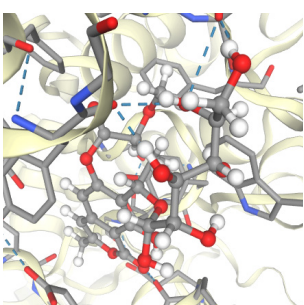
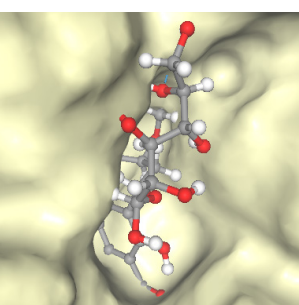
hydrogen donor, 1 hydrogen acceptor, and 1 hydrophobic interaction. Table 10 presents the top 5 ligands for pharmacophore map 4. The RMSD values for these ligands range from 0.016 to 0.021, with the median value at 0.020. This indicates that these ligands are a great fit for the PharmMap 4.

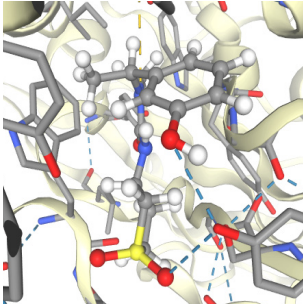
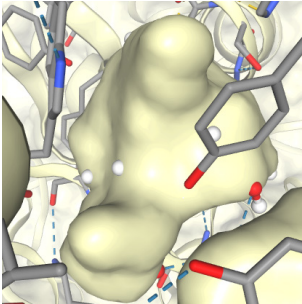
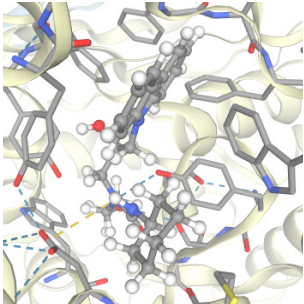
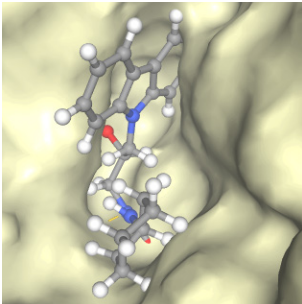
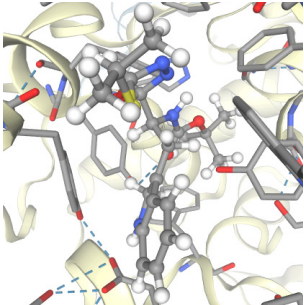
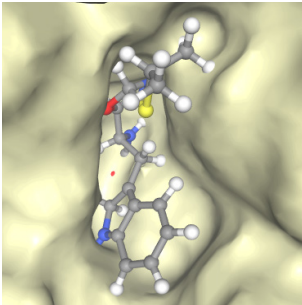
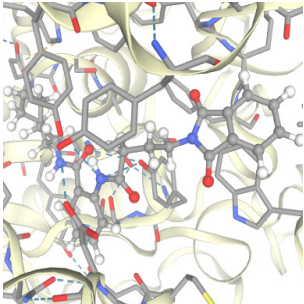
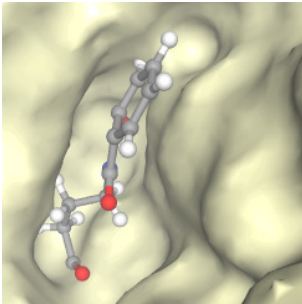
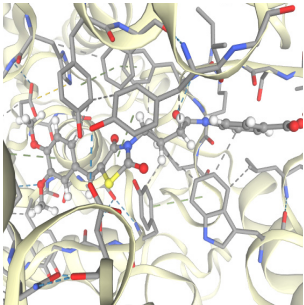
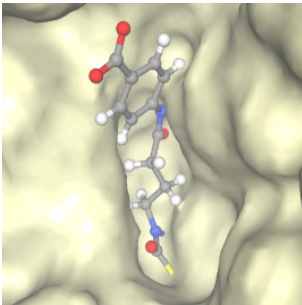
SwissDock Molecular Docking Results

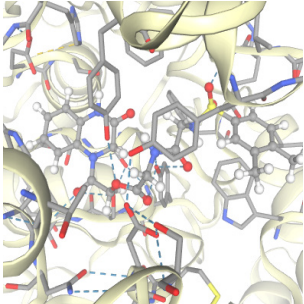
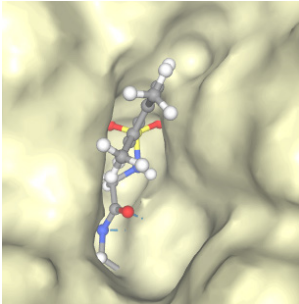
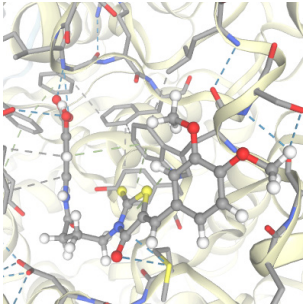
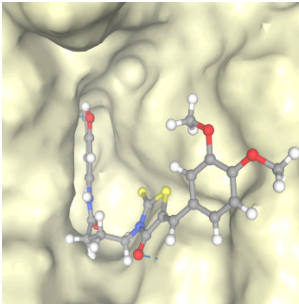
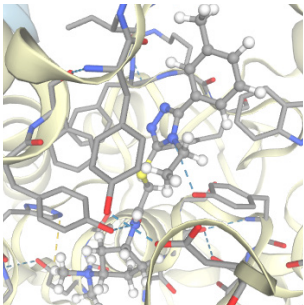
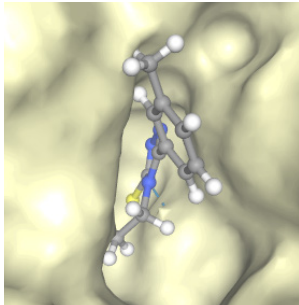
Table 11. Swissdock Results Showing the Docking of the 20 Compounds with AChE. Two Models (Interactions and Protein Surface) are Presented for each Compound, Along with the Top SwissParam Score

Name	Pharm Map #	ZINC ID	Cluster#	Model (with interactions)	Model (with protein surface)	Swiss Param Score (kcal/mol)
L_1	1	64380746	13			-7.1876
L_2	1	67533629	0			-8.1535

Name	Pharm Map #	ZINC ID	Cluster#	Model (with interactions)	Model (with protein surface)	Swiss Param Score (kcal/mol)
L_3	1	19567459	0			-8.2314
L_4	1	89306446	0			-7.9297
L_5	1	95101290	4			-8.1756
L_6	2	12232928	2			-7.0061
L_7	2	92176885	2			-7.1795

Name	Pharm Map #	ZINC ID	Cluster#	Model (with interactions)	Model (with protein surface)	Swiss Param Score (kcal/mol)
L_8	2	69328766	6			-8.3006
L_9	2	92189850	1			-7.5941
L_10	2	74888813	2			-7.6825
L_11	3	64684329	1			-7.9125
L_12	3	31156228	0			-7.7121

Name	Pharm Map #	ZINC ID	Cluster#	Model (with interactions)	Model (with protein surface)	Swiss Param Score (kcal/mol)
L_13	3	67580654	1			-7.4535
L_14	3	12249875	7			-7.3507
L_15	3	63426782	0			-7.5266
L_16	4	01211703	0			-8.6741
L_17	4	33417589	1			-7.5992

Name	Pharm Map #	ZINC ID	Cluster#	Model (with interactions)	Model (with protein surface)	Swiss Param Score (kcal/mol)
L_18	4	03302264	1			-8.9425
L_19	4	35638852	8			-7.2905
L_20	4	93796225	2			-7.9142

The data table above shows 20 selected ligands categorized by 4 pharmacophore map groups. The SwissParam score indicates the binding affinity between the ligand and the specific binding site, with the larger negative value indicating a stronger interaction. The SwissParam score for this dataset ranges from -8.9425 to -7.0061, with the median score being at -7.6973. These promising results indicate that many ligands interact well with AChE and are suitable as potential lead compounds for further investigation. For each ligand, the top cluster number and the member with the best SwissParam score are recorded. The cluster number represents a specific binding site on the target protein and

the cluster member represents one of many ways a ligand can bind to a cluster. Only the cluster number is displayed. The most common cluster numbers are 0, 1, and 2, with 6, 5, and 4 occurrences respectively. For each ligand, the left side figure shows the interaction between the ligand and its environment, including hydrogen bonds, ionic interactions, cation- π interactions, hydrophobic contacts, and π -stacking interactions. The right side figure shows the ligand docking with the protein surface displayed. Visual analysis of these figures suggests that most ligands used in this experiment bind favorably to one specific site on AChE.

Table 12. *SwissParam Scores of Top Ligands Compared with Popular AChE-Is*

Ligand	Cluster	SwissParam Score (kcal/mol)
Donepezil	1	-7.3369
Rivastigmine	1	-7.3763
Galantamine	1	-6.8899
L_18	1	-8.9425
L_16	0	-8.6741
L_8	6	-8.3006
L_3	4	-8.2314
L_5	0	-8.1756

Comparing the SwissParam score of our compounds with popular AChE-I like donepezil, rivastigmine, and galantamine, we found that our top compounds have stron-

ger binding interaction scores than these FDA-approved compounds.

Ligand Absorption, Distribution, Metabolism and Excretion(ADME) Results

Table 13. *SwissADME Result of Top Ligands with Information on the Physicochemical Properties, Water Solubility, Lipophilicity, and Pharmacokinetics of each Compound*

Name	Lipinski	LogP	#H-bond acceptor	#H-bond donor	Molecular Weight (g/mol)	BBB permeant	Water Solubility	GI Absorption
L_6	Yes	3.66	3	1	387.54	Yes	Moderately Soluble	High
L_7	Yes	3.31	3	2	370.51	Yes	Moderately Soluble	High
L_9	Yes	3.01	3	3	358.47	Yes	Moderately Soluble	High
L_16	Yes	3.38	4	2	447.53	No	Moderately Soluble	High
L_3	Yes	2.57	4	3	399.51	No	Moderately Soluble	High
L_8	Yes	2.76	4	3	395.54	No	Soluble	High
L_5	No	2.84	5	2	508.57	No	Poorly Soluble	High
L_18	No	1.59	8	3	488.51	No	Soluble	Low

Table 13 shows that most compounds are able to pass Lipinski's rule with the last two compounds each having 1 violation. Overall, L_6(ZINC12232928), L_7(ZINC92176885), and L_9(ZINC92189850) are our top 3 drug candidates as they showed promising ADME

results while having BBB permeability and high GI absorption. The 5 compounds with the highest SwissParam score had poor ADME results with none of them being able to have BBB permeability and three of them being less soluble than other compounds.

Ligand Toxicity Prediction Results

Figure 12. Toxicity Radar Chart for L_16

Compound L_16:
 Predicted LD50: **2450 mg/kg**
 Predicted Toxicity Class: **5**

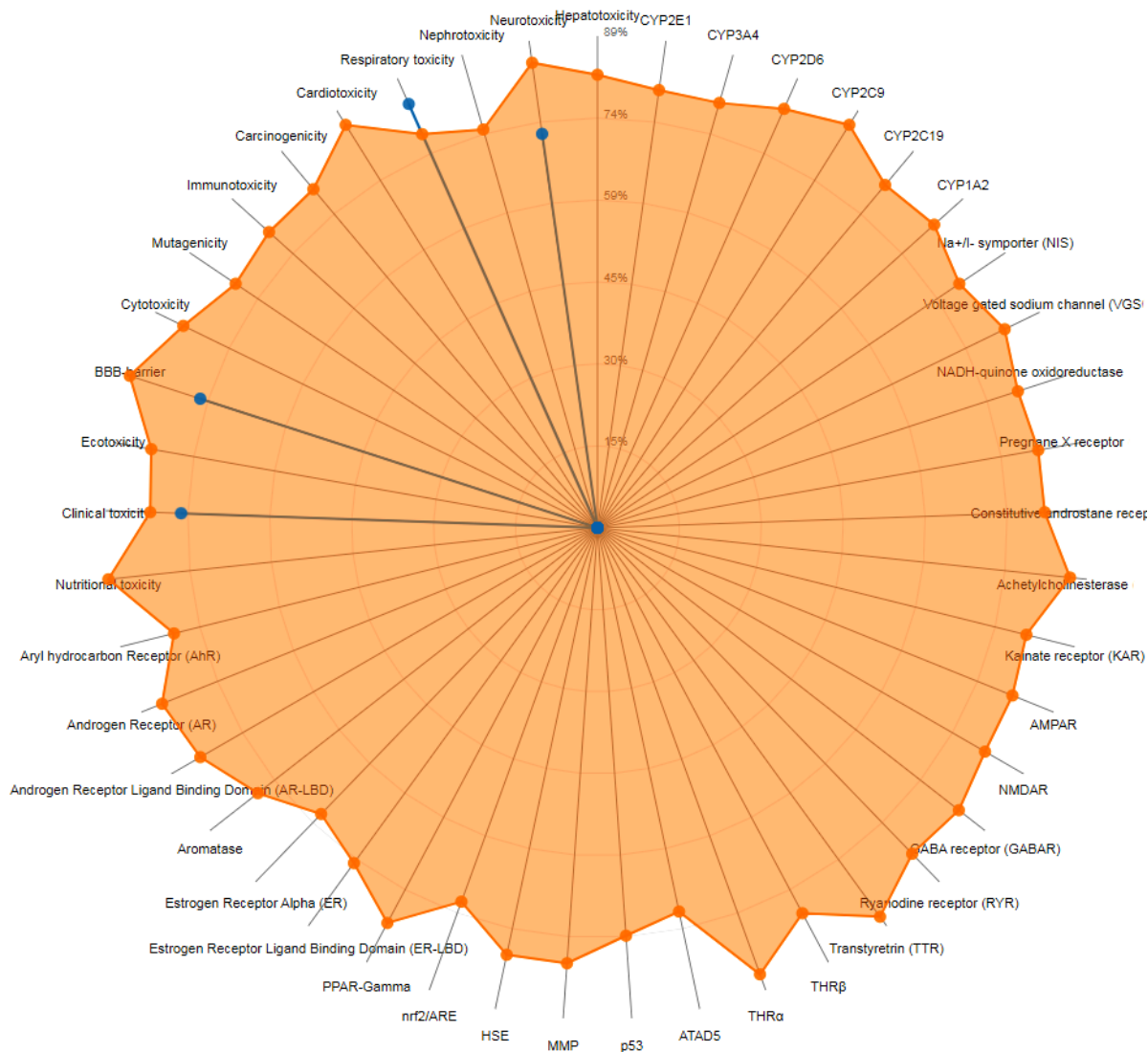


Figure 13. Network Chart for L_16

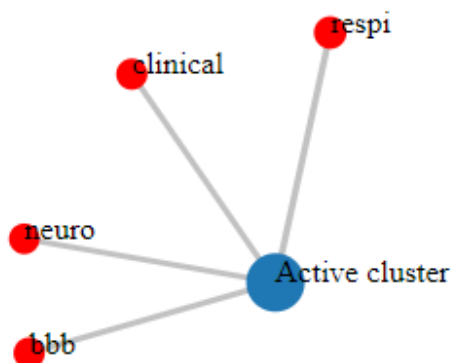


Figure 14. Toxicity Radar Chart for L_3

Compound **L_3**:
 Predicted LD50: **2800 mg/kg**
 Predicted Toxicity Class: **5**

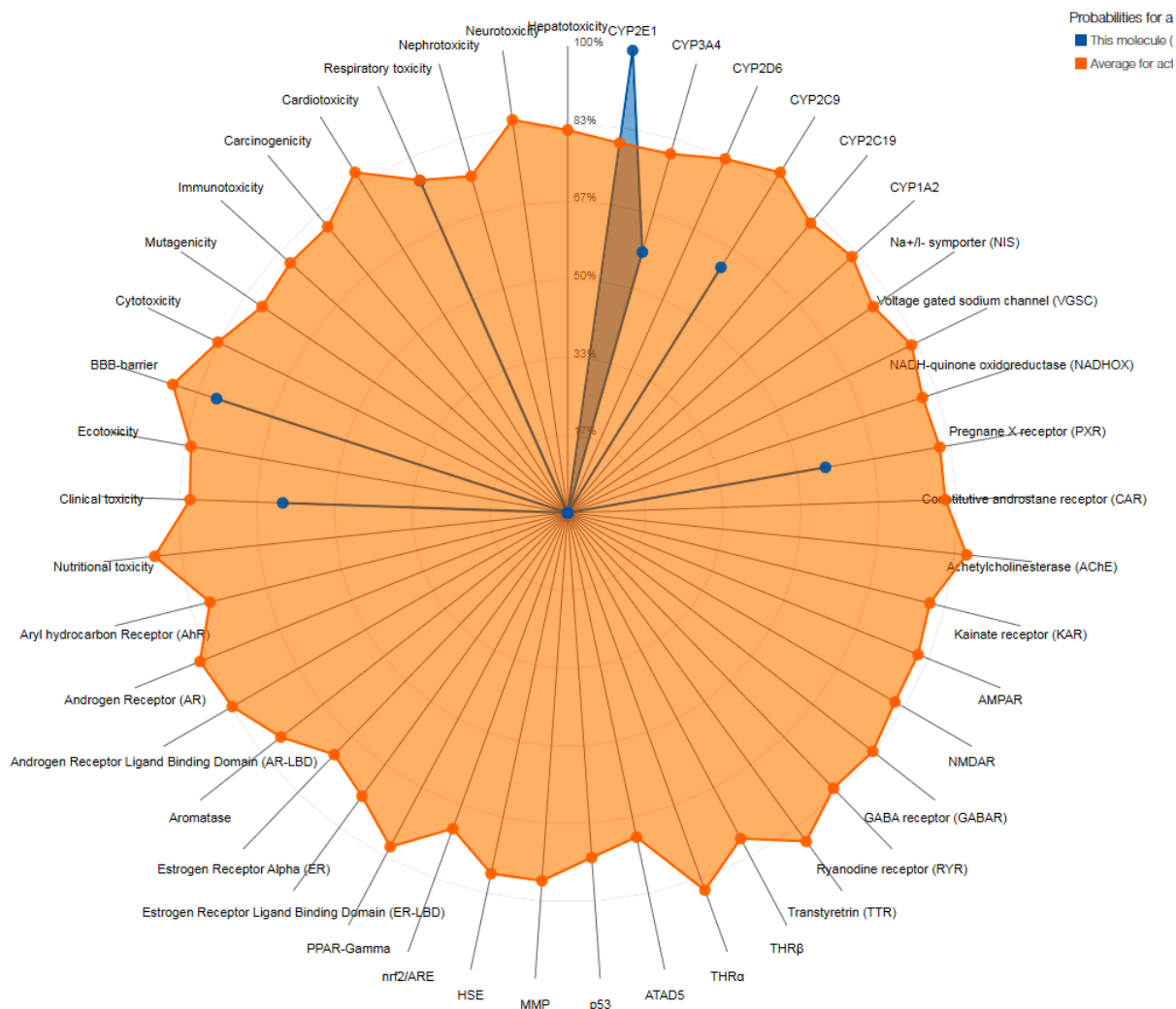


Figure 15. Network Chart for L_3

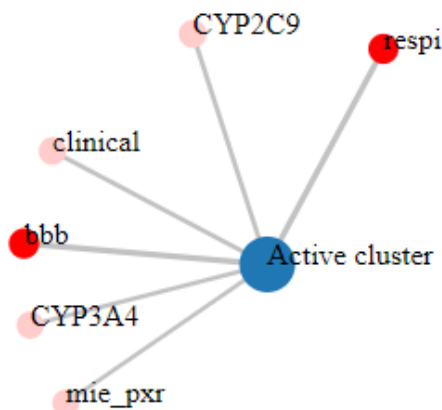


Figure 16. Toxicity Radar Chart for L_8

Compound L_8:
Predicted LD50: 1000 mg/kg
Predicted Toxicity Class: 4

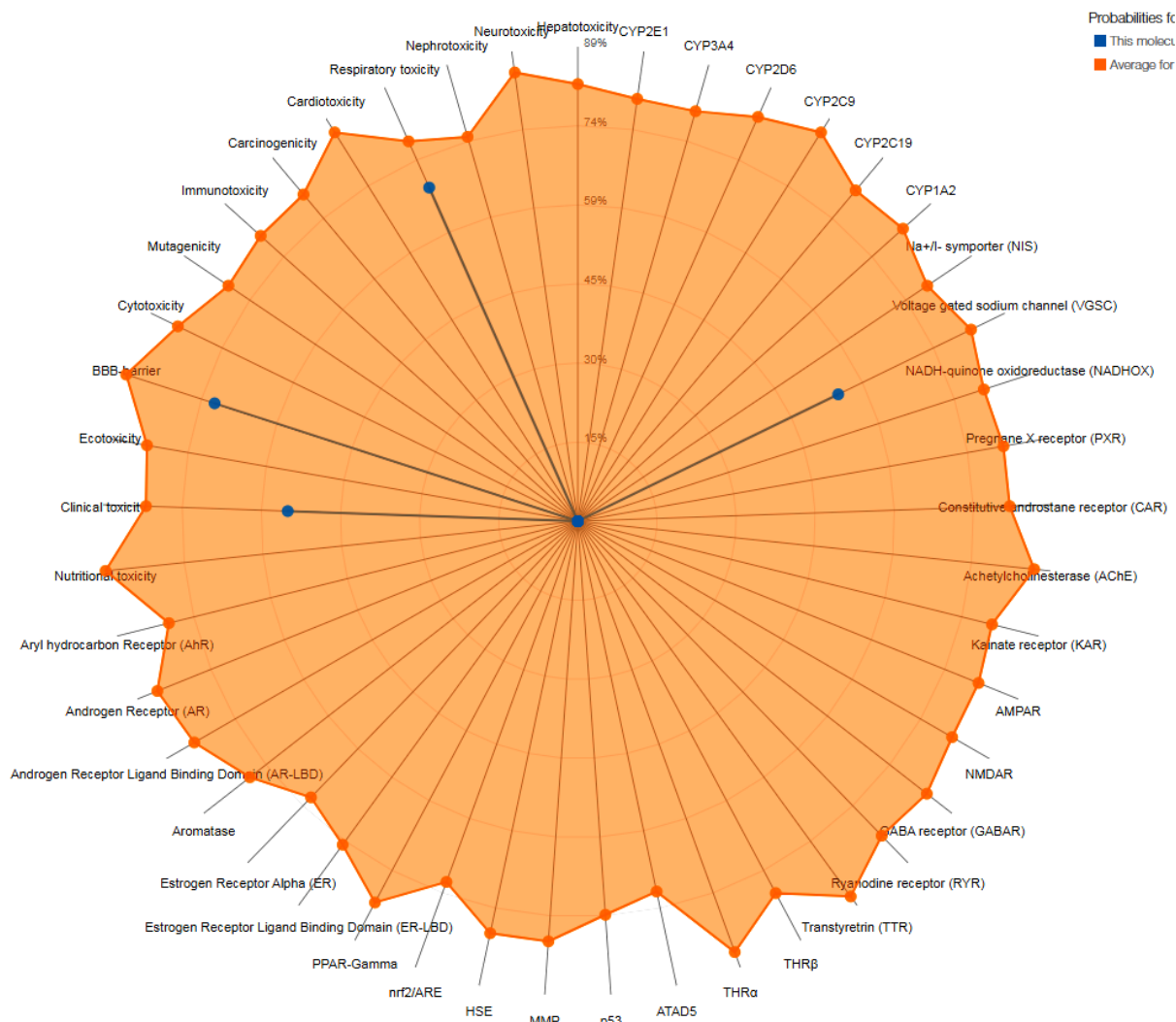


Figure 17. Network Chart for L_8

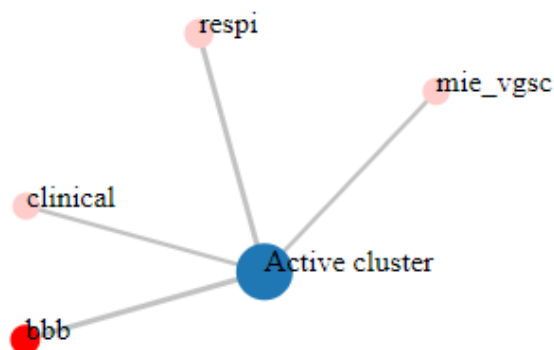


Figure 18. Toxicity Radar Chart for L_5

Compound **L_5**:
 Predicted LD50: **2800 mg/kg**
 Predicted Toxicity Class: **5**



Figure 19. Network Chart for L_5

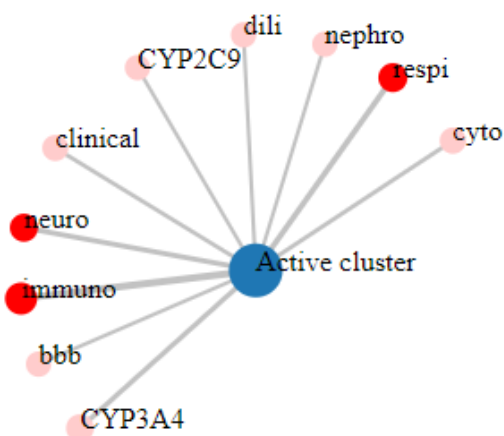


Figure 20. Toxicity Radar Chart for L_18

Compound L_18:
 Predicted LD50: **5240 mg/kg**
 Predicted Toxicity Class: **6**

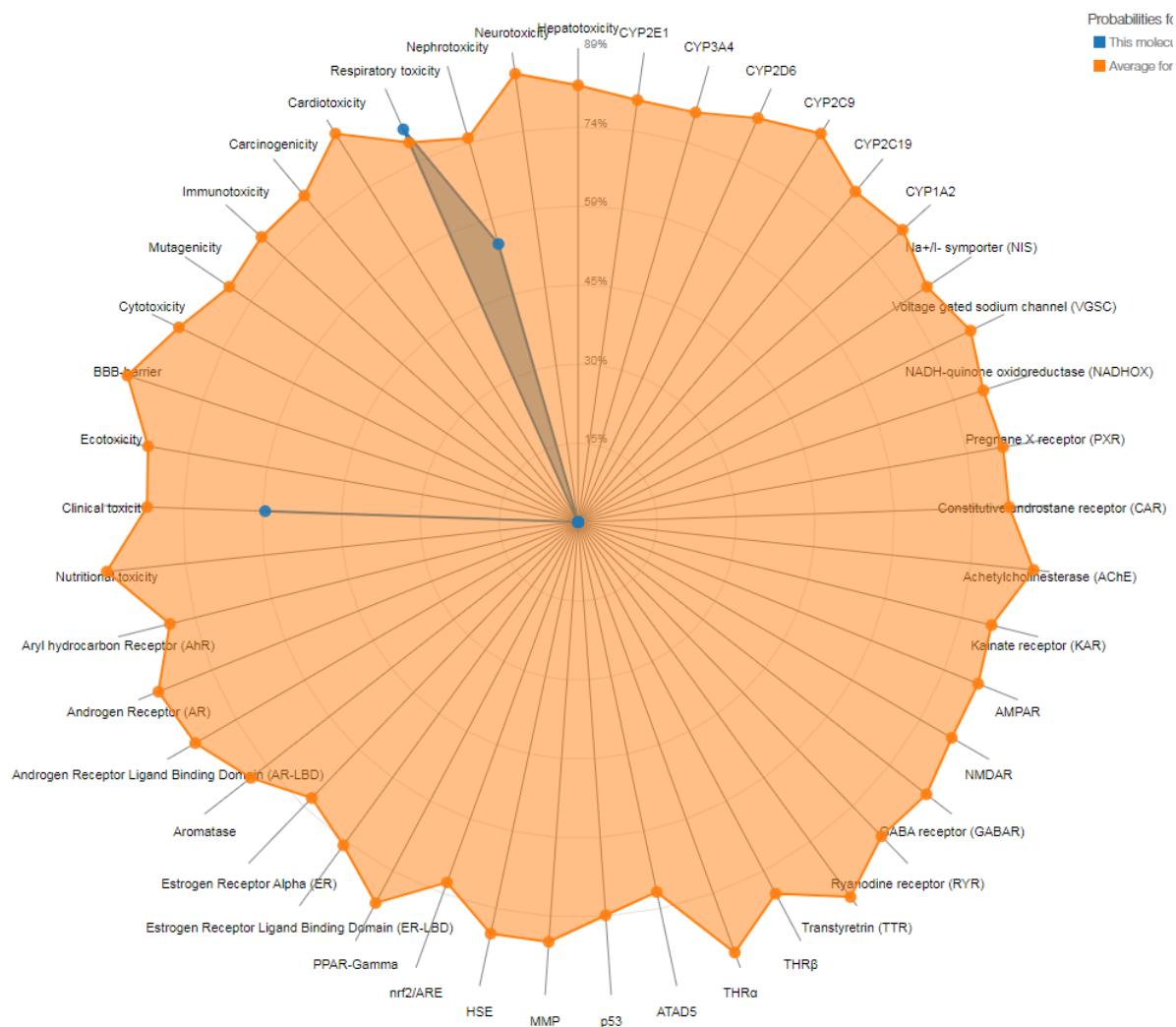


Figure 21. Network Chart for for L_18

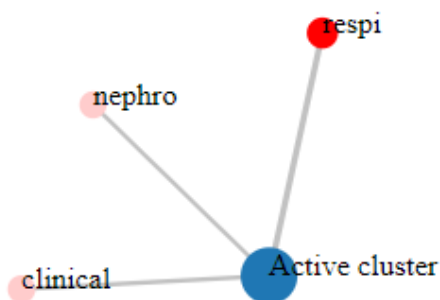


Figure 22. Toxicity Radar Chart for L_6

Compound L_6:
Predicted LD50: 75mg/kg
Predicted Toxicity Class: 3

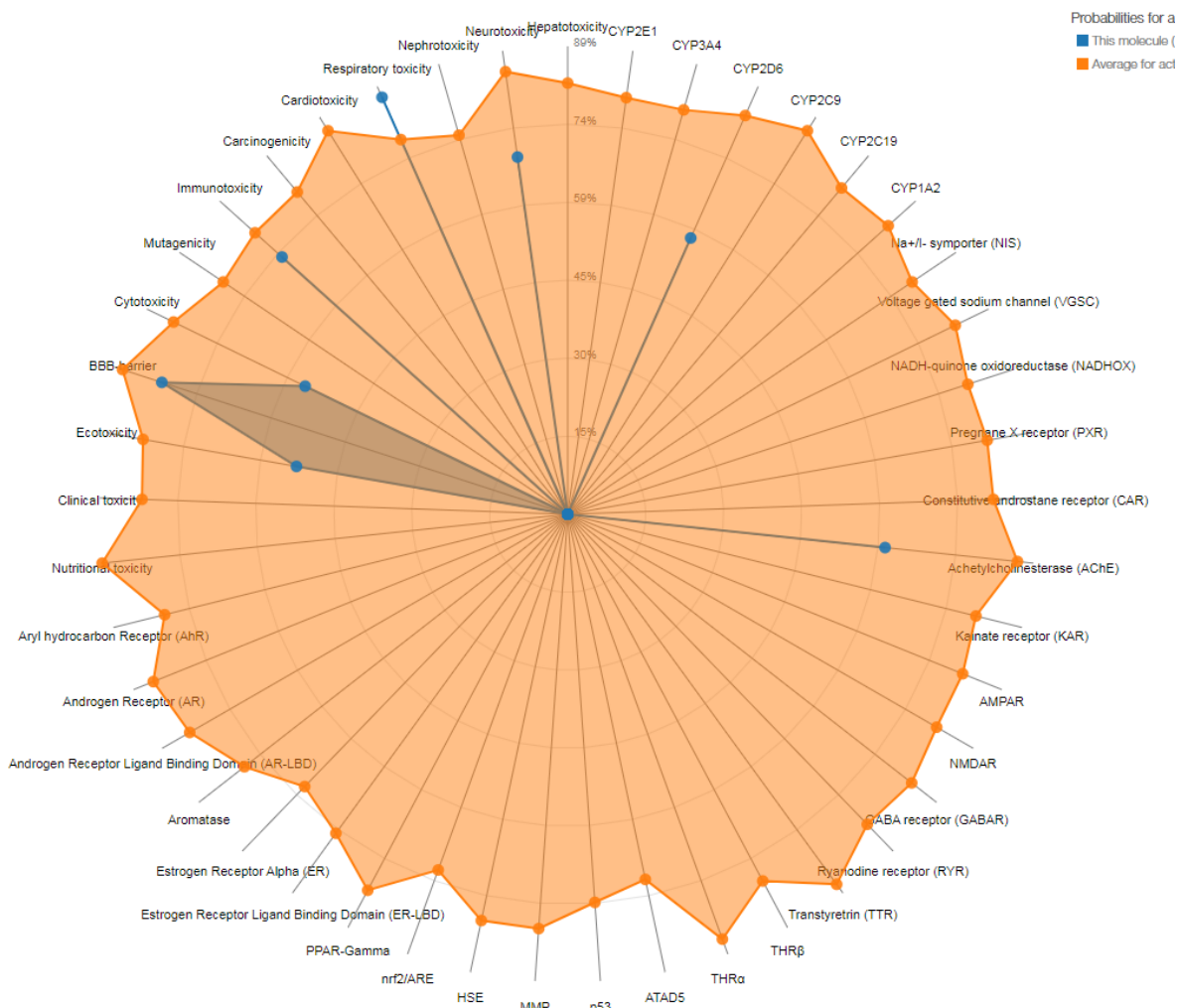


Figure 23. Network Chart for L_6

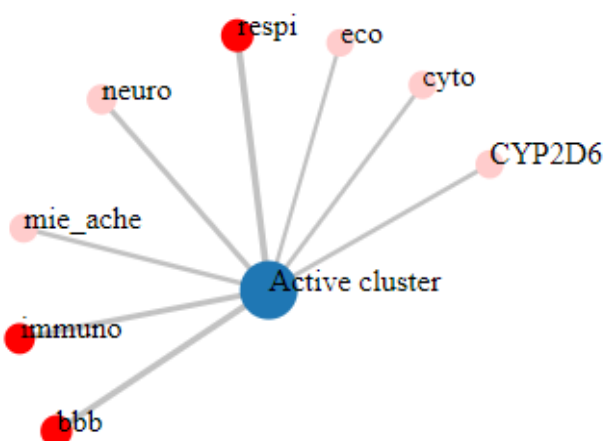


Figure 24. Toxicity Radar Chart for L_7

Compound **L_7**:
 Predicted LD50: **1190 mg/kg**
 Predicted Toxicity Class: **4**

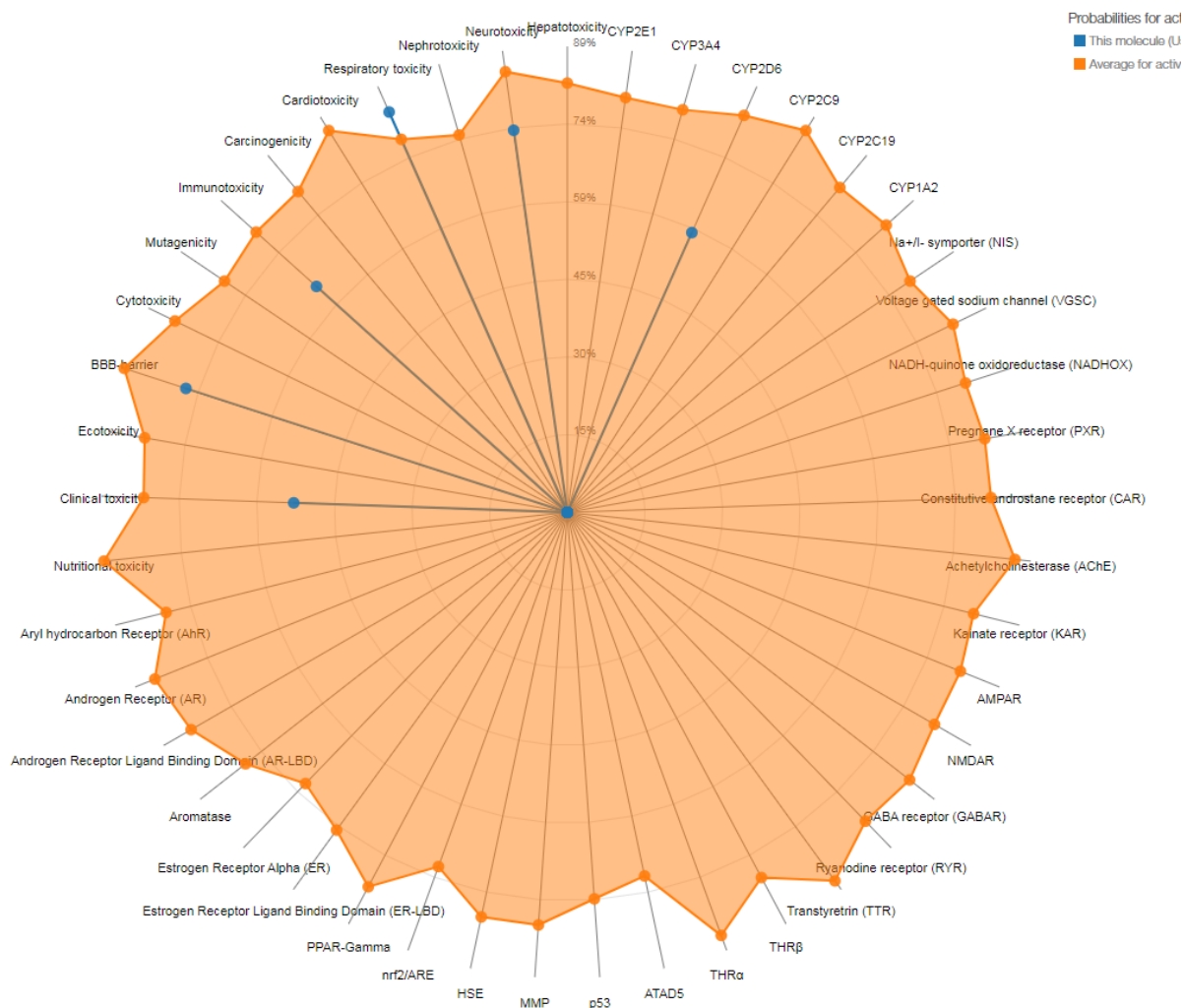


Figure 25. Network Chart for L_7

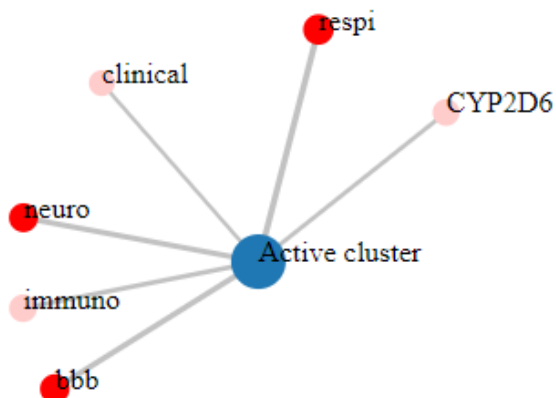


Figure 26. Toxicity Radar Chart for L_9

Compound L_9:
 Predicted LD50: **800 mg/kg**
 Predicted Toxicity Class: **4**

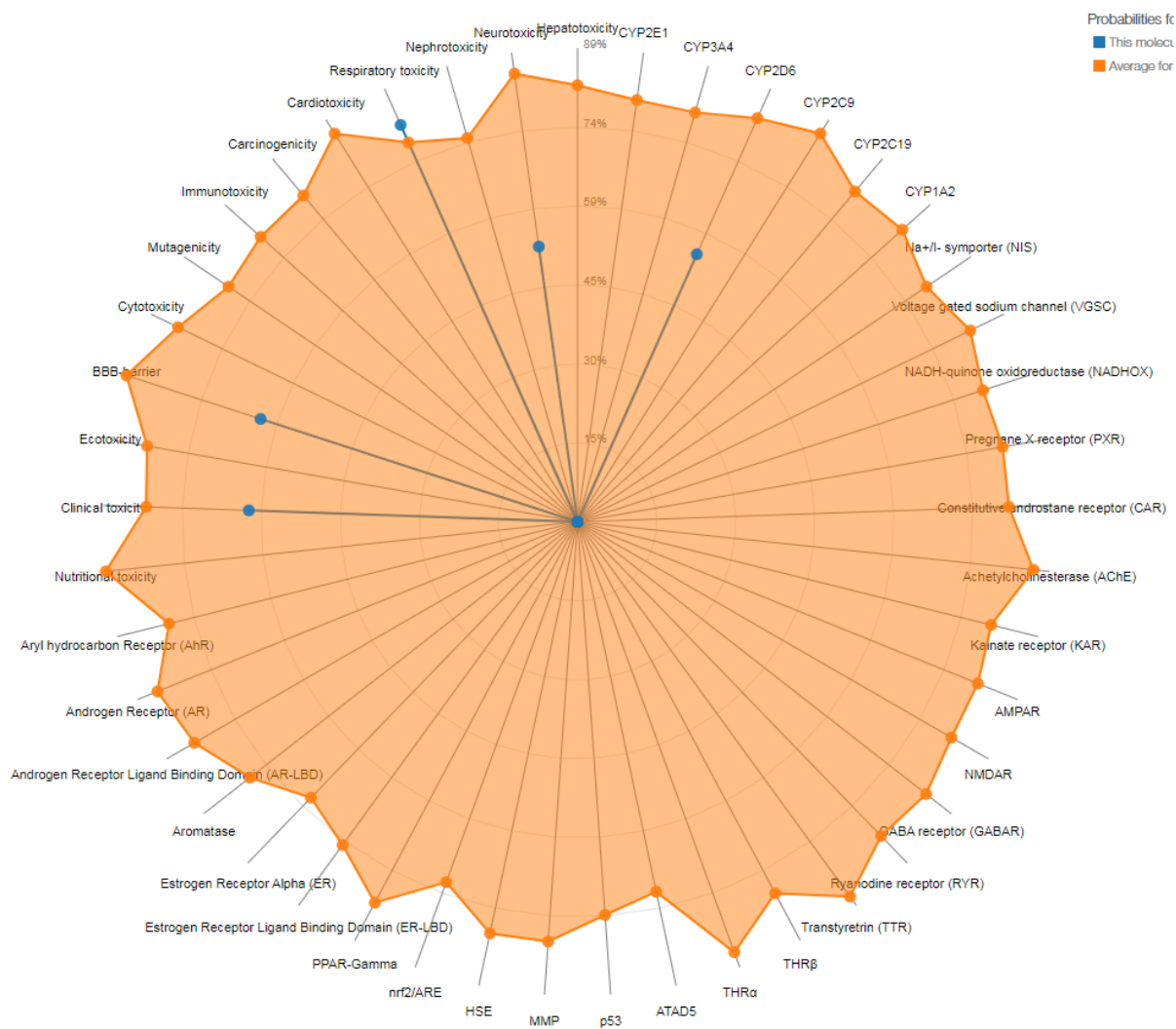


Figure 27. Network Chart for L_9

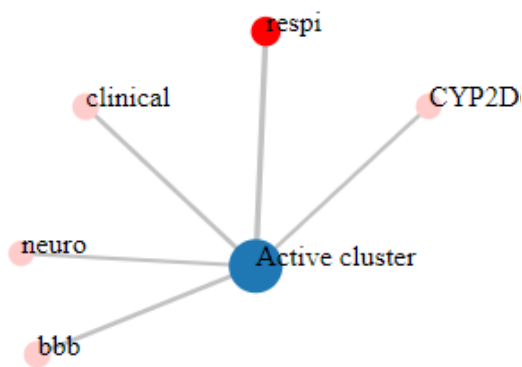


Table 14. ProTox Toxicity Class Description

Class 1	fatal if swallowed	(LD50 ≤ 5)
Class 2	fatal if swallowed	(5 < LD50 ≤ 50)
Class 3	toxic if swallowed	(50 < LD50 ≤ 300)
Class 4	harmful if swallowed	(300 < LD50 ≤ 2000)
Class 5	may be harmful if swallowed	(2000 < LD50 ≤ 5000)
Class 6	non-toxic	(LD50 > 5000)

LD50: the median lethal dose meaning the dose at which 50% of test subjects die upon exposure to a compound (SwissADME. Retrieved from URL: <http://www.swissadme.ch/>. Accessed July 16 2024)

Our results from Pro Tox 3.0 show that most compounds have a toxicity class of 4 or 5 and are harmful or may be harmful if swallowed. The network chart showed us that the clusters most heavily affected by the drugs are respiratory, neurological, clinical, and BBB. Overall, our compound has a median LD50 of 1820 mg/kg with outliers L_18 being surprisingly non-toxic (LD50 of 5240 mg/kg) and L_6 being toxic if swallowed (LD50 of 75 mg/kg). The data for L_6 specifically suggest that although these compounds have strong binding interaction and favorable ADME results, they could be harmful and might require modifications to improve toxicity levels. Regardless, most compounds tested in the Pro-Tox experiment showed appropriate toxicity classes of between 4 and 5.

Statement of limitation

This research has potential limitations. Due to the time constraint of the study, only the top compounds are reported as the results, leading to a limited sample size. Only 4 pharmacophore maps with the top scores were selected from Pocketquery to be used for the ZINCPharmer experiment. In Pocketquery, there are hundreds of other pharmacophore maps for AChE with scores above 0.9 that could potentially lead to new promising ligands. In addition, only 5 compounds with the highest RMSD scores for each of the 4 pharmacophore maps are recorded and analyzed from ZINCPharmer. This limits our sample size for the following SwissDock, SwissADME, and ProTox experiments to only 20 compounds. Additionally, our results from the SwissDock experiment showed that most of our top compounds only dock to one specific binding site on AChE. This is in

contrast to the results from our binding site detection experiment, which showed multiple promising binding sites for small compounds. This discrepancy is likely due to the time limit constraint for the search box on SwissDock, leading to only a portion of the whole AChE enzyme being examined. These limitations could lead to the exclusion of many compounds with potentially promising results. To overcome these limitations, one direction for future studies in the short term is to expand the sample size of the study and examine a larger series of compounds. In addition, the study could explore other regions of AChE and examine the molecular docking of compounds with other binding clusters.

In this study, the 20 compounds selected for further experimentation had the highest RMSD scores from the ZINCPharmer experiment. The series of compounds explored in this study could be biased towards their structural affinity to their respective pharmacophore maps. This bias potentially excluded other important factors in drug development such as binding energy interactions, ADME, and toxicity. This leads to tradeoffs in different characteristics of the compound. For example, L_16(ZINC01211703) has the highest SwissParam score of -8.9425 kcal/mol and the best toxicity result, however, it has unacceptable ADME results. Additionally, L_6(ZINC12232928) has a SwissParam score of -7.0061 kcal/mol and has favorable ADME results, however it is highly toxic, with a predicted LD50 of 75 mg/kg. One potential way to avoid this limitation in future virtual screening studies is to select the top compounds based on a multifactorial analysis of their characteristics and test results instead of only focusing on their RMSD scores. Re-

searchers can give a score for the compound for each factor considered for drug development, and create a composite score with the scores for each factor weighted based on their respective importance. This method might lead to more consistent results as opposed to considering only one factor to narrow compounds for further experimentation.

All experiments in this study are computational and done on free online web tools. These online models and algorithms might produce inaccurate results and fail to precisely simulate real-world interactions. Not all pharmacophore features were selected in the ZINCPharmer experiment which might lead to slightly inaccurate results. Although virtual screening offers a speedier and relatively accurate way to narrow down a large library of compounds, physical screening is needed to validate these results.

Conclusion

Alzheimer's disease (AD), a neurodegenerative disease characterized by memory loss and cognitive deficit, is currently accounting for 60–70% of the 50 million dementia cases worldwide. The costliness and adverse side effects of current AD treatments call for new improved therapy of AD that offers strong efficacy while having tolerable toxicity and favorable ADME. Acetylcholinesterase inhibitors (AChE-I), compounds that are about to reduce the breakdown of acetylcholinesterase (AChE), have shown promising efficacy in recent years in reducing cognitive decline symptoms in AD patients. Our research identifies and examines potential lead compounds for developing better AChE-I using a variety of online virtual screening tools. We first utilized geometric, machine learning, and energetic-based methods to confirm the availability of binding sites for small compounds on AChE. Using Pocketquery and then ZINCPharmer, we were able to narrow down a large library of compounds based on their structural affinity to the features of the top 4 pharmacophore maps we selected from AChE. Using SwissDock, we further narrow down ligands L_18(ZINC03302264), L_16(ZINC01211703), L_8(ZINC69328766), L_3(ZINC19567459), and L_5(ZINC95101290) as the compounds with the strongest binding interaction with AChE. This series of ligands

has a median SwissParam score of -8.3006 kcal/mol, which is nearly 1 kcal/mol higher compared to currently FDA-approved AChE-I. However, in ADME screening, ligands L_6(ZINC12232928), L_7(ZINC92176885), and L_9(ZINC92189850) with slightly worse binding interaction score were the only compounds able to cross the BBB and pass Lipinski's rule. After testing these compounds for their toxicity using ProTox 3.0, ligands L_7 and L_9 maintained excellent testing results as they are our most promising compounds with high SwissParam scores of -7.1795 and -7.5941 kcal/mol, favorable ADME results, and acceptable toxicity levels. In future studies, enzymatic assays and biological screening for these compounds can further investigate and confirm the drug properties of these compounds. The efficacy and toxicity of the compounds can be further verified through in vivo and in vitro studies. Additionally, other laboratory techniques such as microscale thermophoresis (MST), surface plasmon resonance (SPR), isothermal titration calorimetry (ITC), and Kd calculations can be conducted to validate the molecular binding interactions of these ligands.

Acknowledgement

First and foremost, I would like to express my special thanks to Professor Mustafa Gabr from Cornell University for giving me the opportunity to work on this amazing project and mentoring me through the whole process.

I would like to thank my maternal grandfather Fang Ding Chang, who currently has Alzheimer's, for supporting me throughout my childhood. He inspired me to conduct this research on Alzheimer's and I wish the best for him and those suffering from similar conditions. I also want to give my sincere thanks to my paternal grandfather Dr. Bao Han Fei, whose relentless dedication to research to this day inspired me to conduct my very first scientific research.

Finally, I would like to express my sincere gratitude to my parents Ping and Qin for supporting me and encouraging me to embody the scientist's spirit of staying hungry for cutting-edge knowledge and never giving up when faced with adversity.

References

- Abuelezz, Nermeen & Nasr, Fayza & AbdulKader, Mohammad & Bassiouny, Ahmad & Zaky, Amira. (2021). MicroRNAs as Potential Orchestrators of Alzheimer's Disease-Related Pathologies: Insights on Current Status and Future Possibilities. *Frontiers in Aging Neuroscience*. – 13. – 743573 p. 10.3389/fnagi.2021.743573.
- Agu, P.C., Afiukwa, C.A., Orji, O.U. et al. (2023). Molecular docking as a tool for the discovery of molecular targets of nutraceuticals in diseases management. *Sci Rep* – 13, 13398. URL: <https://doi.org/10.1038/s41598-023-40160-2>
- Banerjee P., Kemmler E., Dunkel M., Preissner R.: ProTox 3.0: a webserver for the prediction of toxicity of chemicals *Nucleic Acids Research*, – Vol. 52. – Issue W1, 5 July, 2024. – P. W513–W520. URL: <https://doi.org/10.1093/nar/gkae303>
- Berman H. M., Westbrook J., Feng Z., Gilliland G., Bhat T.N., Weissig H., Shindyalov I.N., Bourne P.E. The Protein Data Bank. *Nucleic Acids Research*. 2000 Jan 1; 28(1): 235-42. Doi: 10.1093/nar/28.1.235. PMID: 10592235; PMCID: PMC102472.
- Breijyeh Z., Karaman R. Comprehensive Review on Alzheimer's Disease: Causes and Treatment. *Molecules*. 2020. Dec 8; 25(24): 5789. Doi: 10.3390/molecules25245789. PMID: 33302541; PMCID: PMC7764106.
- Brenke R., Kozakov D., Chuang G.Y., Beglov D., Hall D., Landon M.R., Mattos C., Vajda S. Fragment-based identification of druggable 'hot spots' of proteins using Fourier domain correlation techniques. *Bioinformatics*. 2009. Mar 1.
- Bugnon M., Röhrig U.F., Goullieux M., Perez MAS, Daina A., Michielin O., Zoete V. Swiss Dock 2024: major enhancements for small-molecule docking with Attracting Cavities and AutoDock Vina. *Nucleic Acids Research*. 2024. Jul 5; 52 (W1): W324–W332.
- Chen Z. R., Huang J. B., Yang S. L., Hong F. F. Role of Cholinergic Signaling in Alzheimer's Disease. *Molecules*. 2022. Mar, 10; 27(6): 1816. Doi: 10.3390/molecules27061816. PMID: 35335180; PMCID: PMC8949236.
- Daina, A., Michielin, O. & Zoete, V. (2017). Swiss ADME: a free web tool to evaluate pharmacokinetics, drug-likeness and medicinal chemistry friendliness of small molecules. *Sci Rep* – 7, – 42717. URL: <https://doi.org/10.1038/srep42717>
- Dávid Jakubec, Petr Škoda, Radoslav Krivák, Marian Novotný and David Hoksza. PrankWeb 3: accelerated ligand-binding site predictions for experimental and modelled protein structures. *Nucleic Acids Research*. May, 2022.
- Dementia medication side effects. Alzheimer's Society. (n.d.)*. Retrieved from URL: <https://www.alzheimers.org.uk/about-dementia/treatments/dementia-medication/dementia-medication-side-effects/> Accessed 13 June 2024.
- Ferreira-Vieira T. H., Guimaraes I. M., Silva F. R., Ribeiro F. M. Alzheimer's disease: Targeting the Cholinergic System. *Curr Neuropharmacol*. 2016; 14(1): 101-15. Doi: 10.2174/1570159x13666150716165726. PMID: 26813123; PMCID: PMC4787279.
- Grossberg G.T. Cholinesterase inhibitors for the treatment of Alzheimer's disease: getting on and staying on. *Curr Ther Res Clin Exp*. 2003. Apr; 64(4): 216-35. Doi: 10.1016/S0011-393X(03)00059-6. PMID: 24944370; PMCID: PMC4052996.
- Kozakov D., Grove L.E., Hall D.R., Bohnuud T., Mottarella S.E., Luo L., Xia B., Beglov D., Vajda S. The FTMap family of web servers for determining and characterizing ligand-binding hot spots of proteins. *Nature Protocols*. 2015. 10(5): 733-755.
- Lukáš Jendele and Radoslav Krivák and Petr Škoda and Marian Novotný and David Hoksza. PrankWeb: a web server for ligand binding site prediction and visualization. *Nucleic Acids Research*. May, 2019.
- Marešová P., Dolejš J., Mohelska H., Bryan L. K. Cost of Treatment and Care for People with Alzheimer's Disease: A Meta-Analysis. *Curr Alzheimer Res*. 2019; 16(14): 1245–1253. Doi: 10.2174/1567205017666200102144640. PMID: 31894748.
- McDade E., Cummings J.L., Dhadda S., Swanson C.J., Reyderman L., Kanekiyo M., Koyama A., Irizarry M., Kramer L.D., Bateman R.J. Lecanemab in patients with early Alzhei-

- mer's disease: detailed results on biomarker, cognitive, and clinical effects from the randomized and open-label extension of the phase 2 proof-of-concept study. *Alzheimers Res Ther.* 2022. Dec 21; 14(1): 191. Doi: 10.1186/s13195-022-01124-2. PMID: 36544184; PMCID: PMC9768996.
- Moustafa T. Gabr, Mohammed S. Abdel-Raziq, Design and synthesis of donepezil analogues as dual AChE and BACE-1 inhibitors. *Bioorganic Chemistry*, – Volume 80, 2018. – P. 245–252. ISSN 0045-2068
- Murphy M. P., LeVine H. 3rd. Alzheimer's disease and the amyloid-beta peptide. *J Alzheimers Dis.* 2010; 19(1): 311-23. Doi: 10.3233/JAD-2010-1221. PMID: 20061647; PMCID: PMC2813509. Professional, Cleveland Clinic medical. "Acetylcholine (ACH): What It Is, Function & Deficiency." Cleveland Clinic, my.clevelandclinic.org/health/articles/24568-acetylcholine-ach/ Accessed 13 June 2024.
- Ngan C.H., Hall D.R., Zerbe B.S., Grove L.E., Kozakov D., Vajda S. FTSite: high accuracy detection of ligand binding sites on unbound protein structures. *Bioinformatics* 2012. 28: 286–287.
- Radoslav Krivák and David Hoksza. P2Rank: machine learning based tool for rapid and accurate prediction of ligand binding sites from protein structure. *Journal of Cheminformatics.* Aug. 2018.
- Ricciarelli R., Fedele E. The Amyloid Cascade Hypothesis in Alzheimer's Disease: It's Time to Change Our Mind. *Curr Neuropharmacol.* 2017; 15(6): 926–935. Doi: 10.2174/1570159X15666170116143743. PMID: 28093977; PMCID: PMC5652035.
- Röhrig U.F., Goullieux M., Bugnon M., Zoete V. Attracting Cavities 2.0: improving the flexibility and robustness for small-molecule docking. *J. Chem. Inf. Model.*, 2023.
- Sam C., Bordonni B. Physiology, Acetylcholine. [Updated 2023 Apr 10]. In: StatPearls [Internet]. Treasure Island (FL): StatPearls Publishing; 2024 Jan-. Available from: URL: <https://www.ncbi.nlm.nih.gov/books/NBK557825>
- Shoab Manzoor, Moustafa T. Gabr, Bisma Rasool, Kavita Pal, Nasimul Hoda, Dual targeting of acetylcholinesterase and tau aggregation: Design, synthesis and evaluation of multifunctional deoxyvasicinone analogues for Alzheimer's disease. *Bioorganic Chemistry*, – Volume 116. 2021. – 105354. ISSN 0045-2068
- Stanciu G. D., Luca A., Rusu R.N., Bild V., Beschea Chiriac S. I., Solcan C., Bild W., Ababei D. C. Alzheimer's Disease Pharmacotherapy in Relation to Cholinergic System Involvement. *Biomolecules.* 2020; 10(1): 40. URL: <https://doi.org/10.3390/biom10010040>
- Tahami Monfared A. A., Byrnes M. J., White L. A., Zhang Q. The Humanistic and Economic Burden of Alzheimer's Disease. *Neurol Ther.* 2022. Jun; 11(2): 525–551. Doi: 10.1007/s40120-022-00335-x. Epub 2022 Feb 22. PMID: 35192176; PMCID: PMC9095804.
- Tansey E.M. Henry Dale and the discovery of acetylcholine. *C R Biol.* 2006. May-Jun; 329(5-6): 419–25. Doi: 10.1016/j.crv.2006.03.012. Epub 2006 May 2. PMID: 16731499.
- Van Dyck C.H., Swanson C.J., Aisen P., Bateman R.J., Chen C., Gee M., Kanekiyo M., Li D., Reyderman L., Cohen S., Froelich L., Katayama S., Sabbagh M., Vellas B., Watson D., Dhadda S., Irizarry M., Kramer L.D., Iwatsubo T. Lecanemab in Early Alzheimer's Disease. *N Engl J Med.* 2023. Jan 5; 388(1): 9–21. Doi: 10.1056/NEJMoA2212948. Epub 2022 Nov 29. PMID: 36449413.
- Volkamer, A., Griewel, A., Grombacher, T., Rarey, M. Analyzing the topology of active sites: on the prediction of pockets and subpockets. *J Chem Inf Model.* 2010. – 50 (11), 2041–52. DOI: <https://doi.org/10.1021/ci100241y>
- Volkamer, A., Kuhn, D., Grombacher, T., Rippmann, F., Rarey, M. Combining global and local measures for structure-based druggability predictions. *J Chem Inf Model.* 2012. – 52 (2). – 360-72. DOI: <https://doi.org/10.1021/ci200454v>
- Zou D., Liu R., Lv Y., Guo J., Zhang C., Xie Y. Latest advances in dual inhibitors of acetylcholinesterase and monoamine oxidase B against Alzheimer's disease. *J Enzyme Inhib Med Chem.* 2023. Dec; 38(1): 2270781. Doi: 10.1080/14756366.2023.2270781. Epub 2023. Nov 13. PMID: 37955252; PMCID: PMC10653629.

FDA Converts Novel Alzheimer's Disease Treatment to Traditional Approval. Retrieved from URL: <https://www.fda.gov/news-events/press-announcements/fda-converts-novel-alzheimers-disease-treatment-traditional-approval/> Accessed 17 June 2024.

Proteins Plus. Retrieved from URL: <https://proteins.plus/3lii/> Accessed June 18 2024

Prankweb. Retrieved from URL: <https://prankweb.cz/viewer?id=3lii&database=v3-conservation-hmm/> Accessed June 18, 2024.

FTSite. Retrieved from URL: <https://ftsitesite.bu.edu/>. Accessed June 18 2024.

SwissDock. Retrieved from URL: <https://www.swissdock.ch/>. Accessed July 9 2024.

SwissADME. Retrieved from URL: <http://www.swissadme.ch/>. Accessed July 16 2024.

ProTox. Retrieved from URL: <https://tox.charite.de/protox3/index.php?site=home/> Accessed July 23 2024.

submitted 02.09.2024;

accepted for publication 16.09.2024;

published 29.10.2024

© Benjamin Liu

Contact: benjaminliu0701@gmail.com

Contents

Section 1. Clinical medicine

Brian Kuo

FIRST-IN-CLASS SMALL MOLECULE BTLA INHIBITORS AS POTENTIAL CANCER THERAPIES	3
--	---

Section 2. Chemistry biology

Guanrong (Rain) Cheng

IDENTIFYING CEACAM 1-TARGETED DRUG CANDIDATES FOR CANCER IMMUNOTHERAPY	21
---	----

Section 3. Life sciences

Yimiao Zou

A REVIEW OF HARP THERAPY AND GENDER DEMOGRAPHICS ANALYSIS IN PUBLISHED STUDIES	39
---	----

Section 4. Pharmaceutical Sciences

Benjamin Liu

VIRTUAL SCREENING OF ACETYLCHOLINESTERASE- CENTERED INHIBITORS AS POTENTIAL THERAPIES FOR ALZHEIMER'S DISEASE	46
---	----